PROBING BOUNDARY LUBRICATION PHENOMENA ON TEXTILE RELEVANT SURFACES

A Dissertation

Presented to the Faculty of the Graduate School

of Cornell University

In Partial Fulfillment of the Requirements for the Degree of

Doctor of Philosophy

by

Yan Li

August 2009

PROBING BOUNDARY LUBRICATION PHENOMENA ON TEXTILE RELEVANT SURFACES

Yan Li, Ph. D.

Cornell University 2009

Boundary lubrication is a fundamental phenomenon in textile processing. While the study on the boundary can provide a unique insight of the chemical interactions between lubricants, finishes, and fibers, boundary lubrication has not received as much attention by the scientific community as hydrodynamic lubrication. The disparity in the scientific efforts to develop a comprehensive understanding of lubrication phenomena can be explained in part by experimental limitations when the characteristic dimensions of the phenomena become submicron. The work reported in this dissertation introduces lateral force microscopy as a feasible tool to probe boundary lubrication phenomena at the nanoscale and establishes correlations between this new technique and more established macroscopic analytical methods. The findings and research contributions of this work are expected to provide a systematic guide to design intelligent and efficient textile finishes and lubricants.

We studied boundary lubrication on model surfaces of common textile materials such as polypropylene (PP), polyethylene (PE), and cellulose. Thin films of these polymeric materials were made using the spin-coating method. The friction coefficient of the films was measured via lateral force microscopy (LFM) under three environmental conditions, in air, in water, and in lubricant solutions. The lubricant solution consisted of aqueous solutions of a PEO-PPO-PEO triblock copolymer

commercially known as Pluronic ® surfactants. LFM results indicated that when the lubricant was applied, PP and PE surfaces exhibited lower values of the friction coefficient than those on the cellulose specimen. This behavior was explained on the basis of the lubricant molecular configuration. It was determined that the PEO segment of the triblock copolymers had higher affinity towards the cellulose surface while the PPO segment exhibited a higher tendency to deposit on the PP and PE substrates. These differences in affinity were responsible for the diverse configurations of the triblock copolymer hence their lubrication performance.

Unique molecular structures of the triblock copolymer were proposed including a buoy (PEO)-anchor (PPO)-buoy (PEO) structure on both PP and PE surfaces and an anchor (PEO)-buoy (PPO)-anchor (PEO) structure on cellulose. The improved lubrication performance of the triblock copolymer on the PP and PE surfaces was attributed to the flexibility of the PEO segments extending from the surface while the poor lubrication on the cellulose surface was attributed to the configuration of the PEO segments being anchored to the surface. Two important parameters, critical normal force and adhesion hysteresis, were found to correlate and to predict lubrication performace. High critical normal force and low values of adhesion hysteresis were good predictors of low friction coefficients.

The reported findings are valuable to explain the behavior of finishing additives and lubricants commonly used in textile and fiber processing operations, as well as to relate the morphology of the adsorbed layers to friction and wear phenomena.

BIOGRAPHICAL SKETCH

Yan Li was born in Dexing, Jiangxi Province, People's Republic of China. After 18 years with her family in her small hometown, she went to college in the Department of Polymer Materials Science and Engineering of Donghua University (Shanghai, China) in the fall of 1996. After she graduated with her BS degree in 2000, she went to graduate school in the same field at Donghua. In 2003, she earned her MS degree in Material Scince and Engineering. After she had worked as an application engineer for one year, she went to North Carolina State University (Raleigh, NC, USA) and worked as research assistant for Professor Hinestroza . In January of 2006, she started working towards her Ph.D. degree in Fiber Science at the Department of Fiber Science and Apparel Design of Cornell University (Ithaca, NY, USA). She married Hongyi Liu in 2008.

ACKNOWLEDGMENTS

The writing of a dissertation can be a lonely and isolating experience, yet it is obviously not possible without the personal and practical support of numerous people.

First, I thank my advisor Dr. Juan P. Hinestroza, for his continuous support. Dr. Hinestroza was always there to listen and to give advice. He is responsible for involving me in the project. He taught me how to ask questions and how to better express my ideas. He showed me different ways to approach a research problem and the need to be persistent to accomplish any goal. Without his encouragement and constant guidance, I could not have finished this dissertation.

Special thanks go to our research collaborators at NCSU. I appreciate Dr. Olando Rojas, who is most responsible for helping me complete the work as well as the challenging research that lies behind it. He was always there to share information, discuss experiments and results, and to proofread and mark up my papers and chapters. I am grateful for great partnership with Dr. Junlong Song and Dr. Hongyi Liu (NCSU).

I would like to thank my special committee, Dr. Lynden Archer, Dr. Anil Netravali, and Dr. Brian Kirby for their support and encouragement. Specially, I appreciate the encouragement from Dr. Archer. His help and time made me confident in completing the dissertation.

During the course of this work at Cornell Univesity (2006 – 2009), I was supported by the National Textile Center under grant C05-NS09.

Last but certainly not least, I would like to thank my husband, Dr, Hongyi Liu, for his endless support and love throughout the completion of this degree. I would like to thank my parents, Jiesheng Li and Yizhen Chen, for their help, support, and encouragement during this momentous time in our lives.

TABLE OF CONTENTS

LIST OF FIGURES

CHAPTER 1

CHAPTER 2

CHAPTER 3

CHAPTER 4

LIST OF TABLES

CHAPTER 2

CHAPTER 3

CHAPTER 4

CHAPTER 5

CHAPTER 1

MOTIVATION OF THE WORK

In order to create a sustainable textile industry, improvements in the efficiency and productivity of fiber generation and textile processes are critical. Friction between fibers and other surfaces in contact is one of critical factors in product processability and quality. Lubricants are applied to fibers and yarns to facilitate the processes of spinning, carding, drafting, and weaving. Surface lubricity is important as it allows smooth transfer of fibers and yarns on metallic or ceramic surfaces with minimum abrasion and breakage of the fibers and yarns. Efforts to develop improved lubricants that control friction, minimize wear and abrasion, and reduce fiber breakage are a significant component in supporting sustainable processes.

Several methods have been used to test friction in textiles. The cylindrical guide remains the most common one. [1] In this method, as an initial approximation the fiber can be treated as an inextensible ribbon as shown in Figure 1.

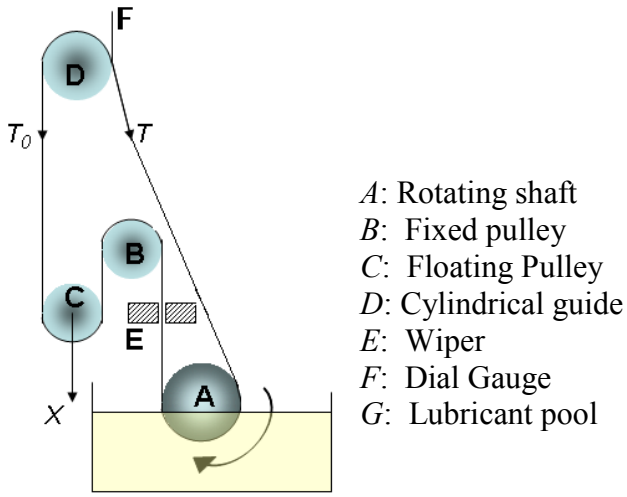

Figure 1. Simple model used in calculation of friction coefficient for a yarn or fiber over a cylindrical guide.

The angle subtended by the fiber over the guide is nearly 180º so the force W, which is

the normal force on the cylindrical guide, is roughly $W = T+T_0$. The resultant force F pulling the fiber around the cylindrical guide is $F = T-T_0$. Therefore, the friction coefficient μ of the system may be deducted as: [1]

$$\mu = \frac{F}{W} = \frac{T - T_0}{T + T_0} \qquad \text{------(1)}$$

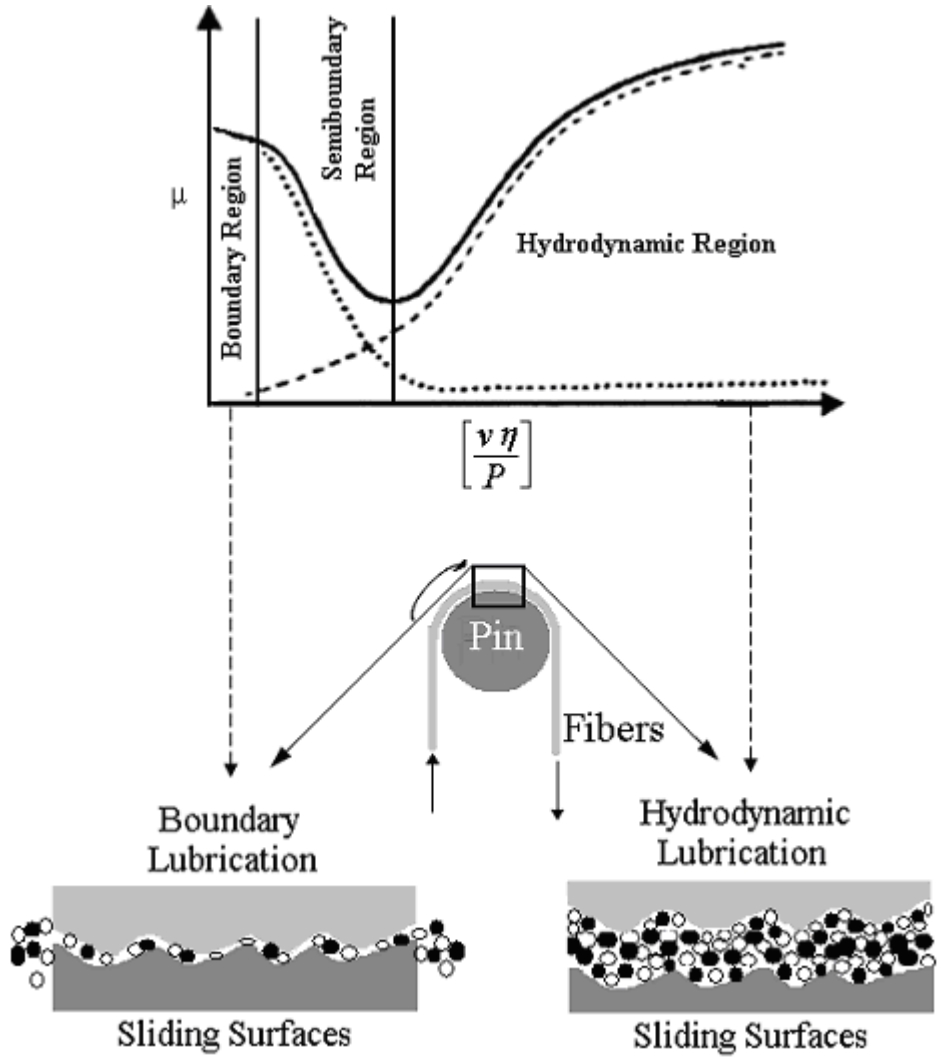

Figure 2. Frictional behaviors of liquid-lubricated textile yarns. Bottom: solid line is experimental curve; dash line is theoretical curve for hydrodynamic friction; dotted line is theoretical curve for boundary friction. The scheme (top) is a micro vision of hydrodynamic and boundary friction on sliding surfaces.

The friction coefficient μ is a dimensionless ratio and must therefore be a function of some other dimensionless parameters. In early studies of friction and lubrication on fibers, process parameters were considered to predict the friction coefficient. Figure 2 gives a common μ vs. $[(v\eta / P)\cdot r]$ curve exhibited by lubricated textiles showing the relationship of processing speed ν, fluid viscosity η, radius of cylinder r, and nominal pressure P to the friction coefficient μ. The solid curve is experimental data. Traditionally this curve is divided into three regimes depending on the gap between the fiber and the sliding surface: boundary lubrication, hydrodynamic lubrication, and semi-hydrodynamic lubrication.

Hydrodynamic lubrication occurs in large interfacial spacing where a continuous and thick fluid film extends between two surfaces at high sliding speeds. Studies on fiber lubrication have focused primarily on hydrodynamic lubrication. [2-5] The hydrodynamic lubrication regime is solely governed by the rheological properties of the lubricant. [6-8] . An empirical equation (see Eq. 2) can be used to predict the friction coefficient in hydrodynamic regime.

$$\mu = k\left((v\eta / P)\cdot r\right)^{1/n} \qquad \textbf{------(2)}$$

Boundary lubrication occurs when a fiber moves over another surface at high contact pressure and low sliding speed. The distance between two sliding surfaces is small, usually in the range of surface roughness. A thin lubricant film is formed in the interface of surfaces. Some key factors in boundary lubrication are (a) the adsorption of lubricants by the fiber surface, [2] (b) the roughness of the surfaces, [7] and (c) the rheological properties of the lubricant. [8] Fort et al. observed that the chemistry of lubricant was critical in boundary friction. Lubricants with polar groups, such as carboxyl groups, significantly reduced friction on synthetic fibers by adsorbing a thin monolayer of lubricant onto the fiber surface. [2] Later, Owsen et al. studied lubrication of the vinylidene chloride-acrylonitrile copolymer thin films using

different lubricants, for example, fatty amides and fatty acids by means of frictional measurements, critical surface tension of wetting, and light microscopy. [9] The authors observed a layer of lubricant formed on surface and the surface coverage by lubricant was dependent of molecular weight. The effectiveness of lubrication decreased as the chain length of the lubricant decreased. Fatty amides were found to more effective in providing lubrication for the polymer systems than fatty acids. It was explained that when the surface of the polymer is completely covered with lubricant, a low energy surface is formed which has low adhesion and consequently a low coefficient of friction. Later, Schick has reported a series of studies on friction and lubrication on synthetic fibers and yarns (eg. polyester, polypropylene, nylon 66, and acrylic). He discussed the effects of fiber luster, guide material, surface charge, and critical surface tension of fibers on friction on synthetic yarns. [10] In this study, friction in the boundary lubrication region increased with the increase in fiber luster,

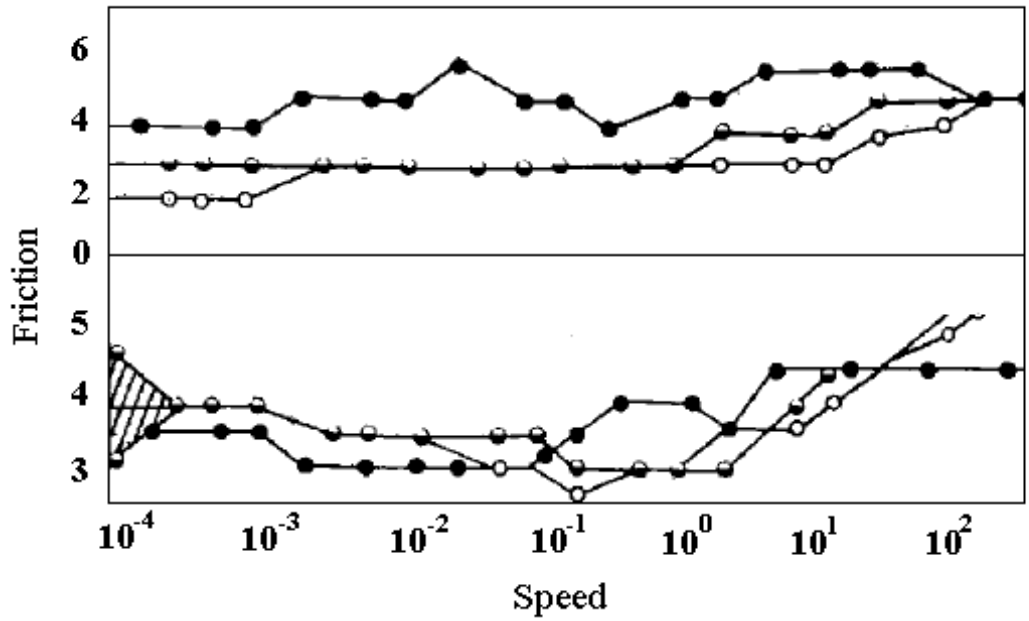

Figure 3. Boundary friction of clean fibers against clean fibers on different substrates. [10]

viscosity in the boundary region, but it was highly dependent on viscosity in the hydrodynamic region. [3, 7, 8]

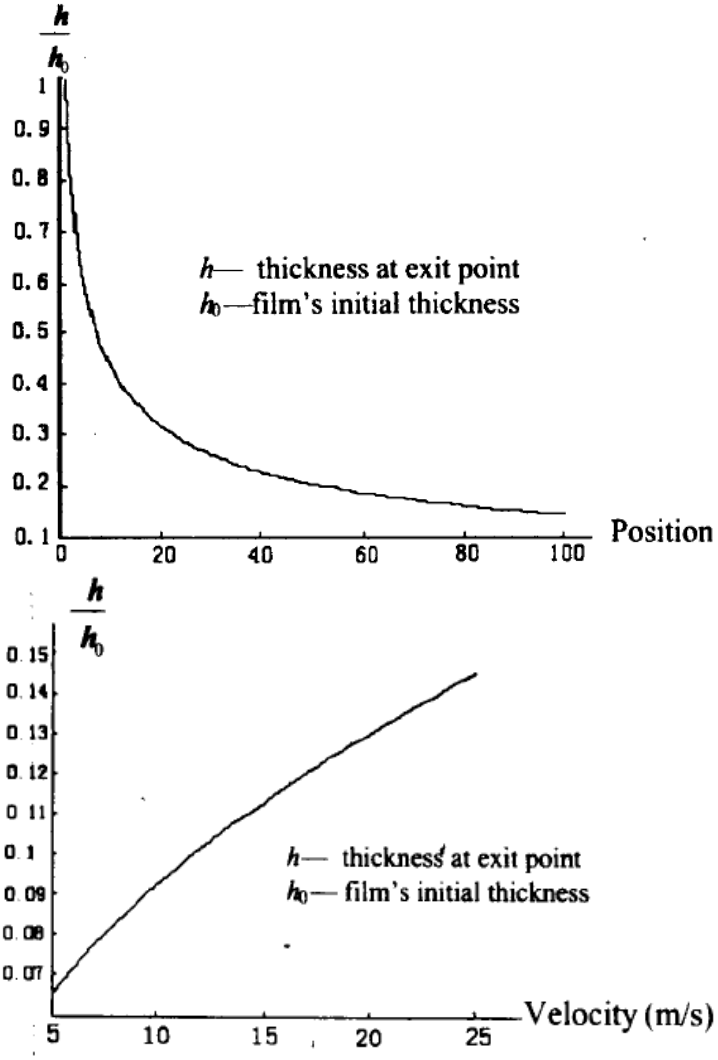

Figure 4. Top: film thickness versus location over the entire friction region (in relative scale). Bottom: relative film thickness versus yarn velocity. [11]

Recently, Lang et al. [11] studied the deformation of the lubricant film on synthetic yarns due to pressure so that the thickness of the lubricant coating decreased. Their theoretical results gave the transition from boundary to hydrodynamic lubrication by showing the changes in the film thickness and friction coefficient (Figure 4). However, all the factors that have been investigated in boundary lubrication were

mostly discussed only qualitatively. [12] No mathematical models have been established to predict boundary friction behavior on fibers, specially regarding to surface chemistry. As far as the author knows, there is no a single equation to model the friction coefficient in boundary regime in terms of adsorption of lubricants and interfacial interaction. Most of the reported has been done macroscopically to investigate and evaluate lubrication systems in terms of friction coefficient which is an industrially relevant parameter for fiber processing. [12] However, little can be found to explain friction phenomena microscopically. We aim at developing a mathematical model in boundary lubrication regime on polymeric fiber surfaces at the molecular scale. The chemistry of the lubricants and fibers will be considered to address the mechanism of boundary lubrication at a molecular scale. The overall objective is to explore friction at the molecular scale and potentially establish a theory, which is able to predict boundary lubrication behavior in fiber processes.

.

REFERENCE

1. Buckle, H. and J. Pollitt, *Shirley Instrument Measurement.* J. Text. Inst.,, 1948. **39**: p. T199-210.

2. Fort, T.J. and J.S. Olsen, *Boundary Friction of Textile Yarns.* Textile Research Journal, 1961. **31**: p. 1007-1011.

3. Schick, M.J., *Friction and Lubrication of Synthetic Fibers: Part II : Two-Component Systems* Textile Research Journal, 1973. **43**(4): p. 198-204.

4. Schick, M.J., *Friction and Lubrication of Synthetic Fibers Part VII: Effect of Guide Temperature'* Textile Research Journal, 1980. **50**(11): p. 675-681.

5. Schlatter, C. and H.J. Demas, *Friction studies on caprolan1 filament yarn.* Textile Research Journal, 1962. **32**(2): p. 87-98.

6. Hansen, W.W. and D. Tabor, *Role of Hydrodynamic Lubrication in the Friction of Fibers and Yarns.* Journal of Applied Physics, 1956. **27**: p. 1558--1559.

7. Schick, M.J., *Friction and Lubrication of Synthetic Fibers Part I: Effect of Guide Surface Roughness and Speed on Fiber Friction* Textile Research Journal, 1973. **43**(2): p. 103-109.

8. Schick, M.J., *Friction and Lubrication of Synthetic Fibers Part IV: Effect of Fiber Material and Lubricant Viscosity and Concentration* Textile Research Journal, 1973. **43**(6): p. 342-347.

9. Owens, D.K., *Friction of polymer films. I. Lubrication.* Journal of Applied Polymer Science, 1964. **8**(3): p. 1465-1475.

10. Schick, M.J., *Friction and Lubrication of Synthetic Fibers Part V : Effect of Fiber Luster, Guide Material, Charge, and Critical Surface Tension of Fibers on Fiber Friction* Textile Research Journal, 1974. **44**(10).

11. Lang, J., S. Zhu, and N. Pan, *Frictional Behavior of Synthetic Yarns During Processing.* Textile Research Journal, 2003. **73**(12): p. 1071-1078.

12. Gupta, B.S., *Friction in textile materials*, ed. B.S. Gupta. 2008, Cambridge, England: Woodhead Publishing Limited.

CHAPTER 2

EXPLORING THE FEASIBILITY OF LATERAL FORCE MICROSCOPY TO PROBE LUBRICATION PHENOMENA IN TEXTILE MATERIALS

1. Introduction

A major part of friction in textiles, given a finish, is governed by the boundary lubrication phenomena. This includes friction during processing of fibers into yarns and fabrics, conversion of fabrics into products, and day to day handling of textiles by consumers. The lubrication phenomenon is considered boundary because the finish applied is usually quite low (~0.1 %) and, in most applications, the speed involved is also small. In this type of lubrication, the finish, ideally a monolayer in thickness, is not considered to totally mask the morphology and the chemical potential of a fiber surface, but to modify them. The chemical interaction involved during a friction process is considered to be at the molecular level. Accordingly, in order to fully understand the boundary lubrication phenomena and determine the role of a finish composition, the interaction between finish and fiber surface must be explored at this level.

The availability of lateral force microscopy (LFM) has made it possible to explore friction and wear at the molecular level and to examine the effectiveness of a finishing treatment in modifying a specific behavior of the textile substrate. The technique is based on scanning probe microscopy, and is one of the few experimental methods capable of assessing forces at the single contact or atomic level.

Chapter 1 is essentially a book chapter published as: "Boundary Lubrication phenomena in coated textile surfaces" by Yan Li and Juan Hinestroza, in "*Friction in Textile Materials*", Woodhead Publishing Limited and CRC Press LLC, 2008, ISBN 978-1-85573-920-8

In this paper, we start out by providing an introduction to the LFM technique, the principle by which it works, the calibration aspects of the forces measured, and the friction phenomenon assessed by it at the atomic level. In the next section, friction and lubrication phenomena are discussed from a molecular perspective and relationships between lubrication performance and lubricant's properties such as its molecular weight, chain configuration, chemical composition, and viscoelastic properties are established. This is followed by a description of the chemical structures and properties of lubricants frequently used in textile processing. Finally, boundary lubrication phenomena is addressed by presenting observations of self-assembled molecular structures over polymeric substrates and describing how these assemblies do influence the friction behavior of the coated surfaces. It is visualized that the discoveries in the field of boundary lubrication will continue with further research and advancement in instrumentation. A fuller understanding of the behavior at molecular level is expected to enable the industry in developing new and better finishing treatments.

2. Lateral force microscopy

2.1 Background

In 1986, the atomic forces between a tip and a sample's surface were measured by Binning *et al* using the first atomic force microscope [1]. One year later, Mate *et al* observed that the atomic structure of a surface manifests itself directly in the frictional properties of the interface [2]. This observation led to the development of the lateral force microscopy (LFM) technique. This technique, also known as friction force microscopy (FFM), translates the lateral force acting on a sliding tip to the frictional properties of the surface. The tips used in LFM can be customized so the contact area between the tip and the probed surface is of molecular dimensions. This allows one to probe single asperity contacts and study behavior with nanoscale resolution. When a

lubricant is applied onto a sliding surface, strong interaction forces arise between the molecules. These forces cause particular molecules to aggregate in the interface and to form self-assembled structures. The conformations and behaviors of these aggregates do influence the friction and wear behavior of the coated materials. Recently, the tips used in LFM have also been functionalized by including specific chemical groups, such as -COOH and –OH. Using chemically functionalized tips, the friction behavior could be directly correlated with the lubrication potential of finishes containing these chemical species.

Following its invention, LFM has been used extensively to study molecular lubrication phenomena on hard surfaces, such as mica, silica, and graphite. Studies on polymer surfaces, relevant to textile applications, however, have been limited, primarily due to the fact that polymer surfaces deform easily, which adds complexity to the experiment and to the interpretation of the data.

2.2 Principle involved

When an atomic force microscopy (AFM) tip slides on a surface, it will be deformed both in the vertical and the horizontal directions (Figure 1). The force F_n, which is

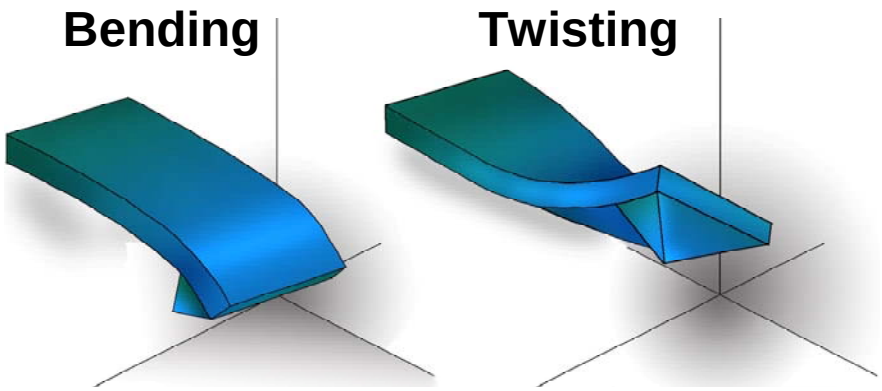

Figure 1. Bending and twisting motions of a rectangular cantilever

normal to the surface of the sample, results in vertical bending of the free end of the cantilever. By contrast, the force F_l, which is parallel to the probed surface and is in the opposite direction to the sliding direction, leads the cantilever into a twisting motion. Both motions, driven by F_n and F_l, are orthogonal and this orthogonality is what enables the simultaneous, yet independent, acquisition of topographic images and lateral force images.

In order to precisely detect the forces between the tip and the surface, a laser beam is reflected off the back of the cantilever onto a quadrant photodiode detector. The output of the quadrant detector is used to determine the degrees of bending and twisting of the cantilever. The laser beam method is the most commonly used monitoring technique as it can achieve a resolution comparable to that of an interferometer while it is also inexpensive and easy to use.

2.3 Calibration, and understanding of friction behavior at atomic level

An accurate quantitative determination of the surface forces is critical for decoupling the LFM signal and obtaining the values of the normal and lateral forces. AFM normal force curves shown in Figure 2 are usually known as force-distance plots. These curves are constructed by monitoring the deflection of an AFM cantilever as its tip. In a force curve, two terms, "steric barrier height" and "steric barrier thickness," are usually defined to interpret the nature of the lubricant layer adsorbed. The steric barrier height is the maximum repulsion force and the steric barrier thickness is the separation distance at a force of 0.2nN. These parameters were initially used by Wang *et al* to study the absorption behavior of silicon and hydrocarbon based lubricants on silica substrates and provided an indication of the lubricity and wear resistance properties of an additive [3].

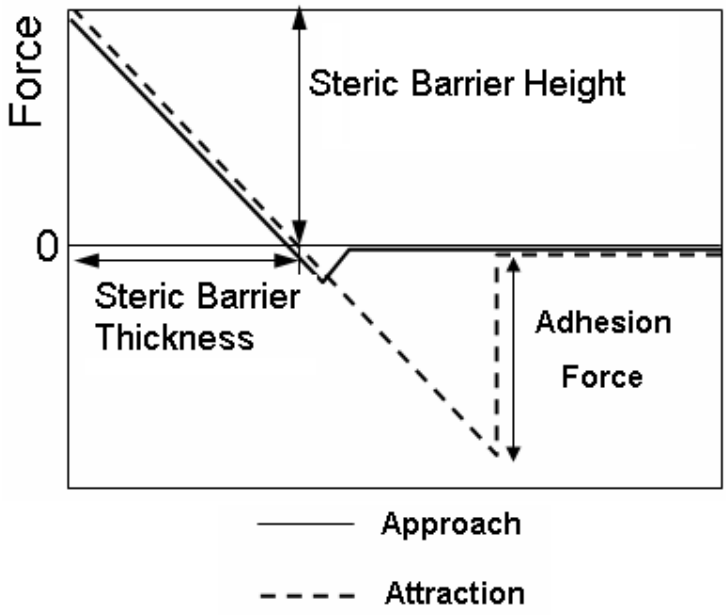

Figure 2. Force curves commonly observed during AFM analysis. The solid line represents the approach curve and the dash line represents the attraction curve.

approaches or retracts from a sample. The movements of approaching and retracting tip are perpendicular to the sample's surface, so the interaction forces measured are indeed normal to the sample's surface.

Figure 3 shows a spring-ball model commonly used to mimic the behavior of the tip-cantilever assembly in an AFM [4]. This simplification is a useful tool to carry out analytical and numerical modeling of the interactions between a tip-cantilever assembly and a sample's surface. The ball represents the tip and a weak spring represents the cantilever used to detect the forces between a sample's surface and the tip. This simple model highlights the central features of AFM as a mechanical sensor for probing interaction forces. The interaction forces between ball and sample depend on many factors, including the tip contact geometry, the tip surface chemistry, and the properties of the sample's surface.

The interaction between ball and surface includes two components: the internal atomic forces between the tip and the surface, and the externally applied force on the

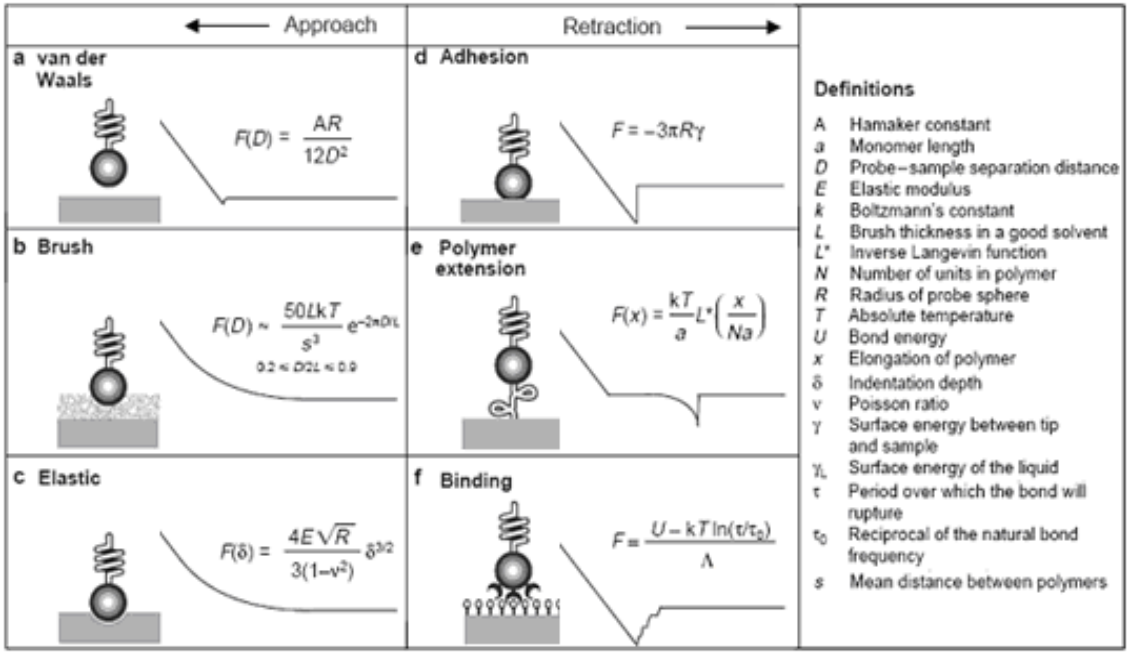

Figure 3. Six types of force curves; (a-c) show approach behavior. (d-f) show retraction behavior. (a): van der Waals (attractive) force; (b): an exponential repulsive force on surface coated with a polymer brush (lubricant); (c): an exponential repulsive force on an elastic surface; (d): a general adhesion force; (e): a retarded adhesion force from an unbroken interlink derived with a polymer extension; (f): multiple adhesion points from multiple unbindings.

spring-ball. The sum of these interactions correlates with the friction behavior of the surface. Therefore, it is essential to know the normal forces in order to study the friction phenomena in LFM**.**

When a tip initially approaches a surface, no interactions between the tip and sample are detected resulting in a flat signal. As the tip-sample distance decreases, short-range forces could be detected. In Figure 3(a), a weak attractive force is explained as van der Waals forces between the molecules of the tip and those of the sample. As the tip gets even closer to the sample's surface, it bends, and the force becomes strongly repulsive. In Figure 3(b), a polymer brush attached to the sample's surface and representing lubricant, depresses as the tip approaches. For a thermally diffused motion of the brush, the entropy of confining these dangling polymer chains results in a repulsive entropic force [5]. In Figure 3(c) the relatively hard tip causes an indent in the elastic sample. The true contact is near the point at which the cantilever begins to deflect [6]. Figures 3(d-f) shows retraction curves. In Figure 3(d), the tip is pulled from the sample and exhibits an adhesion force, which is attractive in nature and it retards the separation between the tip and sample [5]. In Figure 3(e), a polymer chain from the surface is adhered to the tip and stretched until the interlink breaks. The force curve shows a characteristic attraction far from the surface and then a jump back to zero [7-8]. In Figure 3(f), there are multiple adhesion points, so when the tip is moved away, multiple binding points between the tip and the surface's molecules are broken in succession. This is shown by multiple unbinding points in the force curve [9-13]. These details simulate to some extent the frictional forces generated when an asperity on one body slides over the surface of another body.

A force signal obtained by LFM will be the result of the attractive and repulsive forces between the tip and the molecules of the surface as well as the force involved in the tip deforming the surface. These forces shall be decoupled to get a reliable

quantitative measurement of the lateral forces. A number of calibration methods have been developed to interpret the signals. The details of these methods are adequately described in the literature [14-18].

3. Effect of Lubricant's properties on friction behavior observed via LFM

Friction phenomena have been studied on different surfaces via LFM, which discovered a number of effects of lubricant's properties on friction behavior observed via LFM. These findings discussed below help to complement the full understanding of friction and lubrication at a nano scale.

3.1 Molecular weight

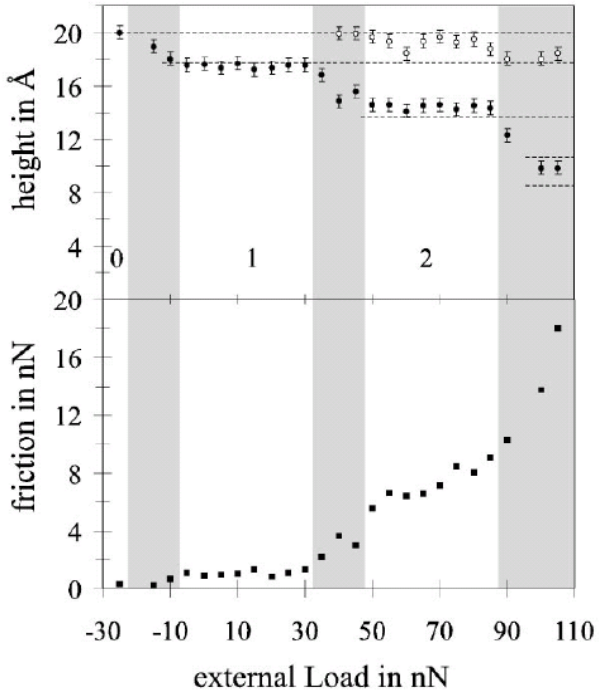

Figure 4. (Bottom) Height of a C12 alkylsilane island vs. load (filled circles). Open circles correspond to the height of the film after the decrease in the load to the lowest practical value for imaging (-25nN). Dashed lines correspond to heights in discrete steps. (Top) A step-like behavior correlated with the height decreases is observed. Transition regions are shaded [19].

Barrena *et al.* [19] studied the friction behavior of alkylsilanols $(CH_3\text{-}(CH_2)_{n-1}\text{-}Si(OH)_3)$ with varying chain length $(n>10)$ using LFM. They observed that the height signal decreased in discrete amounts at critical loads, while the friction signal increased in a stepwise manner which was correlated with the height decreases (Figure 4). Generally, this behavior is assumed to be due to the fact that the upright chains are compressed and they initiate a tilting process under load. The tilting motion is discrete in terms of the packing and the interlocking of the molecules following the zig-zag skeletal structure of the carbon chains. The increase in friction is then consistent with the estimated increase in the activation energy required for the tilting motion.

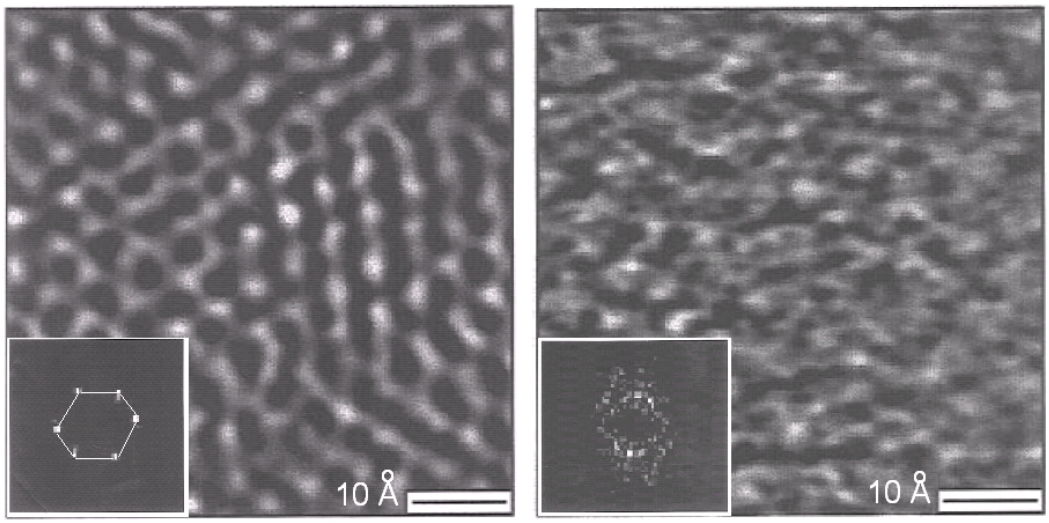

Figure 5. Frictional force images for dodecanethiol C12 on gold and octadecyltriethoxysilane C18 on mica. The corresponding 2D Fourier transform power spectra are shown on the left bottom. Alkanethiol monolayers exhibit a hexagonal ordered structure. Residual short-range order is observed for alkylsilane monolayers [20].

The behavior of shorter chains (n<10) might be distinguished from those of longer ones (n>10) in terms of their mechanical response under load. Lio *et al* [20] discovered that a short chain (n=6) yielded higher adhesion and higher friction forces

for several alkanethiols $(CH_3\text{-}(CH_2)_{n-1}\text{-}SH)$ supported on gold. The initial monolayer may be assumed to be in a close-packed state, so adding more covalent carbon-carbon bonds to the molecular chain provides additional stabilization energy. Therefore, longer chains (n=8, 11, 12, 18) appear to be more stable while maintaining a densely packed configuration. A friction image of a long chain dodecanethiol illustrating hexagonally ordered structures is shown in (Figure 5 left). A disordered structure (not shown) was observed for hexanethiol monolayers (n=6), because a poorly packed structure increased the possibilities of numerous defects and energy dissipation. For long chain alkylsilanes on mica, no long-range order could be detected by the friction image, although residual short-range order was observed (Figure 5 right). A possible explanation for this difference in behavior could be based on the cross-linking of the thiol head groups. In thiols, the disulfide bonds formed between pairs of atoms probably produced a superstructure with C hexagonal periodicity relative to the basic structure. It is important to note that the distance between Si atoms in adjacent molecules forming Si-O-Si bonds (2.5 Å) was larger than their chain radius (2.25 Å). This observation implies the presence of considerable chain distortions near the interface. Although the Si-O-Si networks were observed to form across the surface, the size of their cross-linking network was indeed limited. This behavior was probably at the origin of the lack of long-range order in silane based lubricants.

3.2 Chain configuration

Devaprakasam *et al.* [21] used the LFM technique to characterize the properties of self-assembled perfluorooctyltrichlorosilane (FOTS) and octadecyltrichlorosilane (OTS) monolayers. FOTS has a rigid rod-like helical structure and OTS has a zigzag backbone configuration. Figure 6 illustrates lateral force images of FOTS and OTS self-assembled monlayers on mica. It can be observed that FOTS displays a regular

hexagonal lattice and more symmetrical structures in contrast to OTS, indicating that the helical structures were more ordered than zig-zag backbone molecular configuration.

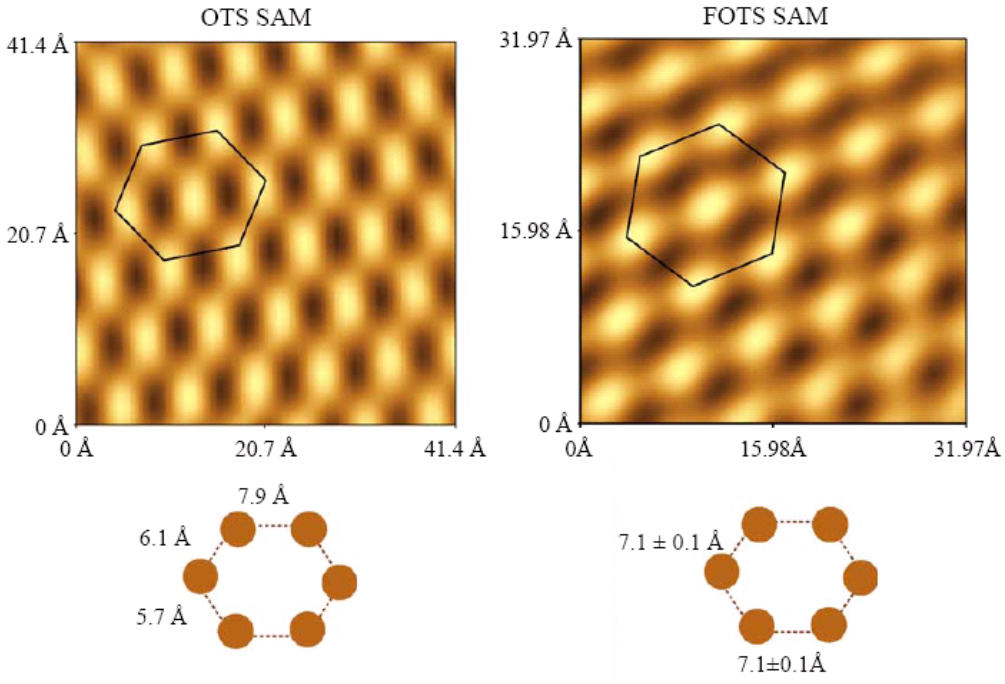

Figure 6. Lateral force images for OTS and FOTS self-assembled monolayers on mica. Both have hexagonal structures. However, there is lack of order in the hexagonal structures of OTS SAM, while FOTS SAM exhibits a regular hexagonal lattice with a lattice constant=7.1±0.1 Å [21].

3.3 Friction anisotropy

Carpick *et al* [22] performed LFM measurements on polydiacetylene coated as monolayer films on mica to correlate the molecular structure of the lubricant with friction anisotropy and friction asymmetry behaviors.

Friction anisotropy refers to the variation of friction relative to the orientation angle between sliding surfaces, or with the sliding direction itself. It was observed that the friction force varied substantially from one domain to the next, but was nearly

uniformly within each domain. Figure 7 illustrates the angular orientational dependence of the friction force, where θ represents the domain orientation measured independently via topographic AFM imaging and polarized fluorescence microscopy. A simple equation, given below, was used to model the angular dependence of friction force:

$$F_f = F_1 + F_2|\sin\theta| \quad (1)$$

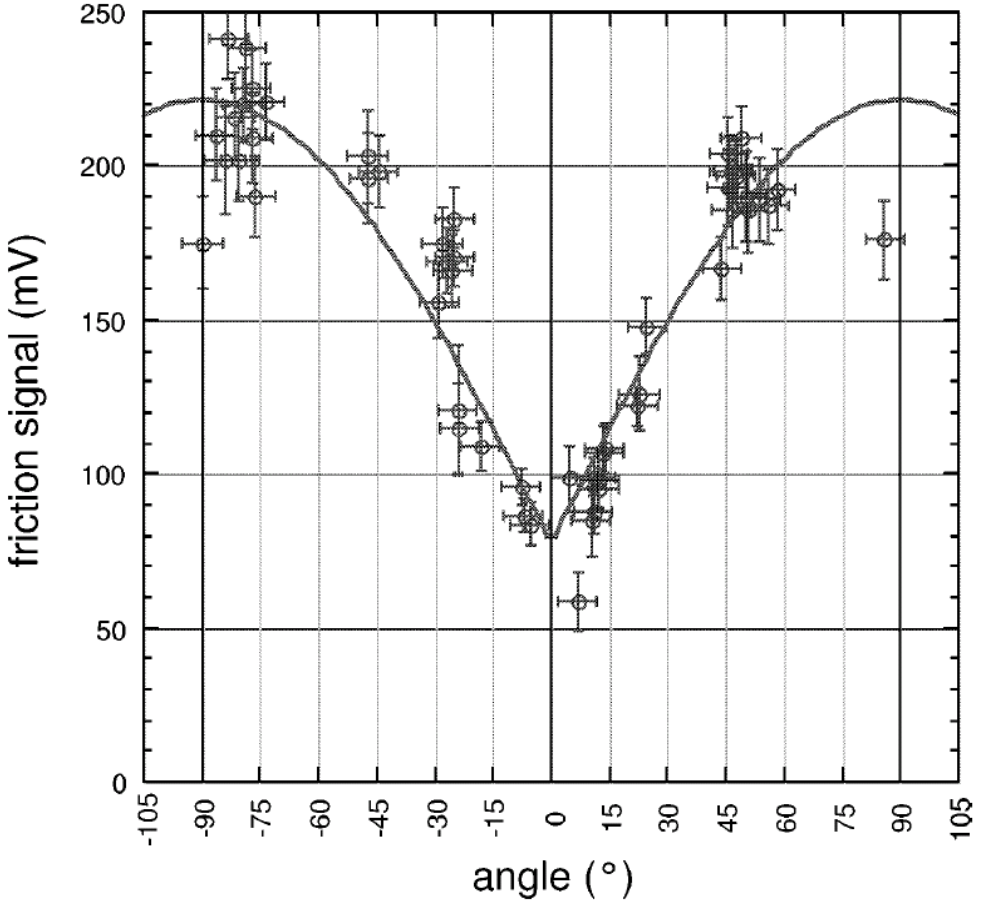

Figure 7. Friction raw signal (relative friction force) vs. orientation angle. The zero degree indicates sliding parallel to the backbone direction. Friction is calculated by taking the difference between forward and backward traverse images on single domains. The standard deviation is used for the friction error bar. The solid line represents the fit of equation (1) to the data [22].

In this equation, F_1 represents the angle-independent contribution to friction and can be thought of as an intrinsic friction force between the tip and the film. F_2 represents an additional contribution to friction that arises when there is a component of sliding motion perpendicular to the polymer backbone direction. It is generally explained that anisotropic packing and/or ordering of the alkyl side chains and the anisotropic stiffness of the polymer backbone itself cause the anisotropic lateral film stiffness, hence resulting in anisotropic friction.

3.4 Friction asymmetry

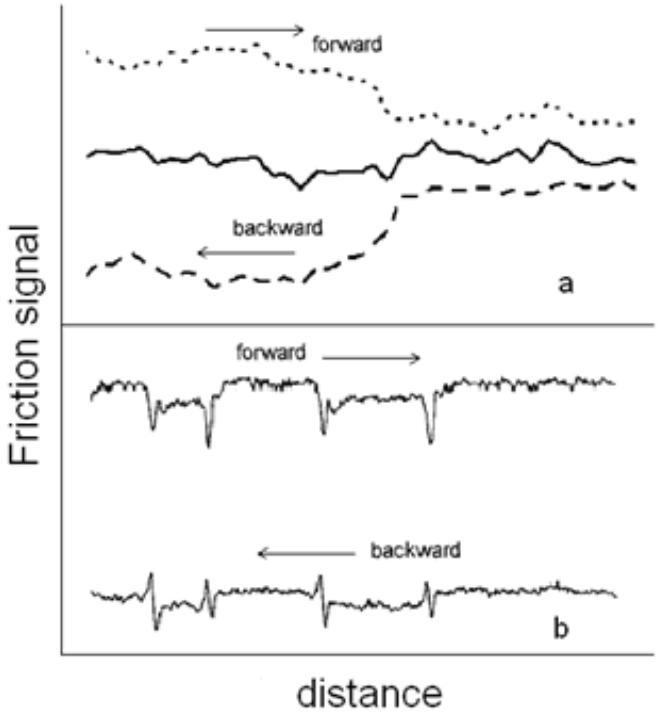

Figure 8. Friction vs. distance in a friction loop. In (a) there is no observable friction asymmetry on domains in Carpick's experiments. In contrast, (b) shows this effect in Bluhm's LFM testings.

Friction asymmetry refers to a change in friction behavior when the sliding direction is flipped by 180°. This effect is possibly induced by molecular groups that tilt from the surface's normal direction. This phenomenon was not clearly observed with a

polydiacetylene monolayer film in Figure 8(a), probably because the spatial fluctuations of the friction forces may have obscured the effect. However, Bluhm *et al* [23] observed friction asymmetry with a ferroelectric triglycine sulfate *(TGS)* (Figure 8(b)). The friction contrast occurred not only between domains with different orientation, but also inside the domains. It was proposed that the crystallography of *TGS*, which features asymmetric molecular arrangement on the surface, caused an asymmetric surface potential detected by the tip.

3.5 Superlubricity

A superlubricity phenomenon was firstly observed by Hirano *et al* [24] when a monocrystalline tungsten tip slid on a *Si* (001) surface. This phenomenon was explained on the basis that the sliding direction of the tip was parallel with the orientation of molecules on the surface. Lateral force microscopy techniques are appropriate for these types of measurements as LFM could magnify molecular anisotropy and asymmetry detecting super-lubricity behavior [25-27].

3.6 Chemical composition

The work by Overney *et al.* [28] using LFM confirmed that friction and elasticity measurements were indeed correlated. A monolayer composed of a mixture of hydrocarbon acid and fluorocarbon acid was examined simultaneously for the local elastic compliance and lateral forces. An island-sea structure was noted in both elasticity and friction images. The hydrocarbon island-like domains with the higher elastic modulus and lower friction were found to be surrounded by the fluorocarbon sea-like areas exhibiting lower elastic modulus and higher friction.

Energy dissipation at the molecular level was examined by Burns *et al* [29-30] on alkanethiol monolayers with *–COOH* and *–CH_3* end groups. They found that under identical experimental conditions, the friction forces of monolayers containing the –

COOH groups were higher than those containing the *–CH₃* groups. A significant fraction of the thiol–*COOH* chains that attached to the substrate with a 30° tilt appeared to have contacted the tip [31]. The molecules seemed to stand up with one end anchoring to the surface and the other end interacting with the tip (Figure 9). For the thiol–*CH₃* chains, a similar tilting arrangement possibly occurred since they have similar backbone molecular chains. However, the effective number of standing thiol–*CH₃* chains is not significant enough to prevent the tip from moving under relatively smaller forces. This behavior is likely caused by the relatively weak atomic interaction forces between the tip and the thiol–*CH₃* chains.

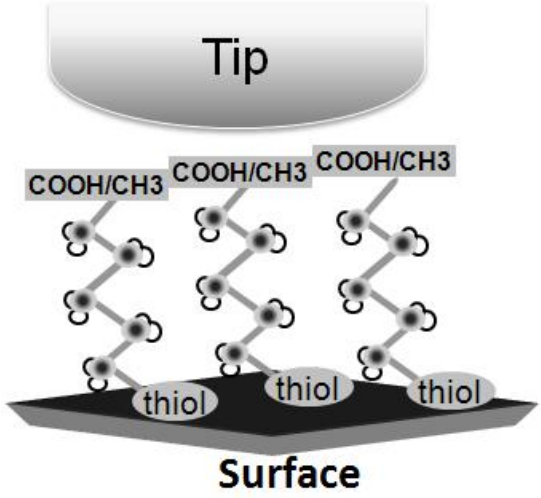

Figure 9. A scheme (not to scale) of a tip interacting with self-assembled head-tail molecular chains that are anchored to a surface. In every chain, the end with the thiol groups is attached on the surface, while the other with the –COOH/-CH_3 groups interacts with the tip.

3.7 Visco-elastic properties

Early in the 18th century, it was determined that if two surfaces adhere to each other, a finite friction force can arise even in the absence of any externally applied load. This effective additional force is due to the molecular attraction between the two surfaces.

Therefore, the general friction force might be composed of two parts. One is a constant force due to adhesion and the other is a force determined by the friction coefficient and is due to the externally applied load [32-33]. However, a general relationship between adhesion and friction forces is not established, although in specific situations they may be correlated [34-35].

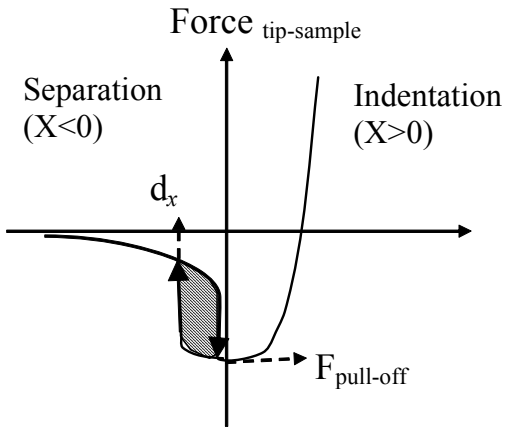

Figure 10. Theoretical force-distance curve presents the total interactions between a tip and a sample during indentation (x<0) or separation (x>0). The adhesion hysteresis (dotted area) is approximated by the product of critical separation δ_x and adhesion forces $F_{pull-off}$.

Yoshizawa *et al* [36] used a conventional surface force apparatus to study friction and adhesion in surfactant monolayers between two mica surfaces. They noticed that the adhesion property, which qualitatively correlates with the friction force, might be more likely given by adhesion hysteresis than adhesion force itself. The term adhesion hysteresis characterizes the energy dissipation when two surfaces approach and then retract from each other. In other words, it is the difference between the energy necessary for separating two surfaces and that restored when the surfaces are brought back together. The dissipated energy in adhesion hysteresis is calculated as the area of a closed loop during an approaching-retracting cycle (Figure 10).

In order to clarify the correlation between adhesion hysteresis and friction force, the monolayers were classified into three categories: solid-like, liquid-like, and amorphous [37]. The classification was based on the difference between the testing temperature T and the material melting point T_m. A surfactant monolayer of dihexadecyl dimethyl ammonium acetate (DHDAA) was studied in dry air in the temperature range 15~35 °C.

Table 1. Friction and adhesion hysteresis of dihexadecyl dimethyl ammonium acetate (DHDAA) monolayers on mica at the temperatures: $T<T_m$, $T \approx T_m$, and $T> T_m$

Temperature (℃)	Status	Friction coefficient	Adhesion hysteresis
15	Solid like	Low	Low
25	Amorphous	High	High
35	Liquid like	Low	Low

Table 11.1 shows that the friction force and adhesion increased and then decreased, with a maximum value being attained at 20~25 °C. It was found in the literature that the melting temperature of DHDAA may be expected to be somewhere between 20~40 °C [38]. If $T < T_m$, a monolayer might be considered to be in a solid-like state. During an approaching-retracting cycle or a back-forth sliding, there is little interdigitation of the chains or rearrangements of the surface molecular groups. The adhesion hysteresis and friction force are both small because the surfaces do not deform significantly.

At $T \approx T_m$, the monolayer chains become more flexible and mobile, but still are not in a truly melted or liquid-like state. This is the amorphous regime. As two surfaces come into contact or slide past each other, there is now significant interdigitation of the chains across the interface, as well as local rearrangements or reorientation of surface molecular groups [39-40]. This interdigitation enhances the effective number of molecular contacts or “bonds” across the interface and results in an increased adhesion hysteresis as the surfaces have to break more bonds on separating than are

recovered when coming into contact. Similarly, the friction force is relatively high, because a small degree of interpenetration causes a great increase in friction force. Analogous trends were observed in the profile of friction force between bulk polymer and rubber surfaces at temperatures close to their glass transition temperature [23].

At $T > T_m$, the interlocks among chains break down and the monolayer becomes truly liquid-like. The surface layer now behaves like a liquid so that while interdigitation readily occurs as soon as two surfaces come into contact, they can relax or disentangle just as rapidly and easily so that the system is always at equilibrium. There is therefore no adhesion hysteresis, just as one finds for a liquid surface where the surface tension is the same on expansion or contraction. For similar reasons, the friction force is expected to be low.

Furthermore, Marti *et al* [41] applied the Johnson-Kendal-Roberts *(JKR)* model [42-43] and calculated the dissipated energy in the interface between a silicon nitride tip and an oxidized silicon surface under aqueous electrolyte solutions. It was shown that a linear relationship between friction force and adhesion hysteresis existed. The relationship was built upon the dissipated energy in the system. The authors also found that the dissipated energy was a function of the pH of the solution hence implying that improved LFM resolution can be achieved by adjusting the electrolytic nature of the solution.

4. Textile lubricants

In general, textile lubricants are a mixture of formulated compounds rather than a single component. The use of mixtures allows the optimization of the lubricity performance as well as minimizing the cost. Low molecular weight polymers have a natural affinity for textile fibers. In most cases, these polymers create self-assembled molecular structures on a fiber's surface. These polymers are fluids at process temperatures, and associatively slide with the fiber surface during the friction process.

High molecular weight polymers are usually formulated as additives, which significantly reduce abrasion and wear to fibers. This is particularly important in dynamic and high-speed operations. Waxes, such as hydrocarbons, polyethylene, and amides, are traditional boundary lubricants that function in both the low-speed (fiber to fiber) and the high-speed (fiber to metal, or fiber to ceramic) processes. Waxes tend to act as solid layers on the fiber's surface enhancing its lubricity. Silicon oils are also commonly chosen as lubricants for their low viscosity, low volatility, and good affinity for most textile fibers. All lubricants are usually applied to textile materials with other finishing agents to assist in processing. The lubricants most generally used in the textiles are fatty acids, mineral oils, as well as synthetic compounds, such as the ethoxylated alcohols, the ethoexylated acids, and the silicone oils. Table 11.2 lists their chemical structures, properties, and common applications in textile processing.

A fatty acid is a carboxylic acid, often coupled to a long unbranched aliphatic chain (C4~C22), which can be either saturated or unsaturated. There are only carbon and hydrogen atoms in each molecule, except for the carboxylic acid group at the end. The unbranched aliphatic chain can be easily packed together tightly due to a linear structure. This characteristic allows fatty acid molecules to form self-assembled structures in some situations. Fatty acids and their derivatives can function as effective lubricants in many applications. Erucoy glycolates are usually found as lubricants for cotton yarn [44]. A patent reported that diesters of glycolic acid are also effective as yarn lubricants, which additionally inhibit the growth of bacteria and fungi on the material [45].

Mineral oil is often used in a number of applications for its relatively low cost. Solvent-refined mineral oil is found in a commercial textile lubricant blend, which also contain methyl oleate and solvent-refined peanut oil [46]. Mixture of low

Table 2. Characteristics and properties of frequently used chemicals in textile lubrications

Lubricant			Chemical structure	characteristics	Textile lubricant application
Fatty acids	Saturated		CH3(CH2)nCOOH , n: 2~20	Easily packing of molecules on an interface;	Cotton yarn lubricant
	Unsaturated		CH3(CH2)n(CH=CHCH2)q(CH2)mCOOH, n: 1, 2, 3, 4, 5, 7; m: 2, 6, 10; q:1 ~ 4		
Mineral oils			CH3(CH2)nCH3, n:13~38	Low viscosity; Low cost; Large production;	Base component; Fiber lubricant
Synthetic lubricants	Polyalkylene glycols		RO(EO)m(PO)n(EO)mH RO(PO)m′(EO)n′(PO)m′H EO: -CH2CHO-; PO: -CH2CO(CH3)- R: alkyl; m/m′≥0; n/n′≥0;	Affinity to synthetic fibers; Self-assembled structures formation; Resistance to bacteria and contaminants	Spin finish for synthetic fibers lubricant
	Silicon oils	Polydimethyl -siloxane	CH3[SiO(CH3)2]nSi(CH3)3	Molecular orientation on fibers; softness;	Lubricant additives; Fabric Softener;
		Silicon polyether	-(EO)m(PO)n[SiO(CH3)2](PO)n(EO)m- EO: -CH2CHO-; PO:-CH2CO(CH3)- m ≥ 0; n ≥ 0;		

viscosity shear reducing mineral oil and high molecular weight oil-soluble polymers has been also reported as a fiber lubricant [47].

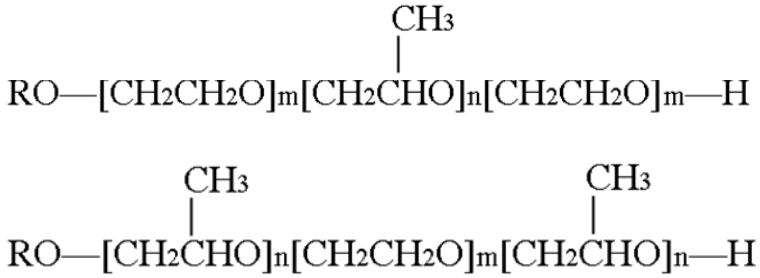

Figure 11. Commercial polyglycol triblock copolymers with alkyl end groups R

Since 1950's synthetic lubricants have become competitive enough, in cost and functionality, to be selected for textile applications. For example, the polyglycols, high molecular weight polymers of ethylene or propylene oxide, are currently available in a wide range of viscosities. The chemical structures for a polyglycol are shown in Figure 11. Polyglycols have high flash points, good viscosity-temperature properties,

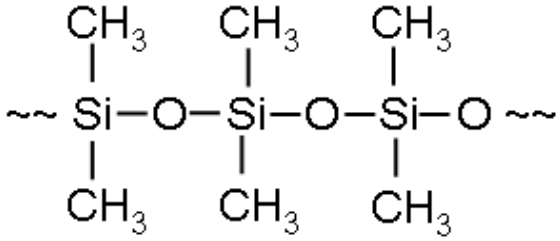

Polydimethylsiloxane (PDMS)

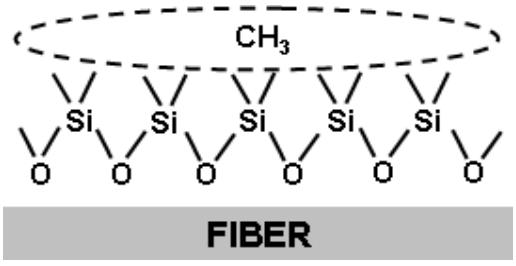

Figure 12. PDMS molecules orientation on a fiber surface provides the lubricity and softness to the fibers

low wax-free pour points, and acceptable shear stability. Water-soluble polyglycols are used primarily as base lubricants for spin finishing of textured fibers, which also can reduce fire hazards in processing and improve oxidation resistance [48]. Polyglycols and other similar compounds, such as ethylene glycols and propylene glycols, have been commercialized as effective textile processing lubricants.

Silicon oils are silicon analogues of carbon based organic compounds, which can form relatively long and complex molecules based on silicon rather than carbon atoms. The most common silicon oil is polydimethylsiloxane (PDMS), which is exclusively used as an additive in the textile lubricant market. A model of this molecule is shown in Figure 12 with the orientation of the PDMS molecules on a fiber surface. PDMS has oxygen atoms that attach to the polymeric fiber surfaces while the methyl groups orient away from the surfaces. The methyl groups are known to reduce friction and enhance abrasion resistance.

5. Current LFM observations of boundary lubrication phenomena in textiles

5.1 materials and methods

Recently, Li and Hinestroza (the authors) initiated lateral force microscopy research work on the lubrication phenomena for three polymers commonly spun into fibers by the textile industry: cellulose, polyethylene, and polypropylene. The purpose of this work was aimed at studying boundary lubrication behavior. Model surfaces of these polymers were created using traditional spin-coating techniques [3,15,49-51]. These specimens were immersed in a liquid cell and studied using LFM. The LFM method allowed the manipulation of a micro-lubrication system at a molecular scale due to the micro dimensions of the contact between the tip and a surface**.** The lubricants chosen in this particular study were Pluronic products manufactured by *BASF* and one commercial product *(LN363-100I)* manufactured by Goulston Technologies Inc.

Pluronic lubricants, commonly used in textile topical treatment formulations, are composed of *ABA* triblock copolymers consisting of polyoxyethylene *(PEO)* as the *A* block and polyoxypropylene *(PPO)* as the *B* block. It has been reported that these molecules can absorb on a hydrophobic surface with the more hydrophobic *PPO* block anchoring on the surface and the *PEO* block extending into the surfactant solution as tail [52-54]. The commercial lubricant *LN363-100I* has been reported to be a mixture of standard polypropylene finishes and silicone surfactants although the exact chemical nature of LN363-100I remains proprietary. This mixture is water-dispersible and can be applied at concentrations below and above the critical micelle concentration (*cmc*) of 0.01%.

5.2 Self-assembled molecular structures and micellization

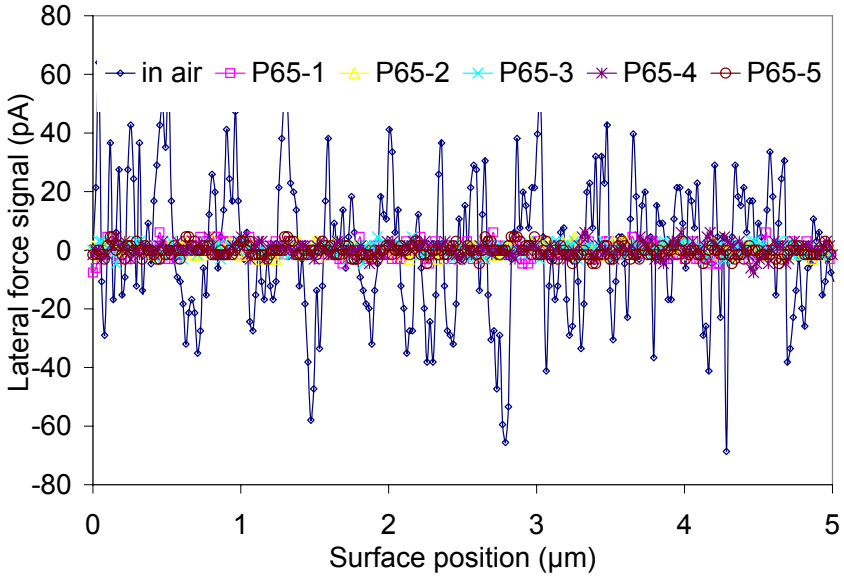

Figure 13. One line scanning profiles for the cellulose coated surface both in the Pluronic lubricant P65 solutions and in air. P65-1~P65-5 represent a series of ethanol solutions with the increase of ethanol concentration. The lateral forces in air are substantially larger than those in lubricant solutions. The force profiles in the five solutions are similar, without difference in amplitude.

When a tip in lateral force microscopy is sliding on a surface, lateral force profiles can be measured both in air (no lubricant applied) and in solution. Figure 13 shows lateral force profiles for a cellulose surface imaged in air and while immersed in Pluronic lubricant P65 solutions. During these experiments, the lubricant was dissolved in ethanol aqueous solutions at various levels of ethanol concentration (22%, 38%, 52%, 66%, and 87%). It is observed that the friction forces measured in air are significantly larger than those in P65 solutions, confirming the lubrication characteristics of P65. However, the force profiles in the five solutions are undistinguishable, making the effect of ethanol concentration unimportant.

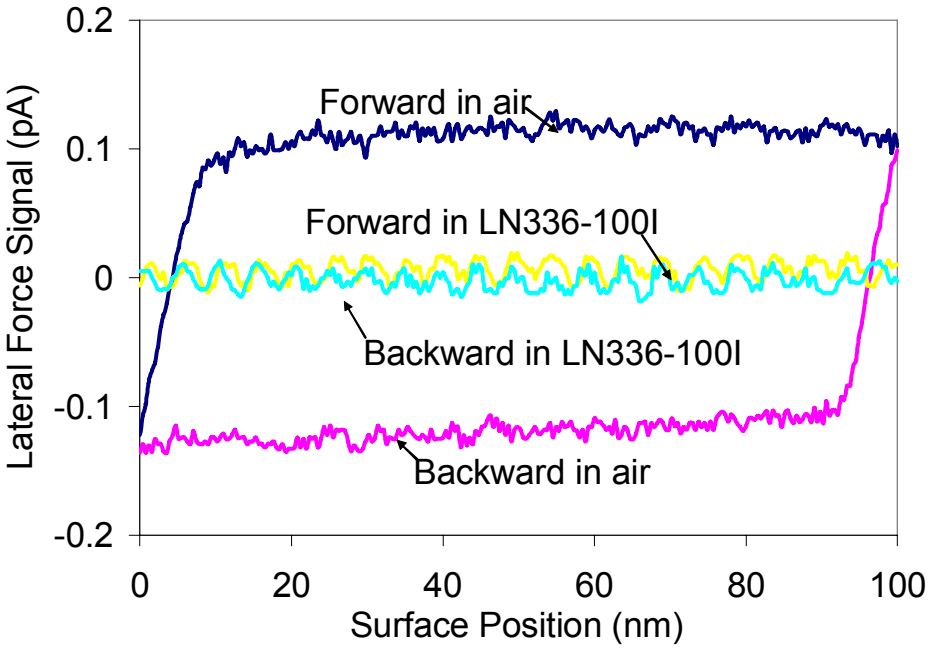

Figure 14. One line scanning profiles (backward and forward) of a PE surface imaged in air and while immersed in commercial lubricant LN336-100I. The lateral forces from the sample immersed in lubricant solution wee smaller than that tested in air.

Figure 14 displays a line scan across a polyethylene surface tested both in air and in the commercial lubricant solution. A static friction force is seen in Figure 14. It is

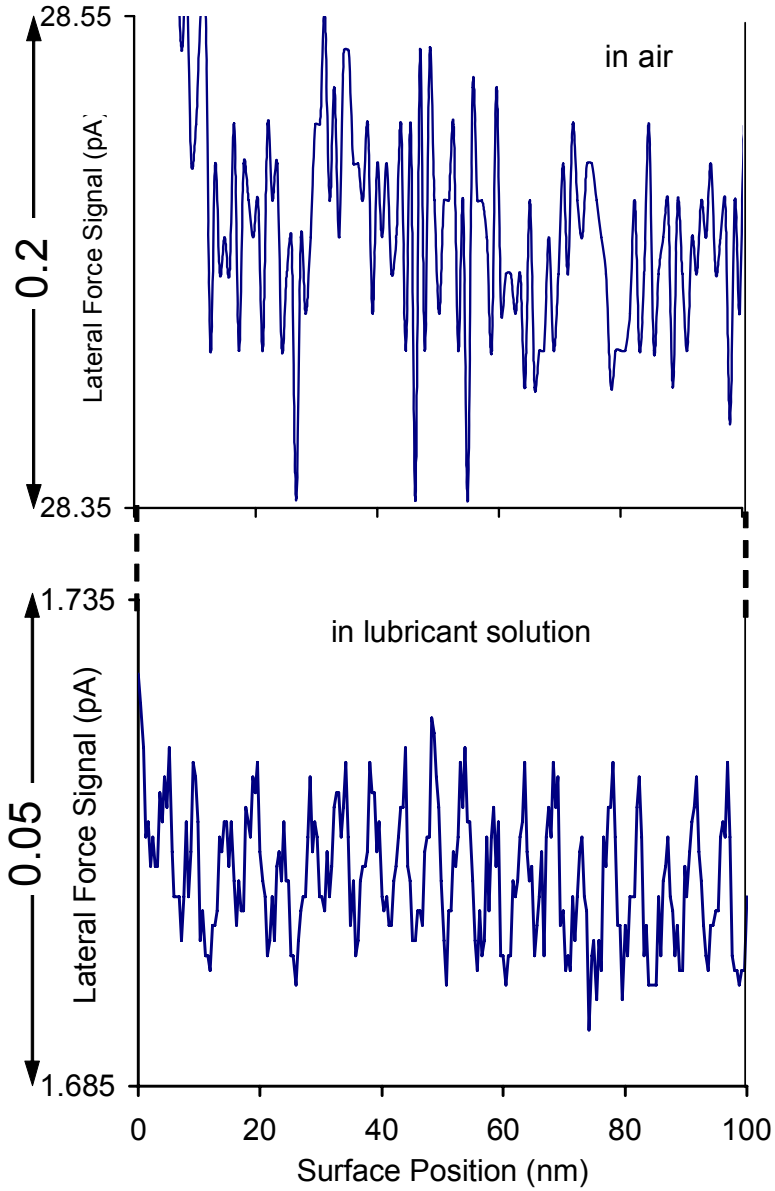

Figure 15. Magnified views of the lateral force profiles on the PE surface both in air and in lubricant solution. The fluctuation of the curve in air is larger and more random than that in lubricant solution. The distance between two neighboring peaks on the force curve in lubricant solution is approximately constant.

known that when a tip starts to move forward on a sample's surface, there is a static friction force on the tip [15,55]. The static friction force was evident in the force

profile imaged in air during the forward and the backward scanning. However, when the tip was sliding on a surface coated with the lubricant solution, the high force corresponding to the static friction disappeared and it was replaced by a regularly oscillating force curve. As expected, and seen in Figure 15, the amplitude of force curve in the solution was smaller than that in the air. The distance between two neighboring peaks in solution was regular and approximately *4.7nm*. These regular peaks possibly indicate that lubricant molecules were aligned along PE surface creating regular oscillation in the force profiles. As stated in the previous section, it is possible that these lubricant molecules align themselves in a preferred direction because of secondary molecular interactions in the interface and that these assemblies could influence the friction behavior.

The LFM technique not only reveals the magnitude of the friction forces but also the molecular structure on the surface. As seen in the left image in Figure 16, self-assembled monolayer (SAM) of the commercial lubricant LN336-100I can be observed on the polyethylene surface. The lubricant layer was not conformal but formed round-shape domains that packed with an average radius of 8~10μm. These domains were found to be evenly distributed on the polyethylene surface. This behavior shows that the interaction between the lubricant monolayer and the polymer surface channels the lubricant molecules into the regular domains through molecular aligning/ordering [56-57]. The micelle forming characteristics of pluronic surfactants in the aqueous solutions has attracted much attention academically and commercially. Freeze-fracture transmission electron microscopy is conventionally employed to visualize this micellization behavior. However, AFM scanning using a liquid cell is equally capable of discovering these micelles with almost molecular resolution but significant lower sample-preparation work. The right image in Figure 16 illustrates distinguishably ribbon-like and rod-like features of Pluronic surfactants on cellulose

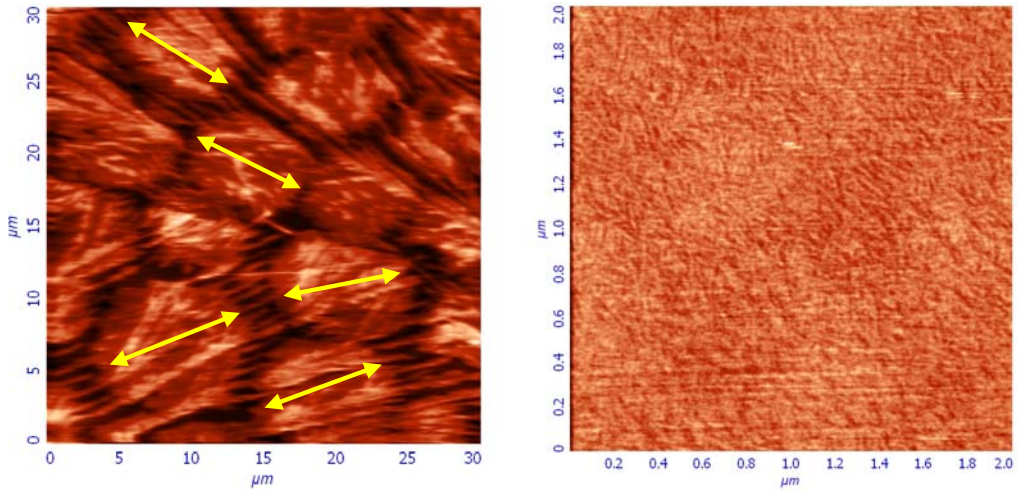

Figure 16. Left: lateral force image of a self-assembled monolayer (SAM) on a PE coated surface. The average radius of the domains are in the range of 8~10μm. Right: lateral force image of a self-assembled monolayer (SAM) on a cellulose coated surface. Ribbon-like structures are seen on the surfaces

surface. It is hypothesized that these self-assembled molecular structures were formed by interaction between the lubricant molecules (P65) with the cellulose surface.

5.3 Hypothesis of molecular structures controlling friction behavior

Figure 17 illustrates the current hypothesis of Li and Hinestroza [58] that particular conformations of lubricants determine friction behavior. In this case, LFM images of cellulose, polyethylene, and polypropylene, surfaces, coated with a commercial lubricant, are presented. The second level of Figure 17 illustrates the conceived conformations of molecular assembled structures and the third level (bottom) shows the friction force curves proposed according to topographical images.

While the samples were coated with the same lubricant, the LFM images obtained are clearly different, highlighting the effect of the three polymer surfaces on the lubricant molecules. On the cellulose surface, the 30μm image may be recognized as a

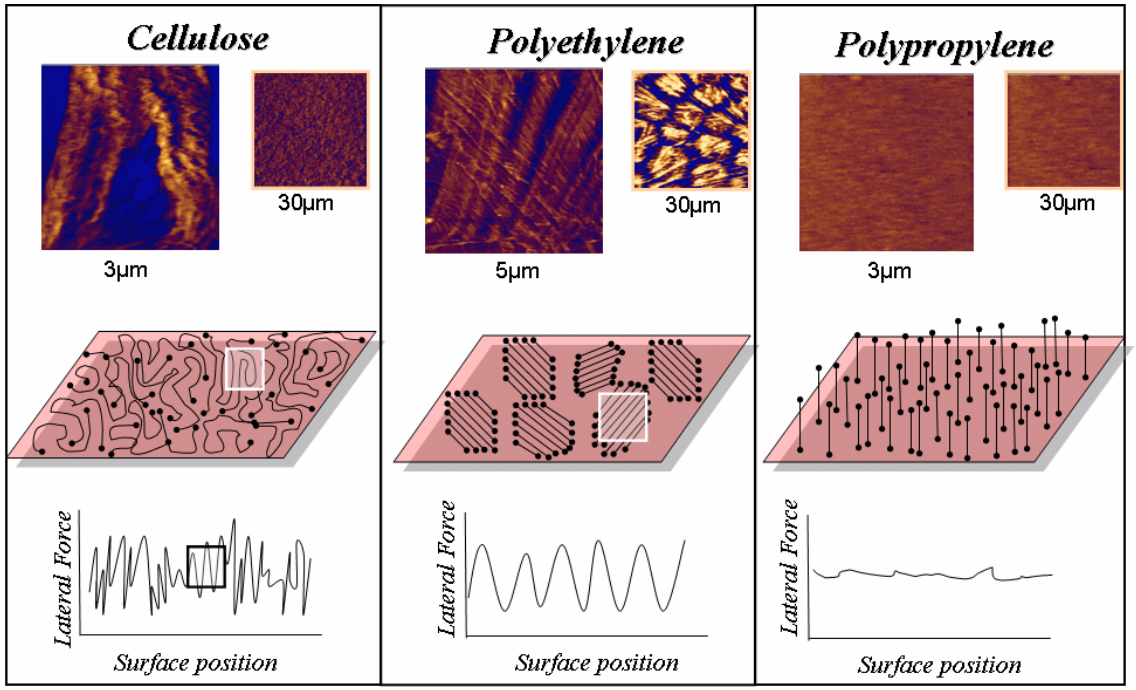

Figure 17. Molecular assembly conformations of the commercial lubricant on cellulose, polyethylene, and polypropylene films. (Top) images: topography; (middle) conformations: self-assembled molecular structures; (bottom) diagrams: friction force curves for a line scanning.

porous-like surface, but the 3μm image reveals local orientation formed by the lubricant molecules. Lubricant molecules appear to randomly lay on the surface without a preferred orientation. The molecular chains may be aligned only in very small local areas, giving short range ordered structures. This arrangement leads to a friction force curve that oscillates randomly.

The molecular conformations of the lubricant molecules on the polyethylene surface indicate the creation of large domains. The friction force therefore has a regular amplitude of oscillation for each domains formed on the surface. For the case in which the polypropylene surface is used, the surface appears uniform and featureless. A standing-up conformation of the molecules is proposed for these lubricant chains, which may be supported vertically on the surface. A thick lubricant layer in term of the chain length may be formed resulting in a relatively flat friction force curve.

These LFM profiles are evidences that the chemistry of polymers and lubricants play a significant role in the lubrication phenomena and it should be explored in depth further.

5.4 Friction coefficients

In a topographical view of a polyethylene surface coated with a commercial lubricant (Figure 18), a bump in the middle of the specimen can be detected. The friction forces on the bump are lower than those on the valley of the samples shown in the lateral force image. This particular bump is created by self-assembled lubricant molecules hence exhibiting low friction.

Another interesting lubrication behavior probed via LFM is illustrated in Figure 19. It is noted that with the increase in normal forces the friction force increases. That is to say: with an increase in pressure, the lubricant layers become thinner and, as expected, lead to an increase in friction. This phenomenon is observed in the cases of both

polyethylene and polypropylene, although the nature of the effects may be somewhat different. The four lubricants used in this experiment were copolymers of polyethylene oxide (EO) and polypropylene oxide (PO).

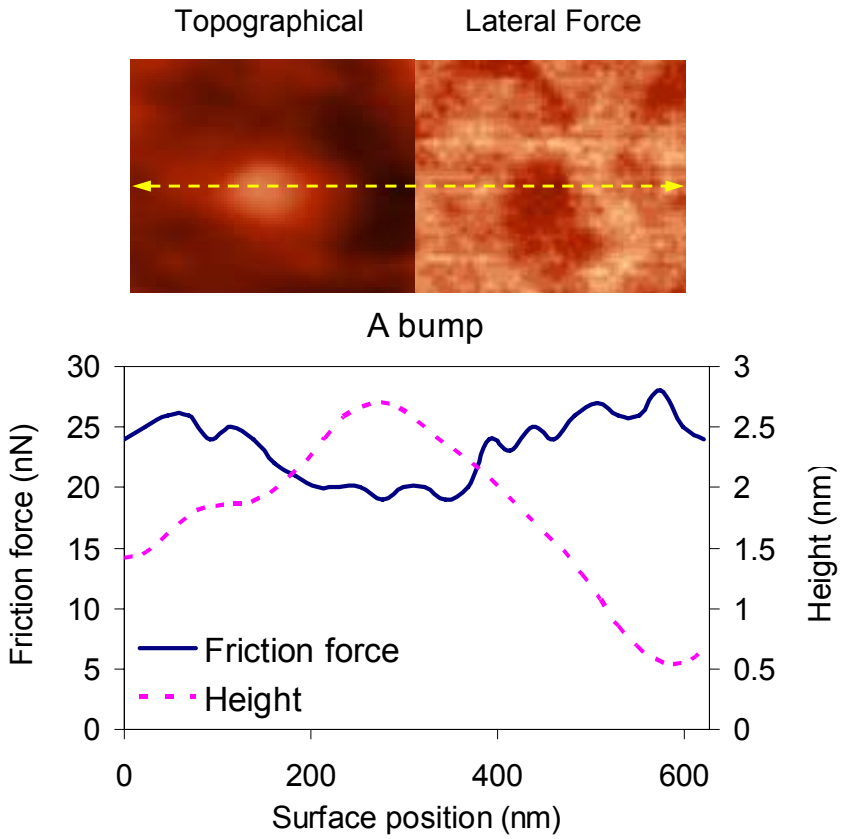

Figure 18. A bump on a polyethylene film (seen in the topographical image) corresponds to lower friction force than the forces represented by the surrounding low areas (seen in lateral force image). The heights (dashed line) and friction forces (solid line) on one cross scanning line (dash line on the images) also show opposite trends.

As an example, EO(133)PO(50)EO(133) molecules (Figure 19) contains 50 repeat units of PO in the middle and 133 repeat units of EO on the both ends. R-PO(10)EO(13) molecules contain another R alkyl groups other than the PO and EO groups. With the EO groups exposed and the PO shielded in all cases, the results show

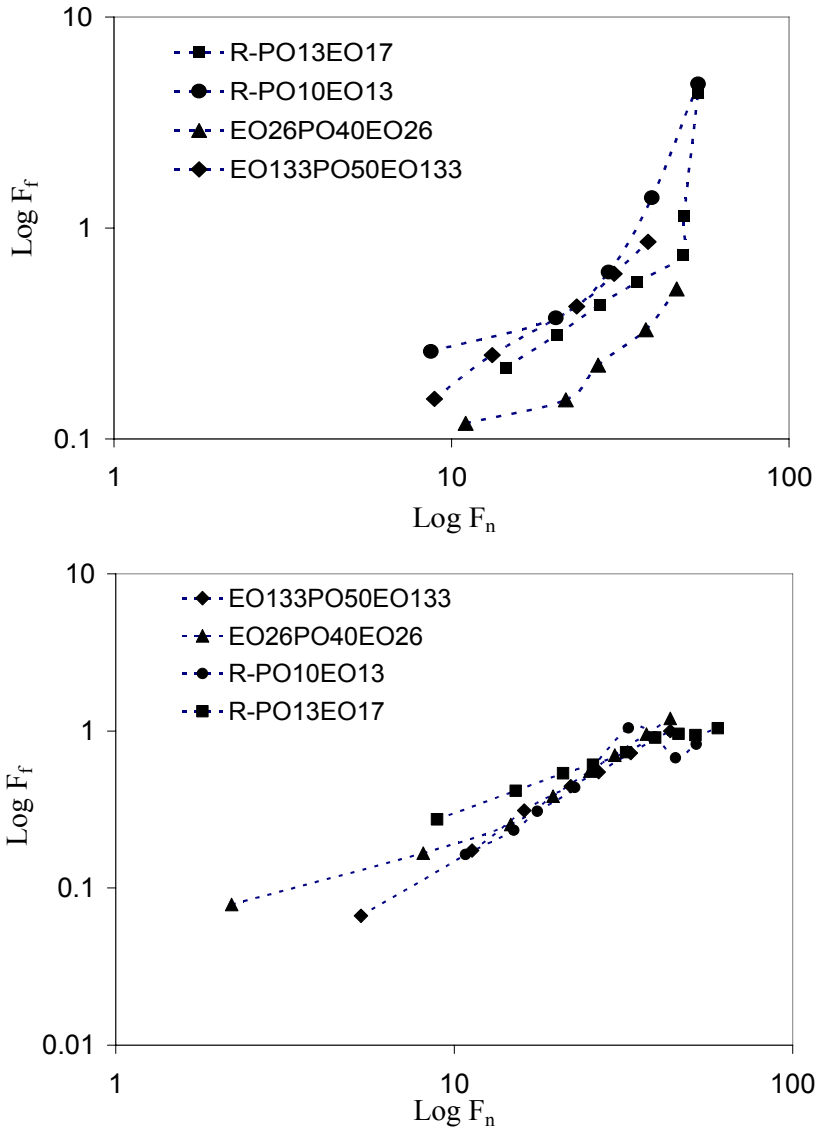

Figure 19. The relationship of friction force (F_f) and normal force (F_n) on polyethylene (left) and polypropylene (right) films using four types of lubricants: (a) EO133PO50EO133, (b) EO26PO40EO26, (c) R-PO10EO13, and (d) R-PO13EO17 (EO: polyethylene oxide; PO: polypropylene oxide; R: alkyl groups). The increase in friction as a function of normal force is valid for both polyethylene and polypropylene surfaces.

that interaction forces between the polymer and the finishes is sensitive to the chemical change in the lubricants in the case of polyethylene (PE), but not in the case

of polypropylene (PP). This is more clearly shown in Figure 20, which gives a comparison of the effects of finishes on the two films. In contrast to PE on which the finish constitution showed a significant effect, on PP all finishes gave approximately the same friction values.

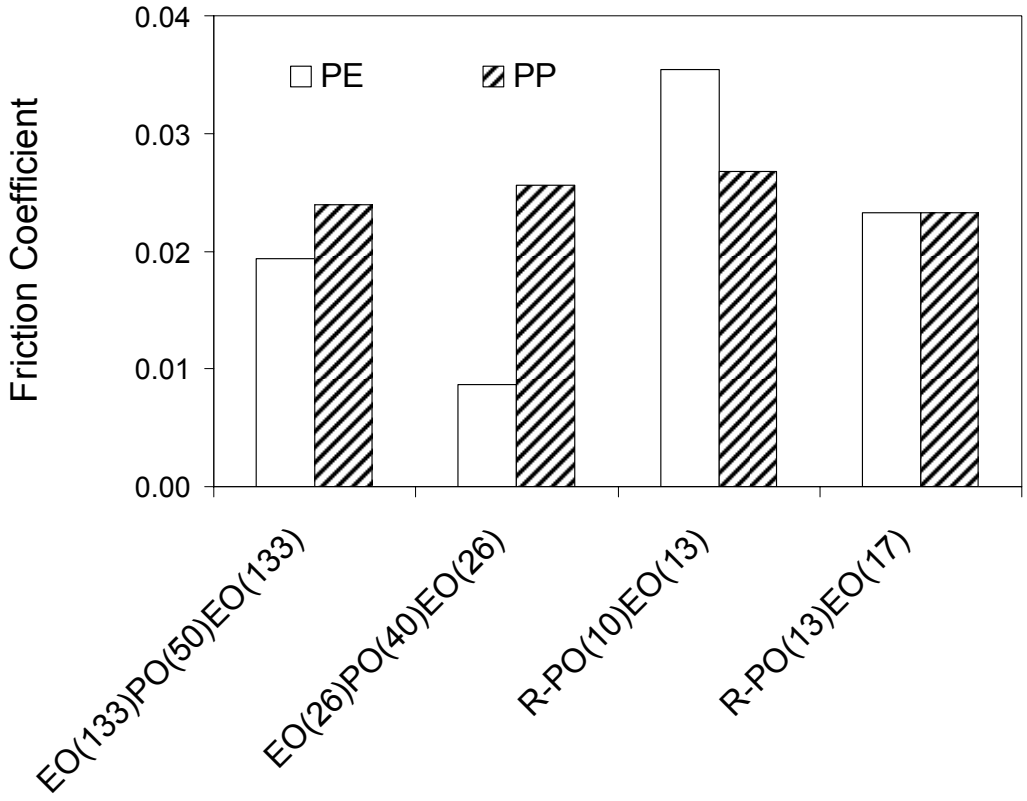

Figure 20. The coefficients of friction (COF) provided by different lubricants on polyethylene and polypropylene films. The COFs for polypropylene films did not change much with lubricant composition.

6. Summary

In boundary lubrication, lubricants might form self-assembled molecular structures on polymer surfaces due to molecular interactions with the surface of the fiber. These interactions appear to determine the alignment modes of the molecules of a lubricant and hence its lubrication efficiency. Lateral force microscopy can be effectively used

not only to measure the friction forces in the interfaces but also to probe on a polymer surface the nature of the self-assemblage of these lubricant molecules. These assemblies are expected to control the friction behavior of the lubricated surfaces. It is foreseen that understanding of the molecular structure conformations of the lubricant's chemical compounds on a fiber surface will serve as a fundamental guide for the formulation of improved finishes and lubricant additives.

REFERENCES

1. Binning G, Quate C F and Gerber Ch, 'Atomic force microscope', Phys. Rev. Lett., 1986, 56(9), 930.

2. Mate C M, McClelland G M, Erlandsson R and Chiang S, 'Atomic-scale friction of a tungsten tip on a graphite surface', Phys. Rev. Lett., 1987, 59, 1942.

3. Wang A, Jiang L, Mao G and Liu Y, 'Direct force measurement of Silicone- and Hydrocarbon-based ABA Triblock surfactants in Alcoholic media by Atomic Force Microscpy', J. Coll. Inter. Sci., 2002, 256, 331.

4. Heinz W F, Hoh J H, 'Spatially resolved force spectroscopy of biological surfaces using the Atomic Force Microscope', Trends in Biotechnology, 1999, 17, 143.

5. Israelachvili J N, Intermolecular and surface forces, Academic press, 1992.

6. Radmacher M, Fritz M and Hansma P K, 'Imaging soft samples with the Atomic Force Microscope: Gelatin in Water and Propanol', Biophys. J., 1995, 69(1), 264.

7. Rief M, Oesterhelt F, Heymann B and Gaub H E, 'Single molecule force spectroscopy on polysaccharides by Atomic Force Microscopy', Science, 1997, 275(5304), 1295.

8. Lee G U, Chrisey L A and Colton R J, 'Direct measurement of the forces between complementary strands of DNA', Science, 1994, 266(5186), 771.

9. Allen S, Chen X, Davies J, Davies M C, Dawkes A C, Edwards J C, Roberts C J, Sefton J, Tendler S J B and Williams P M, 'Detection of antigen-antibody binding events with the Atomic Force Microscope', Biochemistry, 1997, 36(24), 7457.

10. Dammer U, Hegner M, Anselmetti D, Wagner P, Dreier M, Huber W and Guntherodt H-J, 'Specific antigen/antibody interactions measured by Force Microscopy', Biophys. J., 1996, 70(5), 2437.

11. Florin E-L, Moy V T, and Gaub H E, 'Adhesion forces between individual ligand-receptor pairs', Science, 1994, 264(5157), 415.

12. Butt H-J, 'Measuring electrostatic, van der Waals, and hydration forces in electrolyte solutions with an Atomic Force Microscope', Biophys. J., 1991, 60(6), 1438.

13. Butt H-J, 'Measuring local surface charge densities in electrolyte solutions with a Scanning Force Microscope', Biophys. J., 1992, 63(2), 578.

14. Ogletree D F, Carpick R W and Salmeron M, 'Calibration of frictional forces in Atomic Force Microscopy', Rev. Sci. Instrum., 1996, 67(9), 3298.

15. Liu Y, Wu T and Evans D F, 'Lateral force microscopy study on the shear properties of self-assembled monolayers of Dialkylammonium surfactant on Mica', Langmuir, 1994, 10(7), 2241.

16. Liu Y, Evans D F, Song Q and Grainger D W, 'Structure and frictional properties of self-assembled surfactant monolayers', Langmuir, 1996, 12(5), 1235.

17. Gnecco E, Bennewitz R, Pfeiffer O, Socoliuc A and Meyer E, 'Friction and wear on the atomic scale' in Bhushan B, Ed., Nanotribology and nanomechanics: An introduction, Springer, New York, 2005.

18. Cain R G, Biggs S and Page N W, 'Force calibration in lateral Force Microscopy', J Coll. Inter. Sci., 2000, 227(1), 55.

19. Barrena E, Kopta S, Ogletree D F, Charych D H and Salmeron M, 'Relationship between friction and molecular structure: Alkylsilane lubricant films under pressure', Phys. Rev. Lett., 1999, 82(14), 2880.

20. Lio A, Charyc D H and Salmeron M, 'Comparative Atomic Force Microscopy study of the chain length dependence of frictional properties of Alkanethiols on gold and Alkysilanes on Mica', J. Phys. Chem. B., 1997, 101(19), 3800.

21. Devaprakasam D, Khatri O P, Shankar N and Biswas S K, 'Boundary lubrication additives for Aluminum: A journey from nano to macro tribology', Tribol. Intern., 2005, 38(11-12), 1022.

22. Carpick R W, Sasaki D Y and Burns A R, 'Large friction anisotropy of a Polydiacetylene monolayer', Tribol. Lett., 1999, 7(2-3), 79.

23. Bluhm H, Schwarz U D, Meyer K P and Wiesendanger R, 'Anisotropy of sliding friction on the Triglycine sulfate (010) surface', Appl. Phys. A, 1995, 61(5), 525.

24. Hirano M, Shinjo K, Kaneko R and Murata Y, 'Anisotropy of frictional forces in Muscovite Mica', Phys. Rev. Lett., 1991, 67(19), 2642.

25. Hirano M, Shinjo K, Kaneko R and Murate Y, 'Observation of superlubricity by Scanning Tunneling Microscopy', Phys. Rev. Lett., 1997, 78(8), 1448.

26. Overney R M, Takano H, Fujihira M, Paulus W and Ringsdorf H, 'Anisotropy in friction and molecular stick-slip motion', Phys. Rev. Lett., 1997, 72(22), 3546.

27. Takano H and Fujihira M, 'Study of molecular scale friction on Stearic acid crystals by Friction Force Microscopy', J. Vac. Sci. Technol. B, 1997, 14(2), 1272.

28. Overney R M, Meyer E, Frommer J, Güntherodt H–J, Fujihira M, Takano H and Gotoh Y, 'Force microscopy study of friction and elastic compliance of phase-separated organic thin films', Langmuir, 1994, 10(4), 1281.

29. Burns A R, Houston J E, Carpick R W and Michalske T A, 'Friction and molecular deformation in the tensile regime', Phys. Rev. Lett., 1999, 82(6), 1181.

30. Burns A R, Houston J E, Carpick R W and Michalske T A, 'Molecular level friction as revealed with a novel scanning probe', Langmuir, 1999, 15(8), 2922.

31. Dubois L H and Nuzzo R G, 'Synthesis, structure, and properties of model organic surfaces', Annu. Rev. Phys. Chem., 1992, 43, 437.

32. Dowson D, History of tribology, Longman: London and New York, 1979.

33. Derjaguin B, Research in surface forces, Consultants Bureau: New York, 2, 312, 1966.

34. Rabinowicz E, Friction and wear of materials, John Wiley: New York and London, 1965.

35. Homola A M, Israelachvili J N, McGuiggan P M, Gee M L, 'Fundamental experimental studies in tribology: The transition from "Interfacial" friction of undamaged molecularly smooth surfaces to "Normal" friction with wear', Wear, 1990, 136(1), 65.

36. Yoshizawa H, Chen Y and Israelachvili J, 'Fundamental mechanisms of interfacial friction: 1. Relation between adhesion and friction', J. Phys. Chem., 1993, 97(16), 4128.

37. Zeng H, Maeda N, Chen N, Tirrell M and Israelachvili J, 'Adhesion and friction of Polystyrene surfaces around Tg', Macromolecules, 2006, 39(6), 2350.

38. Adam N K and Parkburst A K G, 'Solubility of some Paraffin-chain salts', Trans. Faraday Soc., 1946, 42, 523.

39. Chen Y L, Helm C and Isrealachvili J N, 'Measurements of the elastic properties of surfactant and lipid monolayers', Langmuir, 1991, 7(11), 2694.

40. Maugis D, 'Subcritical crack growth, surface energy, fracture toughness, stick-slip and embrittlement', J. Mater. Sci., 1985, 20(9), 3041.

41. Marti A, Hähner G and Spencer N D, 'Sensitivity of frictional forces to pH on a nanometer scale: A lateral Force Microscopy study', Langmuir, 1995, 11(12), 4632.

42. Johnson K L, Kendall K and Roberts A D, 'Surface energy and the contact of elastic solid', Proc. R. Soc. London A, 1971, 324(1558), 301.

43. Kendall K, 'Inadequacy of Coulomb's friction law for particle assemblies', Nature (London), 1986, 319(6050), 203.

44. Moreau J P and Bailey A V, 'Erucoyl Glycolates as lubricants for cotton yarns', J. Coat. Fab., 1988, 18(Oct.), 85.

45. Moreau J P, Bailey A V, and DeLucca A J, United States Patent 5015419, 1989.

46. Sun C, Baird M, Anderson H. A and Brydon D L, 'Separation of broadly distributed nonylphenol Ethoxylates and determination of Ethylene Oxide oligomers in textile lubricants and emulsions by high-performance liquid chromatography', J. Chroma. A, 1996, 731(1-2), 161-169.

47. Childers J T and Fleming I D, European Patent 261415, 1988.

48. Rodenberg D G, European Patent 0796908, 1997.

49. Helman J S, Baltensperger W and Holyt J A, 'Simple model for dry friction', Phys. Rev. B., 1994, 49(6), 3831.

50. Bennewitz R, Gyalog T, Guggisberg M, Bammerlin M, Meyer E and Güntherodt H –J, 'Atomic-scale stick-slip processes on Cu(111)', Phys. Rev. B, 1999, 60(16), R11301.

51. Zwörner O, Hölscher H, Schwarz U D and Wiesendanger R, 'The velocity dependence of friction forces in point-contact friction', Appl. Phys. A, 1998,

66 (Supplement 1, Scanning Tunneling Microscopy/Spectroscopy and Related Techniques), S263.

52. Eskilsson K, Ninham B W, Tiberg F and Yaminsky V V, 'Effects of adsorption of low-molecular-weight triblock copolymers on interactions between hydrophobic surfaces in water', Langmuir, 1999, 15(9), 3242.

53. Eskilsson K, Grant L M, Hansson P and Tiberg F, 'Self-aggregation of triblock copolymers at the solid silica-water interface', Langmuir, 1999, 15(15), 5150.

54. Karin S, Claesson P M, Malmsten M, Linse P and Booth C, 'Properties of Poly(ethylene oxide)-Poly(butylene oxide) diblock copolymers at the interface between hydrophobic surfaces and water', J. Phys. Chem. B, 1997, 101(21), 4238.

55. Liu Y and Evans D F, 'Structure and frictional properties of self-assembled surfactant monolayers', Langmuir, 1996, 12(5), 1235.

56. Ruths M, 'Boundary friction of aromatic self-assembled monolayers: Comparison of system with one or both sliding surfaces covered with a Thiol monolayer', Langmuir, 2003, 19(17), 6788.

57. Ruths M, Alcantar N A and Israclachvili J N, 'Boundary friction of aromatic silane self-assembled monolayers measured with the Surface and Friction Force Microscopy', J. Phys. Chem. B, 2003, 107(40), 11149.

58. Li Y, Hinestroza J P and Rojas O J, 'Lateral Force Microscopy on thin films of cellulose', Abstracts of Papers, 233rd ACS National Meeting, Chicago, IL, U.S., March 25-29, 2007, Cell-032.

CHAPTER 3

ADSORPTION AND ASSOCIATION OF PEO-PPO-PEO TRIBLOCK COPOLYMER SOLUTIONS ON POLYPROPYLENE, POLYETHYLENE, AND CELLULOSE SURFACES

***ABSTRACT**:* The surface morphology of thin films of polyoxyethylene-polyoxypropylene-polyoxyethylene (PEO-PPO-PEO) tri-block copolymers adsorbed on polypropylene (PP), polyethylene (PE), and cellulose coated silica wafers was probed in air and in aqueous solution by using Atomic Force Microscopy (AFM). The asymmetry ratio, i.e., the relationship between PEO/PPO blocks, was used to explain the adsorption of the tri-block copolymer on the polymer coated surfaces corresponded to the buoy-dominating regime. In order to estimate the affinity between the copolymers and polymer coated surfaces, Molecular Dynamics (MD) simulations were employed to calculate the interaction energy, $E_{interaction}$ (cal/cm^2), between the PEO and PPO blocks and PP, PE and cellulose surfaces. Due to the variation in the surface affinity of the PEO and PPO, the tri-block copolymers were found to assemble in two distinctive configurations including a buoy-anchor-buoy (B-A-B) type structure on hydrophobic PP and PE surfaces, and an anchor-buoy-anchor (A-B-A) type structure on hydrophilic cellulose surfaces. The reported findings are valuable to explain the behavior of finishing additives and lubricants commonly used in textile and fiber processing operations, as well as to relate the morphology of the adsorbed layers to friction and wear phenomena.

KEYWORDS: Adsorption, morphology, self-assembly, tri-block copolymer, polymer thin films, boundary lubrication, atomic force microscopy, molecular dynamic simulation.

1. Introduction

The morphology and chemical interactions between finishes and fiber surfaces is critical to understanding boundary lubrication in textile processing. In typical applications a self-assembled, thin layer is formed at the interface between the lubricant and the surface. The adsorbed layers have been shown to control surface properties, such as surface energy, wetting, coating, friction, and wear. [1-3]

Current understanding of boundary lubrication in textiles processing is very limited and based mainly on empirical observations. In fact, only a few reports are available with regard to finish adsorption and associated nanoscale phenomena in textile fibers. The first attempts to study lubrication on textile fibers were headed by Perwelz and coworkers who related changes in the friction coefficient of polypropylene (PP) filaments to alternating stick-slip cycles. [4-6] They suggested that lubricant molecules might self-assemble on the surface by aligning themselves in distinctive ways, depending on the nature of the involved chemical and physical interactions. It was observed that hydroxylated oils with rigid backbone structures induced higher friction forces than flexible molecules. In particular, the friction coefficients measured on a fiber lubricated with hydroxylated oleate ($CH_3(CH_2)_7CH{=}CH(CH_2)_7COOH$) were higher than those for a fiber coated with hydroxylated stearate ($CH_3(CH_2)_{16}COOH$). [4] The difference in lubrication performance was attributed to molecular features, such as backbone rotation and flexibility brought by the saturated hydrocarbon in the stearate molecules. These early observations clearly attempt to link macroscopic friction behavior to the lubricant's molecular structure. [5, 6]

The surface force apparatus (SFA) has been widely used in tribology studies. [7] However, difficulties in the implementation of this technique in the case of deformable fiber surfaces (or at least those relevant to textile and fiber processing applications) have prevented a complete understanding of fiber tribology at the nanoscale i. Recently, the atomic force microscopy (AFM) has opened new opportunities to probe lubrication phenomena at higher resolutions than conventional techniques used in fiber and finishes industries. [8] There are a significant number of AFM-based tribology studies to probe friction behavior on hard surfaces; materials such as mica,[9] silica, [10] and graphite [11] are typically used in these efforts. Furthermore, these and other reports have shown distinctive correlations between lubrication performance and the lubricant's properties such as molecular weight, [12, 13] chain configuration,[14] chemical composition, [15, 16] and adsorbed layer viscoelasticity. [17, 18]

Lubricants commonly used in textile processing are usually composed of fatty acids, mineral oils, and synthetic compounds, such as ethoxylated alcohols, ethoexylated acids, and silicone fluids. [4] Surface active, tri-block hydrocarbon polymers consisting of polyoxyethylene (PEO) and polyoxypropylene (PPO) have also been used in formulations of fiber lubricants. These copolymers are of interests as they adsorb on hydrophobic surfaces with the more hydrophobic PPO acting as anchor chain while the hydrophilic PEO units extend into solution as tails. [19] Li *et al.* suggested the conformation of the PEO tails were in a relaxed state between a fully extended chain and a random coil conformation. [20] A similar head-tail configuration was also observed when diblock copolymers of polyoxyethylene-polyoxybutylene were used on hydrophobized mica. [21]

2. Theoretical models of self-assemblies on polymer surfaces

Tri-block copolymers of PEO-PPO-PEO vary in their physicochemical properties depending on the ratio between the hydrophilic PEO and the hydrophobic PPO blocks.

These copolymers provide unique properties in formulations of detergents, emulsifiers, dispersants, stabilizers and lubricants. [22] Adsorption and desorption behaviors of tri-block copolymers from aqueous solutions in these formulations have been studied via ellipsometry, [23] total internal fluorescence spectroscopy (TIRF), [24] attenuated total reflection infrared spectroscopy (ATR-FTIR), [25] dynamic and static light scattering, [26] and surface plasmon resonance spectroscopy (SPR). [27, 28]

Many investigators use a so-called buoy-anchor-buoy (B-A-B) model to describe the adsorption of tri-block copolymers on hydrophobic surfaces. [20, 29, 30] This model indicates that in aqueous systems the hydrophobic PPO blocks will strongly bind to the substrate forming a layer while the hydrophilic PEO blocks will dangle from the surface extending into the liquid forming a free "brush" layer. This representation is derived from an earlier wetting model called the "pancake" model, which was used to describe adsorption of homopolymers and copolymers on hydrophobic surfaces. [31] Theoretical work, initially by Whitwore and later by Steroeve, considered several aspects of the adsorption and desorption process including kinetics, thermodynamics, molecular configuration and micellization phenomena using a scaling parameter σ^*. [27-29] (see Equation (1) for tri-block copolymers).

$$\sigma^* = \frac{2\pi R_g^2}{\sum_{area}} \tag{1}$$

In Eqn. (1) σ^* describes the surface density of the tri-block copolymer covering the hydrophobic surface, R_g is the radius of gyration of a brush chain in solution, and $\sum_{area}$ is the average number of molecules per unit area. σ^* is thus the ratio of the cross section area of a free coiled chain in solution to the average area of a grafted chain.

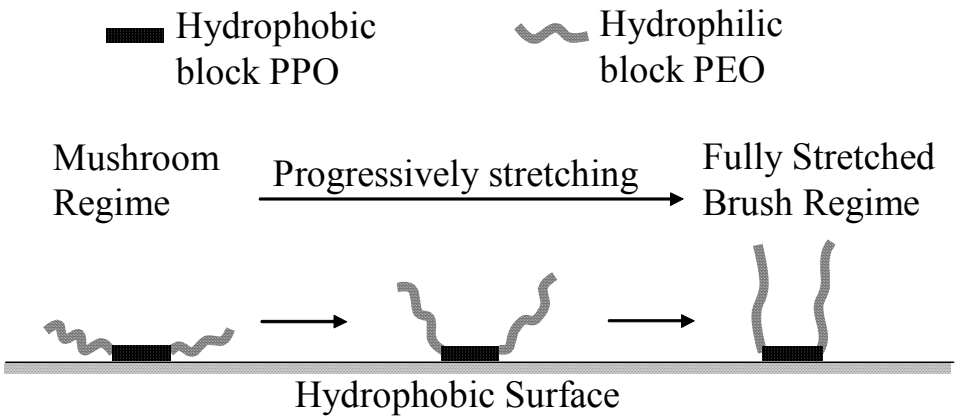

Figure 1. Schematic illustration of the dynamics of a buoy-anchor-buoy model for the self-assembled structures formed by triblock copolymers on a hydrophobic surface. Three regimes are proposed, depending on the conformation of the hydrophilic PEO blocks: "mushroom", "progressively stretching", and "fully stretched" brush regimes.

Numerical analysis indicates the existence of three main assembly regimes which depend on the value of σ^*, as illustrated in Figure 1. One extreme case is the "mushroom" regime, which occurs when $\sigma^* \leq 2$. The σ^* value of the mushroom regime indicates a large average distance between polymer molecules and isolated chains. In this regime the radius of gyration of the tri-block copolymer determines the shape of the "pancake". The opposite extreme is the "brush" regime where $\sigma^* \geq 20$. In the brush regime all dangling hydrophilic blocks stretch away from the hydrophobic surface into the liquid medium. In this regime the average distance between anchoring heads on the pancake blocks is smaller than the dimension of the pancake. This configuration characteristically shows high coverage and adsorption on the surface. A "progressively stretching" transition regime is expected if the value of σ^* falls in the range between 2 and 20, where the "mushroom" tails progressively unfold to become highly stretched "brushes".

Table 1. Effective chemical potential, dominating force, solution concentration, and the asymmetry ratio in the four dynamic regimes of adsorbed triblock copolymer. [31, 34, 55, 56]

Possible asymmetry ratio β*	**Effective chemical potential**	**Regime**	**Dominating force**	**Possible solution concentration**
	$\overline{\mu} << 0$	Rollin Regime	van der Waals force	Extremely dilute
$\beta >> 1$	$\left\|\overline{\mu}\right\| < 0$	Van der Waals-Buoy dominated regime	van der Waals, stretching force of the buoy	Higher than the cmc
$\beta \approx 1$	$\overline{\mu} > 0$ moderate value	Buoy-dominated regime	Stretching force of the buoy	Higher than the cmc
$\beta < 1$	$\overline{\mu} > 0$, very large value	Anchor-dominated regime	Stretching force of the anchor	Higher than the cmc

* The asymmetry ratio is defined by $\beta = N_B^{3/5} \Big/ N_A^{1/2}$, where N_A and N_B are the polymerization indexes of *A* and *B*, respectively.

Besides the adsorbed polymer configuration, the dynamics of the process is of relevance to interfacial phenomena. As such, the adsorption kinetics for tri-block copolymers of PEO-PPO-PEO has been studied using a gold surface modified by a methyl-terminated, self-assembled monolayer. [27] During the adsorption process, the amount of energy dissipated is expected to reach a minimum as equilibrium is

approached. Energy dissipation depends on: a) the capillary energy necessary to insert anchor polymers between an original surface/solvent interface; b) the chemical potential of the adsorbed polymers in equilibrium; c) the van der Waals dispersion energy, which balances the interaction system consisting of the surface, the solvent, and the intermediate anchoring layer; and d) the elastic energy of the buoy layer. These competing energies determine the equilibrium state of tri-block copolymers on the surface. An asymmetry ratio is defined by $\beta = \frac{N_B^{3/5}}{N_A^{1/2}}$, where N_A and N_B are the polymerization indexes of *A* and *B* blocks, respectively. [31] Based on these theoretical considerations we classify the adsorption dynamics into four regimes which depend on the effective chemical potential ($\overline{\mu}$) of the tri-block copolymers, as shown in Table 1.

The quantitative description for the adsorption behavior of triblock polymers presented in Table 1 is the basis for the interpretation of the experimental results presented in this work. We used a tri-block polymers ($EO_{19}PO_{29}EO_{19}$) (specifically a Pluronic® -type) to elucidate its molecular configurations, and adsorption behavior on PP, PE and cellulose surfaces. The study aimed at understanding the molecular configurations of the adsorbed copolymers and their effect on the morphology of adsorbed layers on substrates relevant to textile materials.

In this paper, the surface morphology of thin films of PEO-PPO-PEO tri-block copolymers adsorbed on polypropylene (PP), polyethylene (PE), and cellulose coated silica wafers was probed in air and in aqueous solution by using Atomic Force Microscopy (AFM). As a complementary approach, molecular dynamic (MD) simulations have been recently undertaken to theoretically predict the interaction of polymer-polymer systems. [32] MD simulations were employed to quantitatively evaluate the affinity between the PEO-PPO-PEO tri-block copolymers and PP, PE, and cellulose coated surfaces. The simulation results were used to discuss the

distinctive self-assembled molecular structures of the tri-block copolymers adsorbed on the polymer coated surfaces.

3. Experimental

3.1 Preparation of PP, PE, and cellulose coated surfaces

Three polymers (PP, PE, and cellulose) commonly spun into textile fibers were used in this study. The PP and PE chips, obtained from Sigma Aldrich (St. Louis, MO) were dissolved in xylene. The solution was heated and stirred for more than 2 hours using a condensation system to reflux the evaporated solvent. Silica wafers (Waferworld, FL) were washed in Piranha solution and cleaned with ultraviolet-ozone (UVO) treatment. An IR lamp was used to heat the surfaces of silica wafers and solution-delivery pipettes to a temperature of approximately 85°C. The polymer solution was spin coated (WS-400A-6NPP, Laurell Technologies) onto the silica wafers at 2000 rpm for 20 seconds. The obtained samples were placed in an oven at 80 °C to evaporate residual solvent. An XPS scan of the substrates was used to assess their chemical composition and to verify that no residual solvent was present.

Cellulose films were prepared employing the method reported by Song *et al.* [33] Polyvinylamide was used as an anchoring polymer to bind cellulose to the silica wafers. Clean silica wafers were immersed in a polyvinylamide (BASF Corp.) aqueous solution (100 ppm) for 20 min. The PVAm-coated surface was washed with Milli-Q water to remove excess PVAm and dried with nitrogen. 50 mg of Avicel micro-crystalline cellulose was added to 2.5ml N-methylmorpholine-N-oxide (NMMO) solution (50 vol. %) and heated and stirred at 115 °C until it became transparent. 7.5ml of dimethyl sulfoxide (DMSO) was added to the solution in order to adjust its viscosity. The cellulose solution was spin-coated on the PVAm substrates at 5000 rpm. Figure 2 shows AFM height and phase images of silica the wafers coated with the obtained thin films of cellulose, PE and PP thin films.

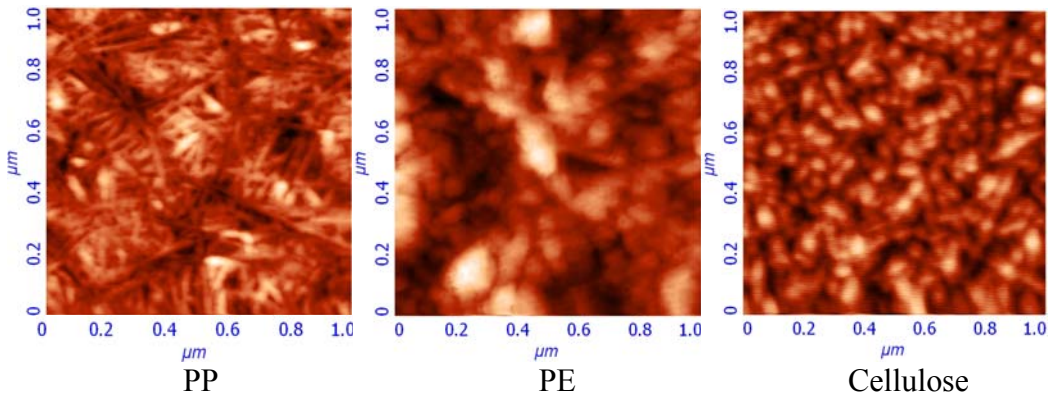

(a) Topography images

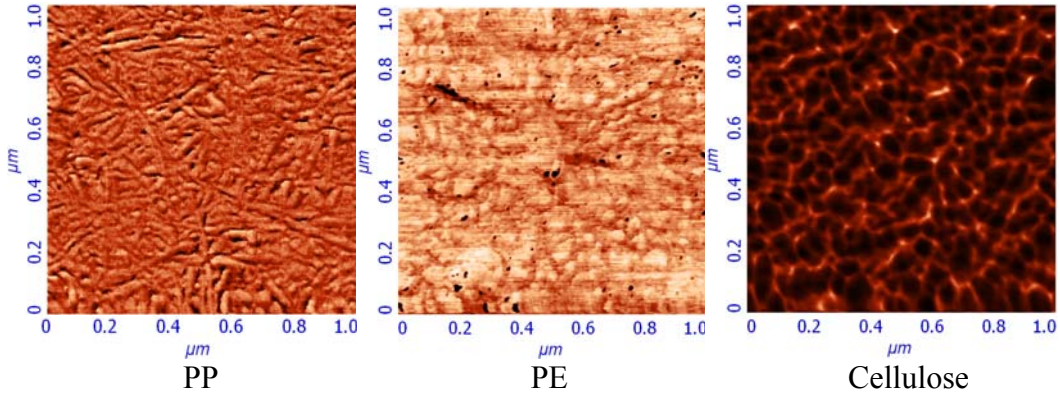

(b) Phase images

Figure 2. 1-μm AFM images of cellulose, PE, and PP thin films spin-coated on silica wafers (images obtained in air).

3.2 Preparation and characterization of lubricant solutions

$EO_{19}PO_{29}EO_{19}$ is a tri-block copolymer of ethylene oxide EO (-C_2H_4O-) and propylene oxide PO (-C_3H_6O-) terminating in primary hydroxyl groups (Figure 3). Its molecular weight and density at 20 ºC are 3400 g/mol and 1.06 g/cm^3, respectively. The asymmetry ratio β of $EO_{19}PO_{29}EO_{19}$ is 1.087 ($\beta = N_B^{3/5} / N_A^{1/2} = 19^{3/5} / 29^{1/2} = 1.087$). Therefore, it is reasonable to postulate

that this system falls into the buoy-dominated regime which predicts the adsorption process is controlled by the stretching forces caused by the buoy segments.

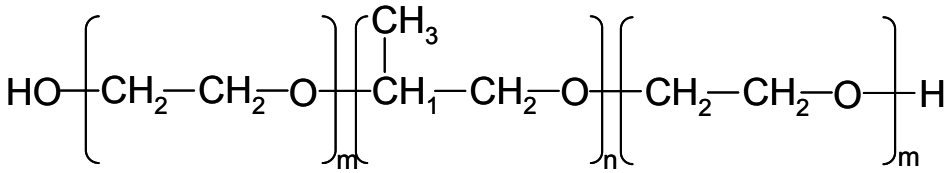

Figure 3. The chemical structure of the triblock copolymer $EO_{19}PO_{29}EO_{19}$

The tri-block copolymers are known to form micelle structures in aqueous solutions [34-36]. The formation of micelles is induced by increasing the block copolymer concentration above the critical micelle concentration (cmc) or exceeding the critical micellization temperature. The cmc of the $EO_{19}PO_{29}EO_{19}$ (0.0001 wt %) was determined via surface tension measurements (Du Nöuy method, Fisher Surface Tensionmat Model 21, Fisher Scientific). The results indicated a critical micelle concentration of 0.0001%. The result was in good agreement with literature values. [37, 38] Therefore, all immersion experiments were performed at a 1% w/w concentration to guarantee operation in a regime significantly higher than the cmc.

Chemical analysis of $EO_{19}PO_{29}EO_{19}$ solutions (at aqueous concentrations of 1%, 2.5%, 5%, and 10% by weight) was carried out via ATR-FTIR (Thermo Nicolet Magna-IR 560 Spectrometer) (see Figure 4) hree characteristic bands were analyzed: 1) the region of 1645-1670 cm^{-1}, assigned to the –OH band of both free and bound water in the system; 2) the region of 1380-1480 cm^{-1}, assigned to the hydrated state of $–CH_3$ and $–CH_2–$ surrounded by water, and 3) the band at 1080 cm^{-1}, assigned to the conjugation of the C–O–C stretching vibration of PPO and PEO blocks. The bands are in agreement with previous reports. [39-41] These bands increased in intensity with the increase of the solution concentration. The increase is especially prominent in the C-O-C bands which play important roles in $EO_{19}PO_{29}EO_{19}$ chain mobility.

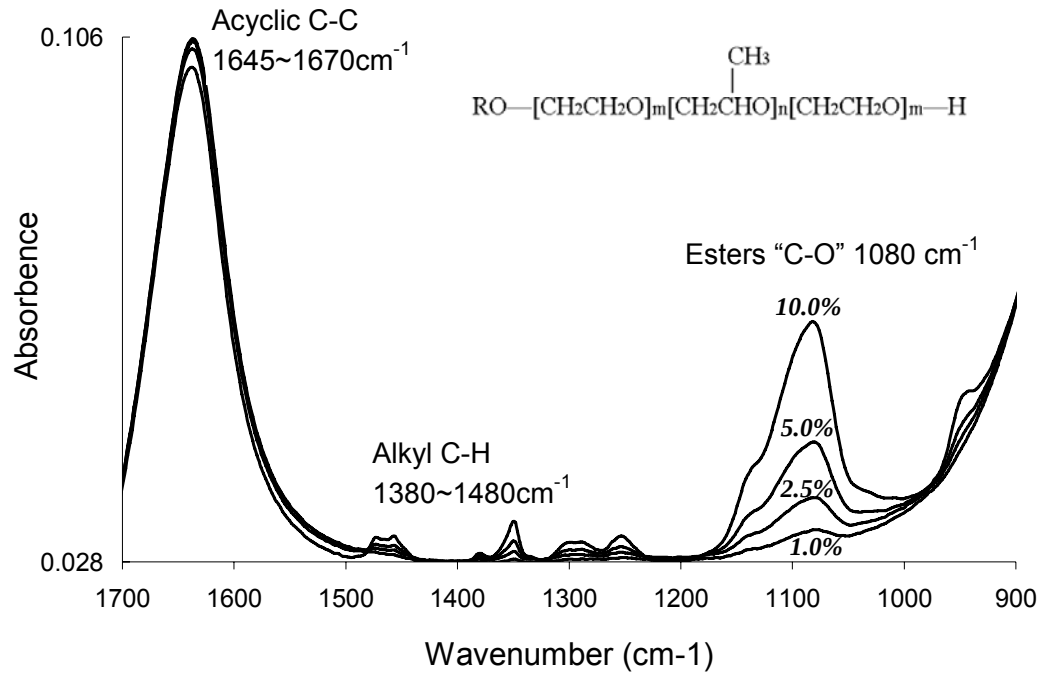

Figure 4. ATR-FTIR spectra of the $EO_{19}PO_{29}EO_{19}$ solutions (1.0%, 2.5%, 5.0%, 10.0% by weight concentrations).

3.3 Water contact angle measurements

The contact angle for Milli-Q water on bare silica wafer, PP, PE, and cellulose surfaces was measured using a goniometer (Ramé-Hart, NJ). 10 μL of Milli-Q water was placed onto the surface. Polymer coated specimens were immersed in an $EO_{19}PO_{29}EO_{19}$ solution (1% by weight) overnight, rinsed with Milli-Q water and dried with qa genlt dry nitrogen jet. The contact angles of the clean and treated (after immersion in the $EO_{19}PO_{29}EO_{19}$ aqueous solution) PP, PE, and cellulose surfaces are shown in Table 2.

Both PP and PE surfaces exhibit large contact angles (>90 degrees), while the cellulose surface has low contact angles (<90 degrees). These values of contact angles were as expected and are suggested here as good indicators of the hydrophobic/hydrophilic character of the substrate, which plays a key role in the creation of adsorbed molecular structures. The treatment with the $EO_{19}PO_{29}EO_{19}$

aqueous solution decreased contact angles for all polymer coated surfaces, indicating the adsorption of the tri-block copolymer on the surfaces.

Table 2. Contact angle of bare and $EO_{19}PO_{29}EO_{19}$–treated silica, PP, PE and cellulose surfaces

Polymer film	**Contact Angle (°)**
Bare silica	25.7 ± 1.5
PP (bare)	102.9 ± 1.7
PP (treated)	92.5 ± 3.3
PE (bare)	95.1 ± 0.7
PE (treated)*	-
Cellulose (bare)	28.6 ± 3.4
Cellulose (treated)	15.8 ± 3.4

* No reliable results were recorded for the treated PE surface since PE layer was not robust in the presence of $EO_{19}PO_{29}EO_{19}$ solution.

3.4 Molecular Dynamic (MD) Simulation

We employed MD simulations to quantify the affinity of the PEO and PPO to the polymer coated surfaces. Previous reports showed that an oligomer can be effectively used in MD simulations as a substitute for a high MW polymer. [32, 42]

3.4.1 Model building

MD simulations were performed using Materials Studio 4.1 software from Accelrys Software Inc (San Diego, CA). [43] The MD calculation was carried out using the Discover module [44] and COMPASS [45] (Condensed-phase Optimized Molecular

Potentials for Atomistic Simulation Studies) force field. First, polymer (PP, PE, and cellulose) surfaces were constructed using the amorphous cell module developed by combining an algorithm by Theodorou and Suter [46] and the scanning method of Meirovitch. [47] The target density of the PP, PE, and cellulose were chosen as 0.873g/cm^3, 0.848g/cm^3, and 1.446g/cm^3, respectively. These densities were comparable to those reported in MD simulations literature. [48-51] The PP, PE, and cellulose oligomer chains were built by monomer units and then were placed into a 30×30×30Å slab (see Figure 5).

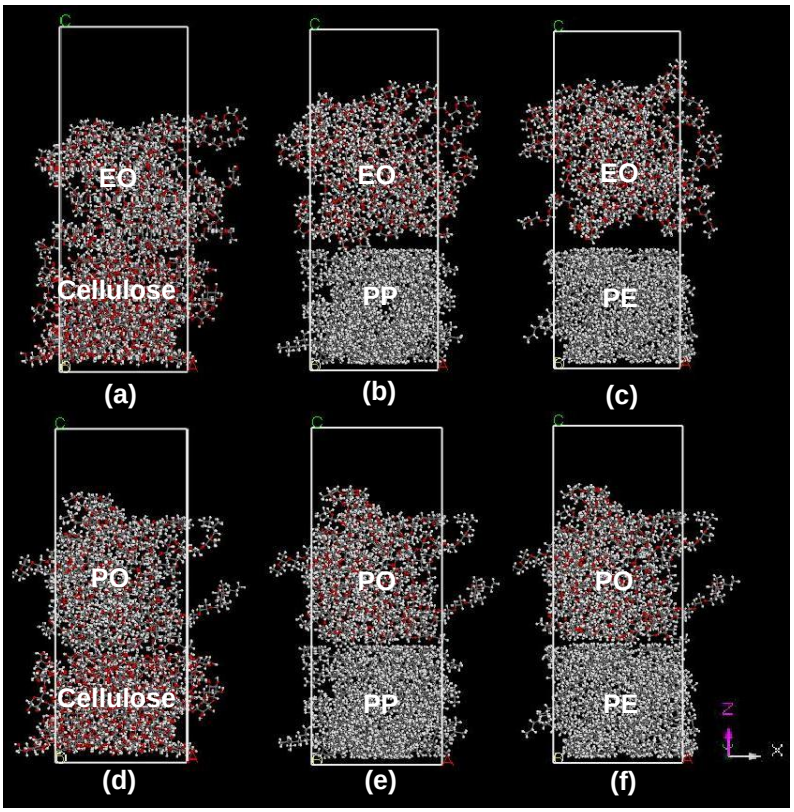

Figure 5. A representative structure of PP, PE, and cellulose surface interacting with the EO or PO. Molecules are packed into the cell in a dimension size 30×30×80Å with their periodic images. (a) PEO-Cellulose; (b) PEO-PP; (c) PEO-PE; (d) PPO-Cellulose; (e) PPO-PP; (f) PPO-PE; (colors: carbon atoms--grey, hydrogen--white, oxygen--red).

In order to construct the same base-size, in a and b dimensions, as the surfaces in the previous step, the 30×30×30Å EO or PO slab was created by the amorphous cell module with 24 EO or 18 PO oligomer chains. Each oligomer chain was composed of 15 EO or PO monomers. The polymer slabs of EO or PO were piled up on the confined oligomeric surface of PP, PE, and cellulose with the same base-size. A 20Å vacuum layer was placed above the polymer slab, which allows the oligomeric systems to expand freely in the c direction as well as to prevent the interaction between the top and the bottom due to the use of a periodic boundary condition. A representative structure of polymer surfaces with the oligomer (EO or PO) is illustrated in Figure 3. Then MD simulations were performed under the constant volume and temperature (NVT) ensemble. Models built with 3D periodicity were equilibrated for 5 ps in the NVT ensemble at 298 K. Systems were then subjected to 1000 ps of dynamics with the trajectories being saved every 1 ps during the last 100 frames to calculate the physical properties of interest.

3.4.2 Interaction energy

The interaction energy is the amount of work necessary to separate the polymer slab of the EO or PO and surface of cellulose, PE, or PP. The interaction energy is proportional to the difference between the energy of the total system, E_{total}, and those of the individual layers, $E_{surface}$ and $E_{polymer}$. The energy difference should be normalized in order to obtain the interaction energy at a molecular level. We adopted the surface area method reported by Chauve *et al.* [52] This method calculates the interaction energy of the polymer in the middle of a sandwich model by dividing the energy difference by twice the surface areas. Because there was only one interacting interface in our model, the energy difference was only divided by the surface area, $S_{surface}$, to obtain the interaction energy, $E_{interaction}$ (cal/cm^2), in equation (1).

$$E_{interaction} = -(E_{total} - E_{surface} - E_{polymer}) / S_{surface} \qquad (1)$$

Results are shown in Figure 6.

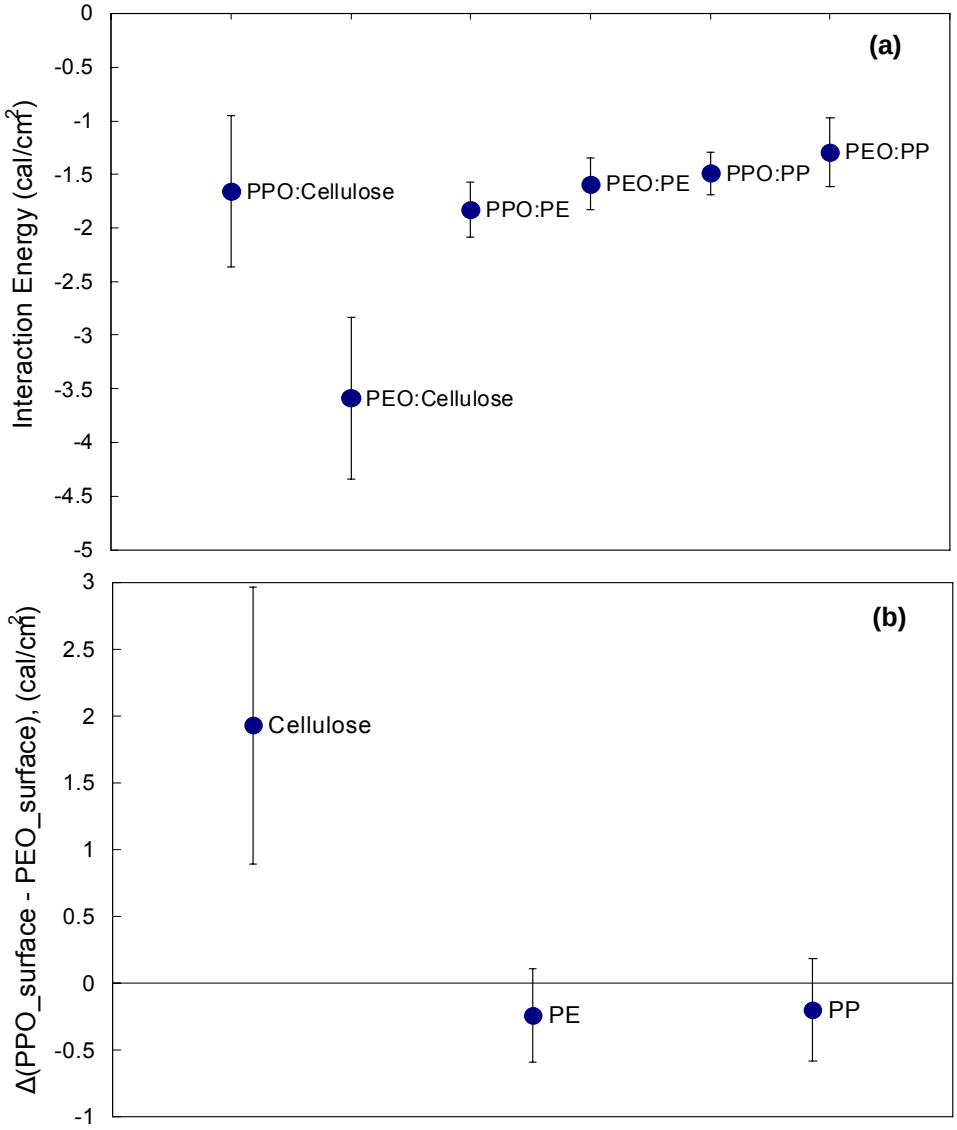

Figure 6. (a) Interaction energy $E_{interaction}$ (cal/cm^2) of the PPO and PEO interacting with the cellulose, PP, and PE model surfaces. (b) Δ (PPO_surface – PEO_surface) represents the interaction energy difference between $E_{PPO\_surface}$ and $E_{PEO\_surface}$. The positive sign of Δ (PPO, PEO) for cellulose indicates the PEO block has higher tendency towards cellulose than the PPO block. By contrast, the negative sign of Δ (PPO, PEO) for PP and PE indicates that the PPO block has higher tendency towards PP or PE.

3.5 Surface morphology by Atomic Force Microscopy

A Scanning Probe Microscope (NTEGRA Prima, NT-MDT) was employed to characterize the topography of the bare and treated (coated) substrates. Scans were performed in air (air-test), in DI water (water-test), and in 1% w/w $EO_{19}PO_{29}EO_{19}$ solutions ($EO_{19}PO_{29}EO_{19}$-test). Before imaging, each surface was cleaned with DI water and 95% ethanol, and dried with compressed air. AFM was performed in tapping mode using a MikroMasch probe with a force constant of 0.35N/m and resonance frequency of 145Hz. In the water-test and $EO_{19}PO_{29}EO_{19}$-test, the respective solution was injected onto the surfaces in a liquid metal cell. All tests were performed with a scanning frequency of 1Hz and a scan size of 1 μm. Both topography and phase signals were collected and each image consisted of 256×256 pixels.

4. Results and discussion

4.1 Interaction energy

MD simulations provided a theoretical prediction of interaction energy, $E_{interaction}$ (cal/cm^2), between the PPO and PEO blocks and the polymer surfaces of PP, PE, and cellulose. The interaction energy quantified the affinity between the PEO or PPO and polymer surfaces shown in Figure 6 (a). Negative values indicated the attractive forces between the polymers and surfaces. The variation in the interaction energy illustrated the variant affinity between the polymers and surfaces due to differing chemical nature. The interaction energy difference $\Delta\ (E_{PPO\_surface}–E_{PEO\_surface})$, shown in Figure 6 (b), illustrated the difference in affinity of PEO and PPO interacting with a given polymer surface. It was found that the PEO block had higher affinity towards the cellulose surfaces than the PPO block, and the PPO block had higher affinity towards the PP and PE surfaces. These values were in good agreement with the fact that both of the PP and PE are hydrophobic polymers, while the cellulose surface is hydrophilic.

[53, 54] The relative interaction energy of the PPO block with the PE surface was larger than the PPO block with the PP surface. These differences in chemical affinity could be responsible for the formation of self-assembled molecular structures of the tri-block copolymer $EO_mPO_nEO_m$ when deposited over the polymer coated surfaces. The affinity differences between the PEO and PPO could give rise to variations in the self-assembling modes of molecular structures. Consequently, the self-assembling modes of the PEO/PPO copolymers affected adsorption phenomena.

4.2 Self-assembled patterns of tri-block copolymers on different polymer surfaces by AFM analysis

4.2.1 Polypropylene

Figure 7a shows the fibrillar morphology of the PP coated surface imaged in air. These fibrillar structures might form after crystallization of PP during the spin-coating process. The fibrillar structure was seen more clearly when imaged in water (see Figure 7b) due to the improved resolution by the elimination of Laplace (capillary) forces between the tip and the surface. When the specimen was imaged while immersed in $EO_{19}PO_{29}EO_{19}$ solution, the crystallite fiber-like structures became obscure (Figure 7c). The MD simulation indicated the hydrophobic PPO blocks of the tri-block copolymers had a higher affinity to the PP surface and thus easily anchored on the surface. The blocks of PEO were hydrophilic hence they had less affinity with the surface and were expected to remain in the liquid phase. Figure 7d illustrates a buoy-anchor-buoy (B-A-B) structure formed on the PP hydrophobic surface. [55] Small and fine crystallite structures of the PP thin film were most likely shielded from AFM detection by large crystallite formations.

4.2.2 Polyethylene

According to Figure 8a, microcrystal structures of PE were formed on the silica wafers. In contrast to the fibrous-like structures exhibited by PP, the PE crystal

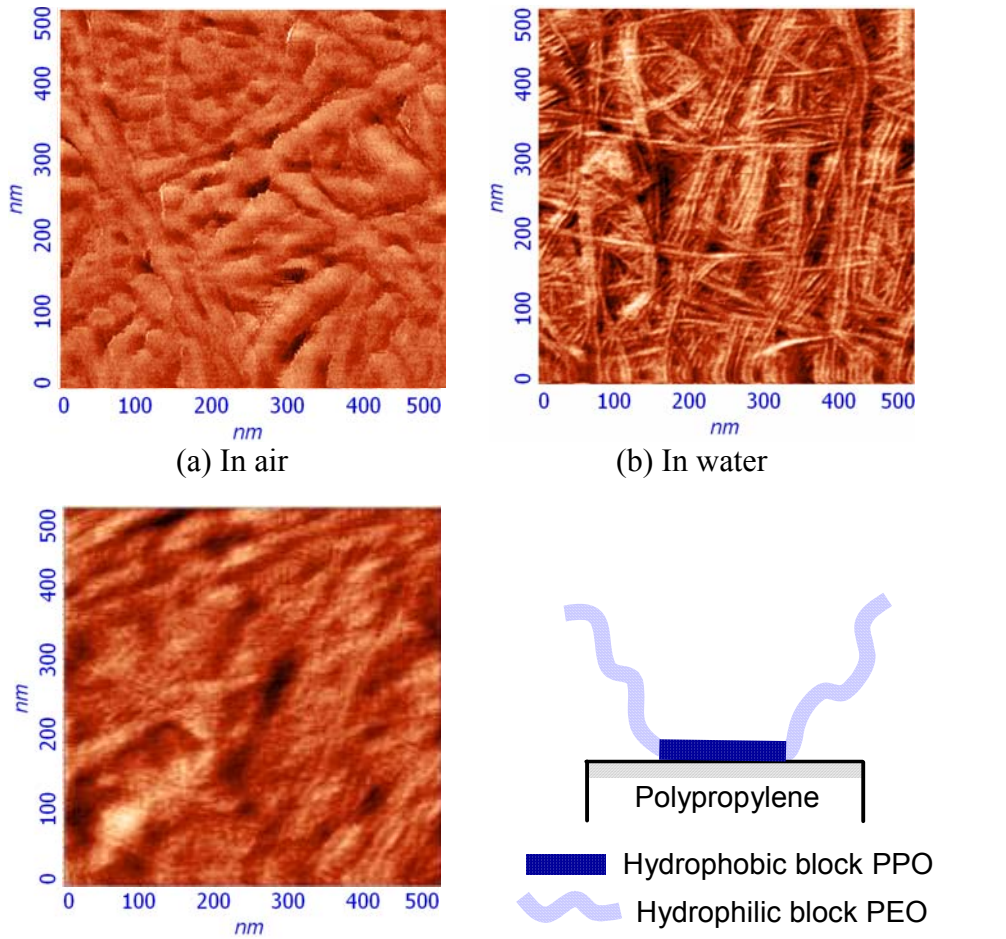

(a) In air (b) In water

(c) In $EO_{19}PO_{29}EO_{19}$ soluti (d) An $EO_{19}PO_{29}EO_{19}$ chain on a PP surface

Figure 7. (a) Phase image of PP thin film in air, illustrating fibrillar structures; (b) Phase image of PP thin film in water, showing clearer fibrillar structures than (a); (c) Phase image of PP thin film immersed in $EO_{19}PO_{29}EO_{19}$ solution, presenting large pores; (d) A buoy-anchor-buoy structure on a hydrophobic PP surface consists of a hydrophobic PPO segment binding on the surface and hydrophilic PEO segments extending from the PP surface.

structures were round. During imaging in water, these circular domains became larger and more distinguishable (Figure 8b). The enlargement might be due to water

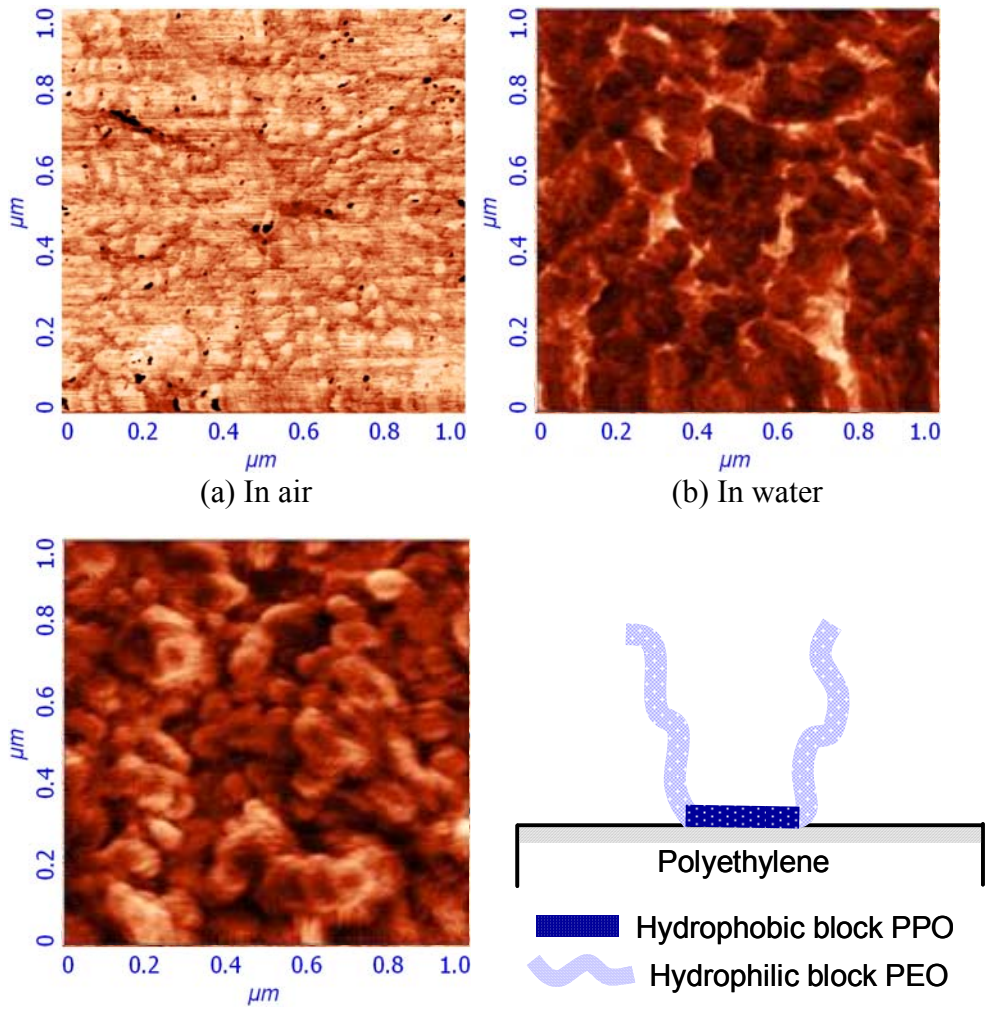

(a) In air (b) In water

(c) In $EO_{19}PO_{29}EO_{19}$ solution (d) An $EO_{19}PO_{29}EO_{19}$ chain on a PP surface

Figure 8. (a) Phase image of PE thin film in air, illustrating circular microcrystal structures; (b) Phase image of PE thin film in water, showing larger and more distinguishable structures that in (a); (c) Phase image of PE thin film immersed in $EO_{19}PO_{29}EO_{19}$ solution, presenting larger and more circular features than (a) and (b); (d) A pancake structure of triblock copolymers on a hydrophobic PE surface has both PEO and PPO segments spread on the surface.

penetrating and swelling areas of the PE thin film. After immersing the PE specimen in $EO_{19}PO_{29}EO_{19}$, the surface morphology appeared flatter. The reduction in contrast

suggested the $EO_{19}PO_{29}EO_{19}$ molecules diffused and filled the spaces between the crystals. In the previous discussion of interaction energy, the buoy stretching force of the PEO blocks still appeared to dominate the behavior of the tri-block copolymers adsorbed on the hydrophobic PE surface, resulting in a similar B-A-B structure of the tri-block copolymers on the PP surface. However, the difference between the PP and PE surfaces shown in Figure 6 illustrated the affinity difference between the PPO and PEO block toward the PE surface, $\Delta (E_{PPO\_PE}–E_{PEO\_PE})$, was slightly larger than that for the PP surface. Therefore, compared with the PP surface, a larger stretching force is applied to the PEO blocks thus extending them further away from the PE surface. The outer PEO layer is more flexible on the PE surface than on the PP surface.

4.2.3 Cellulose surface

Reports on the adsorption of tri-block copolymers on hydrophilic surfaces were less frequent than on hydrophobic surfaces. [56] The AFM image of the cellulose film shown in Figure 9a allowed the detection of hexagonal crystal structures on the cellulose surface using a two-dimensional Fast Fourier Transform (2D FFT) image, [13] Figure 9b shows the morphology of the cellulose surface immersed in water. A 2D FFT transformation of Figure 9b indicated that the hexagonal configuration disappeared and was developed to circular structures. Cellulose is known to interact with water due to the presence of free hydroxyl groups. Therefore, it was hypothesized that the changes in crystal configuration on the cellulose surface were mainly due to hydration of the film. Figure 9c presents the morphology of the cellulose surface while immersed in the $EO_{19}PO_{29}EO_{19}$ solutions. It was observed that the fine crystal structures tend to fade away and are replaced by a random morphology.

The interaction energy in MD results suggested that the PEO block had higher affinity towards the cellulose surfaces than the PPO block. Therefore, a different molecular configuration, the anchor-buoy-anchor (A-B-A) model, was proposed to

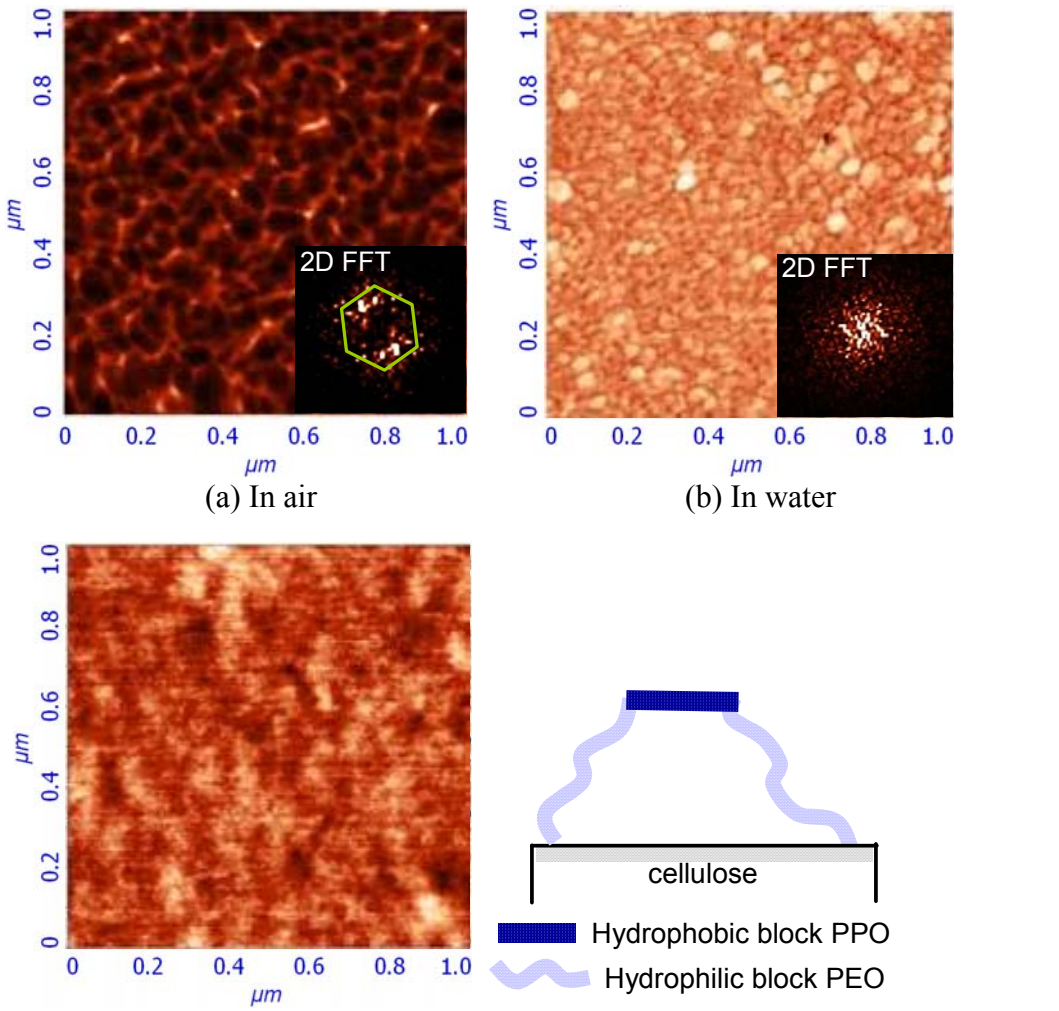

(a) In air (b) In water

(c) In $EO_{19}PO_{29}EO_{19}$ solution (d) An $EO_{19}PO_{29}EO_{19}$ chain on a PP surface

Figure 9. (a) Phase image of cellulose thin film in air, illustrating hexagonal crystal structures in 2D FFT figure; (b) Phase image of cellulose thin film in water, showing analogous circular structures; (c) Phase image of cellulose thin film in $EO_{19}PO_{29}EO_{19}$ solution; No regular structures are detected; (d) an anchor-buoy-anchor structure on a hydrophilic cellulose surface consists of two hydrophilic PEO segments binding on the surface and a hydrophobic PPO segment repelling from the surface.

form on the hydrophilic cellulose surface, as illustrated in Figure 9d. Similar model was reported previously by Wu *et al.* where they used AFM to study the adsorption of an $EO_{99}PO_{69}EO_{99}$ tri-block copolymer onto hydrophilic silica surfaces. [19]

5. Conclusions

Atomic Force Microscopy was employed to directly observe $EO_{19}PO_{29}EO_{19}$ self-assemblies on PP, PE, and cellulose surfaces. According to the asymmetric ratio β, the systems in this study fell into a dynamically buoy-dominated regime for the three polymer coated surfaces. Therefore, the adsorption process was hypothesized to be controlled by the stretching force caused by the PEO buoy segments. The interaction energy from MD simulations illustrated that the PEO block had higher affinity towards the cellulose surfaces than the PPO block, and the PPO had a higher affinity towards the PP and PE surfaces. Due to the affinity difference, the B-A-B structure was proposed for the PE and PP surfaces while the A-B-A structure for the cellulose surface. The self-assembled configurations of the triblock copolymer were found to be influenced by the nature of the substrate: a B-A-B structure on the hydrophobic PP and PE and an anchor-buoy-anchor structure on hydrophilic cellulose. Observation of these molecular assemblies via AFM may serve as a fundamental means to engineer better lubricant and additive systems for fiber processing operations.

Acknowledgement

This work was supported by the National Textile Center under Grant No. C05-NS09. We are grateful to Dr. Laura McJilton and Christina Diaz for their English correction of the manuscript.

REFERENCES

1. Hill, R.M., *Silicon Surfactant*. Surfactant Science Series, ed. R.M. Hill. 1999, New York: Marcel Dekker.

2. Michielsen, S.J., *Device for Measuring Sliding Friction on Highloft Nonwovens.* Journal of Engineered Fibers and Fabrics, 2006. **1**(1): p. 23-31.

3. Sim, W.S. and F.Y. Goh, *Molecular self-assembly of sulfonated polyaniline thin films.* Surf. Rev. Lett. 2001. **8**(5): p. 491-496.

4. Behary, N., *et al.*, *Using an electronic microbalance technique to study the stick-slip behavior of lubricated polypropylene fibers.* J. Appl. Polym. Sci. 2003. **89**(3): p. 645-654.

5. Behary, N., *et al.*, *Tribology of sized glass fibers Part I: Friction analysis by lateral force microscopy and electronic microbalance technique.* Text. Res. J. 2000. **70**(8): p. 700-708.

6. Behary, N., *et al.*, *Tribology of sized glass fibers. Part II: Using an electronic microbalance technique to study stick-slip behavior.* Text. Res. J. 2001. **71**(3): p. 187-194.

7. Israelachvili, J.N., *Intermolecular and surface forces*. 1992, New York: Academic Press.

8. Mate, C.M., *et al.*, *Atomic-scale friction of a tungsten tip on a graphite surface.* Phys. Rev. Lett. 1987. **59**(17): p. 1942-5.

9. Marti, O., J. Colchero, and J. Mlynek, *Combined scanning force and friction microscopy of mica.* Nanotechnology, 1990. **1**(2): p. 141-144.

10. Bhushan, B., H. Liu, and S.M. Hsu, *Adhesion and Friction Studies of Silicon and Hydrophobic and Low Friction Films and Investigation of Scale Effects.* Journal of Tribology, 2004. **126**(3): p. 583-590.

11. Sasaki, N., K. Kobayashi, and M. Tsukada, *Atomic-scale friction image of graphite in atomic-force microscopy.* Physical Review B, 1996. **54**(3): p. 2138-2149.

12. Barrena, E., *et al.*, *Relationship between Friction and Molecular Structure: Alkylsilane Lubricant Films under Pressure.* Phys. Rev. Lett. 1999. **82**(14): p. 2880-2883.

13. Lio, A., D.H. Charych, and M. Salmeron, *Comparative Atomic Force Microscopy Study of the Chain Length Dependence of Frictional Properties of Alkanethiols on Gold and Alkylsilanes on Mica.* J. Phys. Chem. B 1997. **101**(19): p. 3800-3805.

14. Devaprakasam, D., *et al.*, *Boundary lubrication additives for aluminum: A journey from nano to macro tribology.* Tribol. Int. 2005. **38**(11-12): p. 1022-1034.

15. Burns, A.R., *et al.*, *Friction and Molecular Deformation in the Tensile Regime.* Phys. Rev. Lett., 1999. **82**(6): p. 1181-1184.

16. Burns, A.R., *et al.*, *Molecular Level Friction As Revealed with a Novel Scanning Probe.* Langmuir, 1999. **15**(8): p. 2922-2930.

17. Yoshizawa, H., Y.L. Chen, and J. Israelachvili, *Fundamental mechanisms of interfacial friction. 1. Relation between adhesion and friction.* J. Phys. Chem., 1993. **97**(16): p. 4128-40.

18. Zeng, H., *et al.*, *Adhesion and Friction of Polystyrene Surfaces around Tg.* Macromolecules, 2006. **39**(6): p. 2350-2363.

19. Wu, C., *et al.*, *Atomic force microscopy study of E99P69E99 triblock copolymer chains on silicon surface.* Langmuir, 2000. **16**(2): p. 656-661.

20. Li, J.-T., K.D. Caldwell, and N. Rapoport, *Surface Properties of Pluronic-Coated Polymeric Colloids.* Langmuir, 1994. **10**(12): p. 4475-82.

21. Schillen, K., *et al.*, *Properties of Poly(ethylene oxide)-Poly(butylene oxide) Diblock Copolymers at the Interface between Hydrophobic Surfaces and Water.* J. Phys. Chem. B, 1997. **101**(21): p. 4238-4252.

22. Alexandridis, P., J.F. Holzwarth, and T.A. Hatton, *Micellization of Poly(ethylene oxide)-Poly(propylene oxide)-Poly(ethylene oxide) Triblock Copolymers in Aqueous Solutions: Thermodynamics of Copolymer Association.* Macromolecules, 1994. **27**(9): p. 2414-25.

23. Malmsten, M. and F. Tiberg, *Adsorption of ethyl(hydroxyethyl) cellulose at polystyrene.* Langmuir, 1993. **9**(4): p. 1098-103.

24. Fu, Z. and M.M. Santore, *Kinetics of Competitive Adsorption of PEO Chains with Different Molecular Weights.* Macromolecules, 1998. **31**(20): p. 7014-7022.

25. Frantz, P. and S. Granick, *Exchange Kinetics of Adsorbed Polymer and the Achievement of Conformational Equilibrium.* Macromolecules, 1994. **27**(9): p. 2553-8.

26. Nolan, S.L., *et al.*, *Light scattering study on the effect of polymer composition on the structural properties of PEO-PPO-PEO micelles.* J. Colloid Interface Sci., 1997. **191**(2): p. 291-302.

27. Brandani, P. and P. Stroeve, *Adsorption and Desorption of PEO-PPO-PEO Triblock Copolymers on a Self-Assembled Hydrophobic Surface.* Macromolecules, 2003. **36**(25): p. 9492-9501.

28. Brandani, P. and P. Stroeve, *Kinetics of Adsorption and Desorption of PEO-PPO-PEO Triblock Copolymers on a Self-Assembled Hydrophobic Surface.* Macromolecules, 2003. **36**(25): p. 9502-9509.

29. Baranowski, R. and M.D. Whitmore, *Theory of the structure of adsorbed block copolymers: detailed comparison with experiment.* J. Chem. Phys., 1995. **103**(6): p. 2343-53.

30. Wang, A., *et al.*, *Direct force measurement of silicone- and hydrocarbon-based ABA triblock surfactants in alcoholic media by atomic force microscopy.* J. Colloid Interface Sci., 2002. **256**(2): p. 331-340.

31. Marques, C., J.F. Joanny, and L. Leibler, *Adsorption of block copolymers in selective solvents.* Macromolecules, 1988. **21**(4): p. 1051-9.

32. Prathaba, B., V. Subramanianb, and T.M. Aminabhavia, *Molecular dynamics simulations to investigate polymer–polymer and polymer–metal oxide interactions.* Polymer, 2006. **48**(1): p. 409-416.

33. Song, J., *et al.*, *Development and Charaterization of thin polymer films relevant to fiber processing.* Thin Solid Films, 2009.

34. Alexandridis, P., *Poly(ethylene oxide)/poly(propylene oxide) block copolymer surfactants.* Curr. Opin. Colloid Interface Sci., 1997. **2**(5): p. 478-489.

35. Patel, K., *et al.*, *Salt induced micellization of very hydrophilic PEO-PPO-PEO block copolymers in aqueous solutions.* Eur. Polym. J., 2007. **43**(5): p. 1699-1708.

36. Zhou, B.C.Z., *Z. Physical Chemistry of polyoxyalkylene block copolymer surfactants*, in *In Nonionic surfactants, surfactant science series*, V.M. Nace, Editor. 1996, CRC Press.

37. Wanka, G., H. Hoffmann, and W. Ulbricht, *The aggregation behavior of poly-(oxyethylene)-poly-(oxypropylene)-poly-(oxyethylene)-block-copolymers in aqueous solution* Colloid & Polymer Science, 1990. **268**(2): p. 101-117.

38. Diakova, B., M. Kaisheva, and D. Platikanov, *Thin liquid films from polyoxyethylene-polyoxypropylene-block copolymer on the surface of fused quartz.* Colloids and Surfaces A: Physicochemical and Engineering Aspects, 2001. **190**(1-2): p. 61-70.

39. Dissanayake, M. and R. Frech, *Infrared Spectroscopic Study of the Phases and Phase Transitions in Poly(ethylene oxide) and Poly(ethylene oxide)-Lithium*

Trifluoromethanesulfonate Complexes. Macromolecules, 1995. **28**(15): p. 5312-5319.

40. Kimura, N., J. Umemura, and S. Hayashi, *Polarized FT-IR Spectra of Water in the Middle Phase of Triton X100-Water System.* Journal of Colloid and Interface Science, 1996. **182**(2): p. 356-364.

41. Meng, S., *et al.*, *Two-dimensional correlation ATR-FTIR studies on PEO–PPO–PEO tri-block copolymer and its phosphorylcholine derivate as thermal sensitive hydrogel systems* Polymer, 2008. **49**(11): p. 2738-2744.

42. Chauve, G., *et al.*, *Cellulose Poly(Ethylene-co-vinyl Acetate) Nanocomposites Studied by Molecular Modeling and Mechanical Spectroscopy.* Biomacromolecules, 2005. **6**(4): p. 2025-2031.

43. Accelrys, I., *Material Studio modeling*. 2006: San Diego, CA.

44. Lippa, K.A., L.C. Sander, and R.D. Mountain, *Molecular Dynamics Simulations of Alkylsilane Stationary-Phase Order and Disorder. 1. Effects of Surface Coverage and Bonding Chemistry.* Analytical Chemistry, 2005. **77**(24): p. 7852-7861.

45. Sun, H., *COMPASS: An ab Initio Force-Field Optimized for Condensed-Phase ApplicationsOverview with Details on Alkane and Benzene Compounds.* The Journal of Physical Chemistry B, 1998. **102**(38): p. 7338-7364.

46. Theodorou, D.N. and U.W. Suter, *Detailed molecular structure of a vinyl polymer glass.* Macromolecules, 1985. **18**(7): p. 1467-1478.

47. Meirovitch, H., *Computer simulation of self-avoiding walks: Testing the scanning method.* The Journal of Chemical Physics, 1983. **79**(1): p. 502-508.

48. Chen, W.L., G. C.; Yang, C. Q., *Molecular modeling of cellulose in amorphous state part II: Effects of rigid and flexible crosslinks on cellulose.* Polymer, 2004. **45**(21): p. 7357-7365.

49. Derecskei, B.D.-K., A., *Molecular dynamic studies of the compatibility of some cellulose derivatives with selected ionic liquids.* Molecular Simulation, 2006. **32**(2): p. 109-115.

50. Mazeau, K.H., L., *Molecular Dynamics Simulations of Bulk Native Crystalline and Amorphous Structures of Cellulose.* The Journal of Physical Chemistry B, 2003. **107**(10): p. 2394-2403.

51. Sun, C.C., *Quantifying errors in tableting data analysis using the Ryshkewitch equation due to inaccurate true density.* Journal of Pharmaceutical Sciences, 2005. **94**(9): p. 2061-2068.

52. Chauve, G., *et al.*, *Cellulose poly(ethylene-co-vinyl acetate) nanocomposites studied by molecular modelling and mechanical spectroscopy.* Biomacromolecules, 2005. **6**(4): p. 2025-2031.

53. Pooley, C.M. and D. Tabor, *Friction and Molecular Structure: The Behaviour of Some Thermoplastics* Proceedings of the Royal Society of London. Series A, Mathematical and Physical Sciences, 1972. **329**: p. 251-274.

54. Wu, S., *Polymer Interface and Adhesion*. 1982, New York: Marcel Dekker.

55. Eskilsson, K. and F. Tiberg, *Equilibrium and kinetic properties of triblock copolymers at hydrophobic surfaces.* Macromolecules, 1997. **30**(20): p. 6323-6332.

56. Eskilsson, K. and F. Tiberg, *Interfacial Behavior of Triblock Copolymers at Hydrophilic Surfaces.* Macromolecules, 1998. **31**(15): p. 5075-5083.

CHAPTER 4

PROBING BOUNDARY LUBRICATION PHENOMENA OF PEO-PPO-PEO TRI-BLOCK COPOLYMERS ON TEXTILE RELEVANT SURFACES VIA LATERAL FORCE MICROSCOPY

ABSTRACT: Boundary lubrication of polyoxyethylene-polyoxypropylene-polyoxyethylene (PEO-PPO-PEO) tri-block copolymers on polypropylene (PP), polyethylene (PE) and cellulose surfaces was investigated via lateral force microscopy (LFM). The molecular configuration formed by the tri-block copolymers on the surface controlled its friction and lubrication behavior. A significant friction reduction was observed on PP and PE surfaces lubricated by PEO/PPO tri-block copolymers. On the contrary, no significant reduction was found for the cellulose surface. A two-layer model was proposed to explain the variation in boundary lubrication on the different surfaces. For PP and PE surfaces, an outer flexible layer was formed by the PEO (buoy) blocks. This layer acted like a liquid resulting in a reduction of friction. The inner well-packed layer, composed of the PPO (anchor) block, was able to tightly adhere to the surface, preventing friction-induced removal of the lubricant. For the cellulose surface the conformation of the outer and inner layers was reversed, and no significant reduction in friction was noticed. X-ray photoelectron spectroscopy (XPS) analysis unveiled a low-oxidation state induced by the adsorbed PEO-PPO-PEO layers on the PP and PE surfaces, corresponding to the buoy-anchor-buoy (B-A-B) configuration of the lubricant on the surface. This was not observed in the case of cellulose surfaces, where an anchor-buoy-anchor (A-B-A) structure of the PEO-PPO-PEO was found to self-assemble during upon treatment.

KEYWORDS: Boundary lubrication, self-assembled structure, multilayer, polypropylene, polyethylene, cellulose, intelligent textile finishes

1. Introduction

During conventional textile manufacturing processes, lubricants are used to reduce friction on the fiber surface and prevent fiber damage. Fiber lubrication can be divided into three categories depending on the gap between the fiber and the sliding surface: boundary lubrication, hydrodynamic lubrication, and semi-hydrodynamic lubrication. Boundary lubrication occurs when a thin lubricant film is formed in the interface of surfaces at low sliding speeds and high contact pressures. Hydrodynamic lubrication occurs in large interfacial spacing where a continuous fluid film extends between two surfaces at high sliding speeds. Studies on fiber lubrication have focused primarily on hydrodynamic lubrication. [1-4] This regime is solely governed by the rheological properties of the lubricant. [5-7] The regime between the boundary and hydrodynamic lubrication is known as the semi-hydrodynamic regime. Semi-hydrodynamic lubricants offer the lowest coefficients of friction. [2, 8]

Boundary lubrication plays an important role in fiber processing, particularly when the fiber surface slides over other surfaces at slow speeds. In the 1960s, Fort et al. [3] studied the boundary regime on synthetic yarns using a conventional boundary friction apparatus. They found that lubricants with polar groups, such as carboxyl groups, significantly reduced friction on synthetic fibers by adsorbing a thin monolayer of lubricant onto the fiber surface. This was not observed when working with non-polar lubricant compounds. More recently, boundary lubrication has been linked to process parameters, such as spinning velocity, normal pressure, and lubricant viscosity. [6, 7, 9]

Little work has been done to correlate of the chemical composition of lubricants and fibers with textile lubrication. [10] In order to gain a fundamental understanding of boundary lubrication, we consider the chemistry of the lubricants and fibers to address the mechanism behind boundary lubrication at a molecular scale.

The lubricants most commonly used in textiles are fatty acids, mineral oils, ethoxylated acids and silicones. [11] They can be cationic, anionic, or nonionic. [12] Recently, nonionic surfactants have been of great interest due to numerous advantages, including good solubility in both water and organic solvents, compatibility with most surfactants, and availability as electrolyte-free material. [13] PEO-PPO-PEO (Pluronic) tri-block copolymer is a nonionic surfactant consisting of two hydrophilic PEO blocks and a hydrophobic PPO block. [14, 15] Pluronic forms bubbles above the critical micelle concentration (cmc). [14-17] The molecular weight and the ratio of PEO to PPO can be adjusted to tailor its properties to various applications including lubricants, texturizers, softeners, emulsifiers, dispersers, antistatic agents and wetting agents. [18] Pluronic copolymers have high wetting and spreading ability which allow the copolymers to form uniform coatings on textiles resulting in low friction, antistatic properties, dye-leveling improvement, and easy-cleaning.

Advanced techniques such as ellipsometry, [19] total internal fluorescence spectroscopy (TIRF), [20] surface plasmon resonance spectroscopy (SPR), [21] and atomic force microscopy (AFM) [22] have been employed to probe molecular structures formed by the hydrophilic and hydrophobic blocks of copolymers on surfaces. Marques *et al.* first proposed a so-called buoy-anchor-buoy model of tri-block copolymers to explain their adsorption on polymer surfaces. [23-25] The model correlates chemical compositions with the molecular self-assembled structures formed on the surface. In this model, the hydrophobic PPO blocks bind strongly to the surface

forming a thin layer while the hydrophilic PEO blocks dangle from the surface, extending into the liquid and forming a free "brush" layer.

Zhang *et al.* reported that when the packing density in the lubricant layers was kept the same, a self-assembled monolayer containing both short and long polymer chains provided lower friction coefficients and improved wear resistance when compared with single-component self-assembled monolayers. [26, 27] Although these studies discuss the PEO-PPO-PEO molecular structures formed on polymer surfaces, the polymers they use are not used in fibers and textile products. To date, no work has been done to relate these studies to polymers used in textile produces. Extending this work to textile relevant polymers would allow the examination of the lubricant molecular structure formed at textile interfaces. This could allow for intelligent design of effective lubrication systems for fiber surfaces.

Lateral force microscopy (LFM) (or friction force microscopy, FFM) has been employed to study molecular structures on hard substrates at micro and nano scales. [28-30] LFM was used to determine that self-assembled perfluorooctyltrichlorosilane (FOTS) and octadecyltrichlorosilane (OTS) monolayers unfolded into different molecular configurations when deposited onto silica wafers. [31] While FOTS has a rigid rod-like helical structure, OTS has a zigzag backbone configuration, offering different lubrication performance.

Friction anisotropy and friction asymmetry were discovered via LFM on monolayers of polydiacetylene. [32, 33] The surfaces in these studies were mica, [34] silica, [35] and graphite[36] substrates. Polymer and fiber surfaces are quite different as they are soft, deformable and highly energy-dissipative. Thus, the study of boundary lubrication on fiber surfaces is more complex. To date, LFM has not been used to determine the molecular structures formed by lubricants on fiber surfaces. [37]

In this paper, thin films of three polymers commonly made into fibers, polypropylene (PP), polyethylene (PE), and cellulose, were spin coated on silica substrates and used as model surfaces. Two solutions of tri-block copolymers varying in the length of their blocks, $EO_{26}PO_{40}EO_{26}$ and $EO_{133}PO_{50}EO_{133}$, were applied to the surfaces. The lateral forces were measured via LFM and the coefficients of friction were calculated to examine lubrication on the model surfaces. X-ray photoelectron spectroscopy (XPS) was employed to analyze chemical composition of the model polymer surfaces before and after lubrication application.

2. Experimental

2.1 Preparation of model surfaces

Polymeric surfaces were prepared following the procedure reported by Song *et al.* [38] 20 mg PE (M_n≈1110, M_w/M_n≈1.11, Sigma Aldrich) or PP (M_n≈5000, M_w/M_n≈2.4, Sigma Aldrich) was dissolved in 10 ml xylene. The solutions were stirred for more than 2 hours under a condensation system. Silica wafers (Waferworld, FL) were washed with H_2SO_4:H_2O_2 (70:30) solution and cleaned by ultraviolet-ozone (UVO) treatment. An IR lamp was used to heat the surfaces and pipettes to a temperature of 85°C. One or two drops of PE or PP solution were spin coated onto the cleaned silicon wafer at 2000 rpm for 20 seconds using a WS-400A-6NPP spin coater (Laurell Technologies). Samples were placed in an oven at 80 °C to evaporate residual solvent. XPS demonstrated the films were pure and no residual solvent was present.

To prepare cellulose surfaces, a method proposed by Gunnars was followed. [39] Clean silica wafers were immersed in polyvinylamide (PVAm, BASF) aqueous solution (100ppm) for 20 min. The PVAm-coated surface was washed with milli-Q water to remove excess PVAm and dried with nitrogen. Polyvinylamide was used as an anchoring polymer to bind cellulose to the silicon wafers. To prepare cellulose solutions, 50 mg of micro-crystalline cellulose (Avicel) were added to a 2.5ml N-

methylmorpholine-N-oxide (NMMO) solution (50 vol. %). The solution was heated and stirred at 115 °C. After the solution became transparent, 7.5ml DMSO was added to adjust the viscosity. A drop of the cellulose solution was filtered through a disc-filter and spin coated at 5000 rpm onto the PVAm-coated silica wafers. Figure 1 shows the height and phase images of silica wafers coated with PP, PE, and cellulose thin films. All polymer coatings were flat and uniform at the macro scale and presented unique topography at the nano scale: granular features for cellulose and PE and fibrillar structures for PP. The root-mean-square roughness (RMS) was less than 6 nm.

2.2 Preparation of lubricant solutions

Two copolymers were used to prepare 1% w/w lubricant solutions: $EO_{26}PO_{40}EO_{26}$ and $EO_{133}PO_{50}EO_{133}$ (BASF). Their chemical structures are shown in Figure 2. The solution concentration of 1%, w/w was larger than the cmc, which is previously reported as being in the range of 10^{-5} to 10^{-3} % w/w. [17, 40]

2.3 X-ray Photoelectron Spectroscopy analysis

XPS spectra were acquired using a Surface Science Instrument SSX-100 X-ray photoelectron spectrometer employing monochromatic AlK α X-rays at 1486.6ev with operating pressure < $2x10^{-9}$ Torr. Photoelectrons were collected at an angle of 55º from the surface. The pass energy of 150V was used for survey scans and the pass energy of 50V for high resolution C 1s peaks. The spot size was 1000 μm.

The polymer substrates (polymer-coated silicon wafers) were submerged in 1% w/w $EO_{19}PO_{29}EO_{19}$ solutions for 24hrs. The wafers were cleaned with DI water and 95% ethanol, and dried with a gentle jet of compressed, filtered air. The lubricant treated polymer thin films were examined by XPS and compared to the XPS spectra of silica and neat lubricant.

2.4 Lateral force microscopy

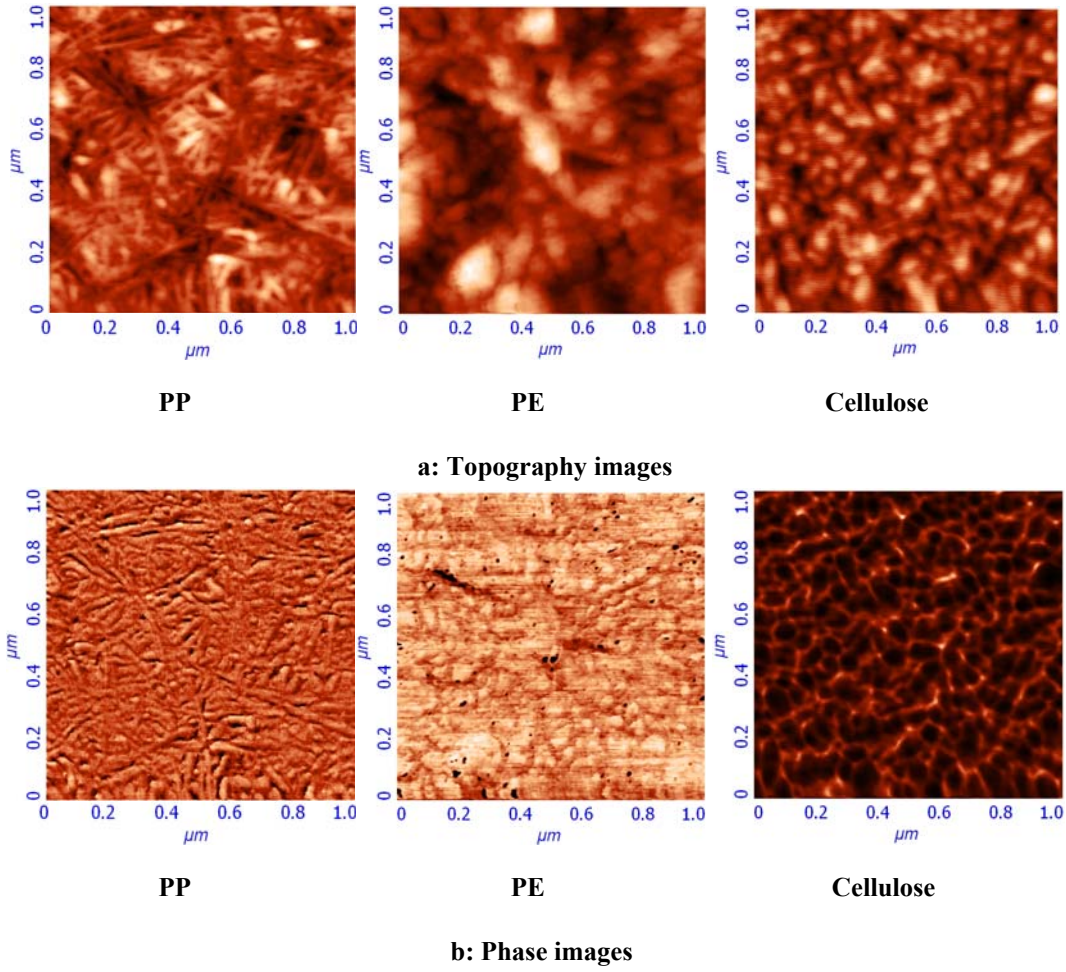

Figure 1. 1-µm AFM images of PP, PE, and cellulose thin films spin-coated on silica wafers in a dry state.

Lateral force microscopy (TEGRA Prima, NT-MDT) was employed to probe friction properties of the model polymer surfaces. Measurements were conducted in air (air-test), in DI water (water-test), and a 1% by weight lubricant solution (lubricant-test). Before imaging, each surface was cleaned with DI water and 95% ethanol and dried with compressed air. A MikroMasch contact mode probe with a force constant of 0.35N/m was used. In both immersion tests (water-test and lubricant-test), the respective solution was injected into a liquid metal cell in which the wafer

samples were positioned. All of the tests were performed with a scan frequency of 1 Hz and a scan size of 1 μm. Both topography and lateral force images of the samples were collected simultaneously. Each image consisted of 256×256 pixels (see Figure 1).

3. Results and discussion

3.1 XPS analysis

Relative element percentages (C, O, Si) on each surface from XPS measurements are given in Table 1. The bare silicon wafer showed peaks for oxygen, carbon, and silicon. The oxygen peak is likely due to silicon oxide formed when the wafer was exposed to air. [41] The untreated PE and PP surfaces showed more than 96% carbon indicating that the silicon wafers were well covered by the polymers during the spin-coating process. The polymer surfaces were treated with $EO_{19}PO_{29}EO_{19}$ and measured by XPS after rinsing and drying. The treated PE surface showed only 28.8% carbon, 37.2%

Table 1. Relative element percentages on surfaces from XPS measurements

Sample	Element (%)		
	"C"	**"O"**	**"Si"**
bare silicon	15.33	41.12	43.56
$EO_{19}PO_{29}EO_{19}$	72.42	27.58	-
PE	96.35	2.43	1.23
PE + $EO_{19}PO_{29}EO_{19}$	28.80	37.21	34.00
PP	99.26	0.74	-
PP + $EO_{19}PO_{29}EO_{19}$	98.76	1.24	-
Cellulose	58.49	40.05	1.46
Cellulose + $EO_{19}PO_{29}EO_{19}$	55.84	39.47	4.68

oxygen, and 34.0% silicon. Due to the significant amount of silicon, it was likely that PE coating was removed by rinsing. After rinsing, carbon remained as the primary element on the PP surface, suggesting the PP remained as a continuous layer on the silica. This suggests that the PP layer was more robust than the PE surface. XPS spectra on the cellulose surface showed a chemical composition of 58.5% carbon,

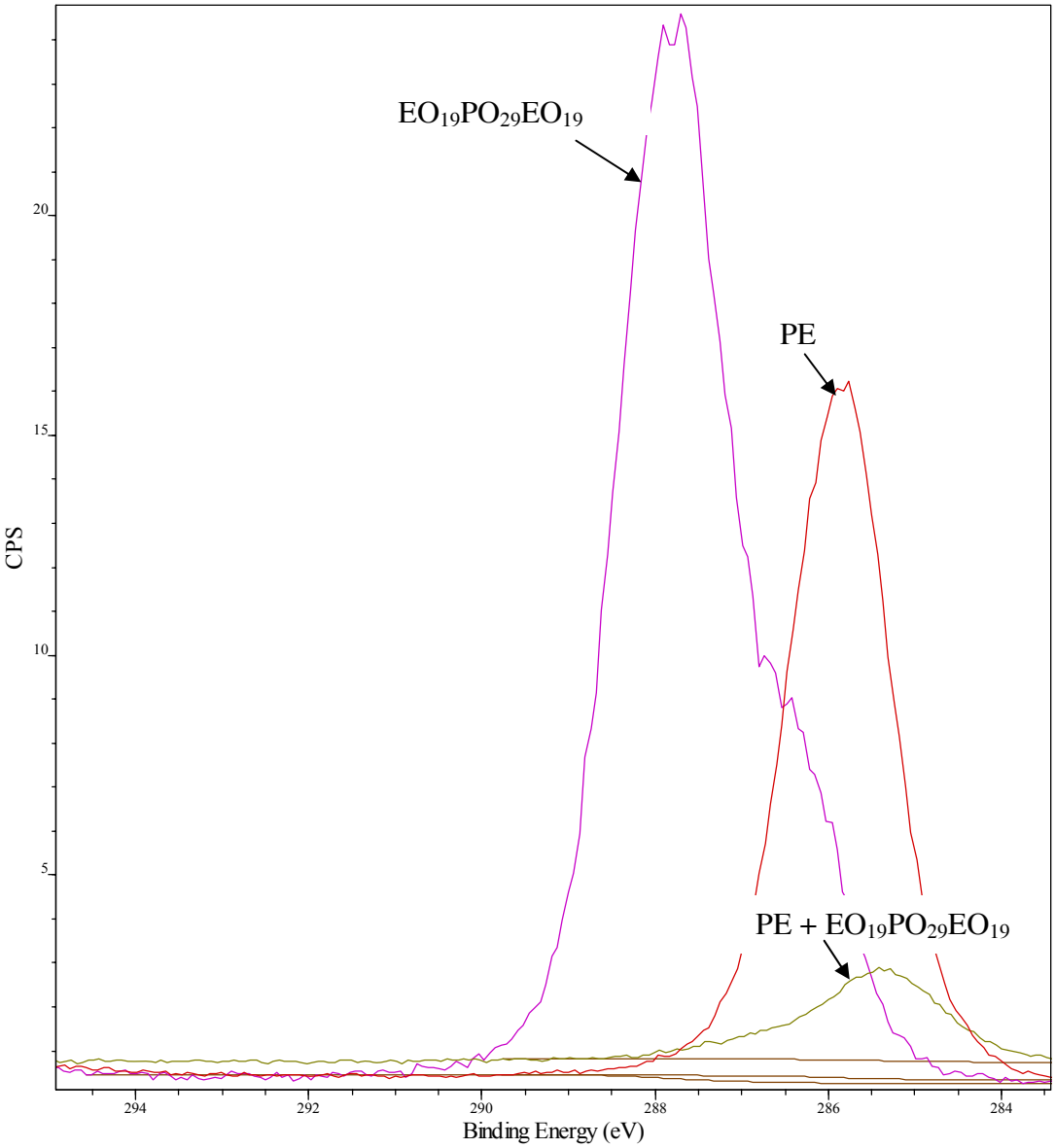

Figure 2. Normalized C 1s spectra: $EO_{19}PO_{29}EO_{19}$, PE, and PE+ $EO_{19}PO_{29}EO_{19}$.

40.1% oxygen, and 1.5% silicon. After treatment, XPS showed a small increase in silicon and a small decrease in carbon and oxygen on the surface, indicating some cellulose may have been removed by rinsing. A thinning of the cellulose layer may place the underlying silicon layer within the probe depth of XPS (10 nm). [42] The small increase in silicon was due to signal contributions from the silica substrate in areas where the thickness of cellulose films was less than 10 nm.

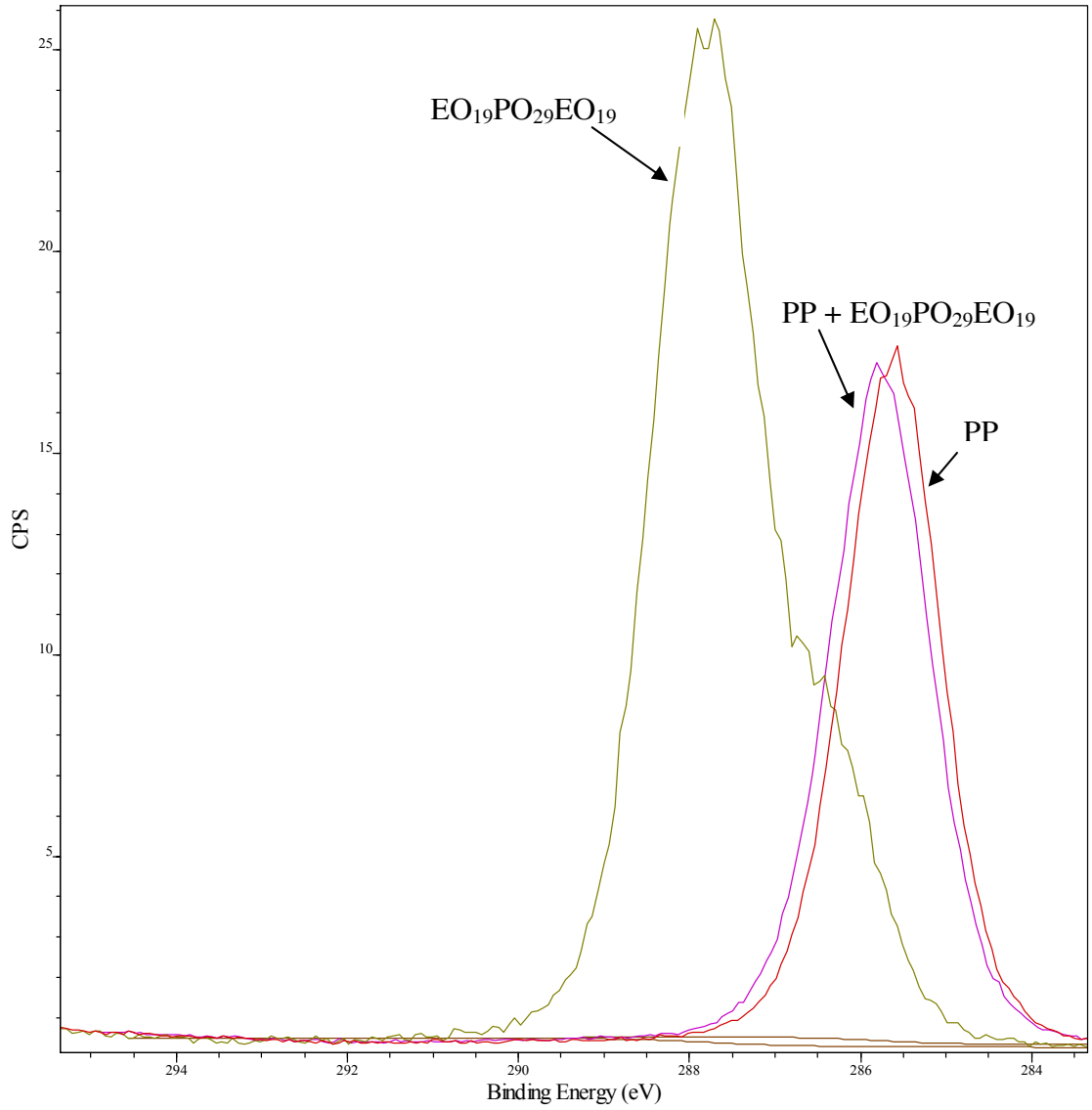

Figure 3. Normalized carbon 1s spectra: $EO_{19}PO_{29}EO_{19}$, PP, and PP+ $EO_{19}PO_{29}EO_{19}$.

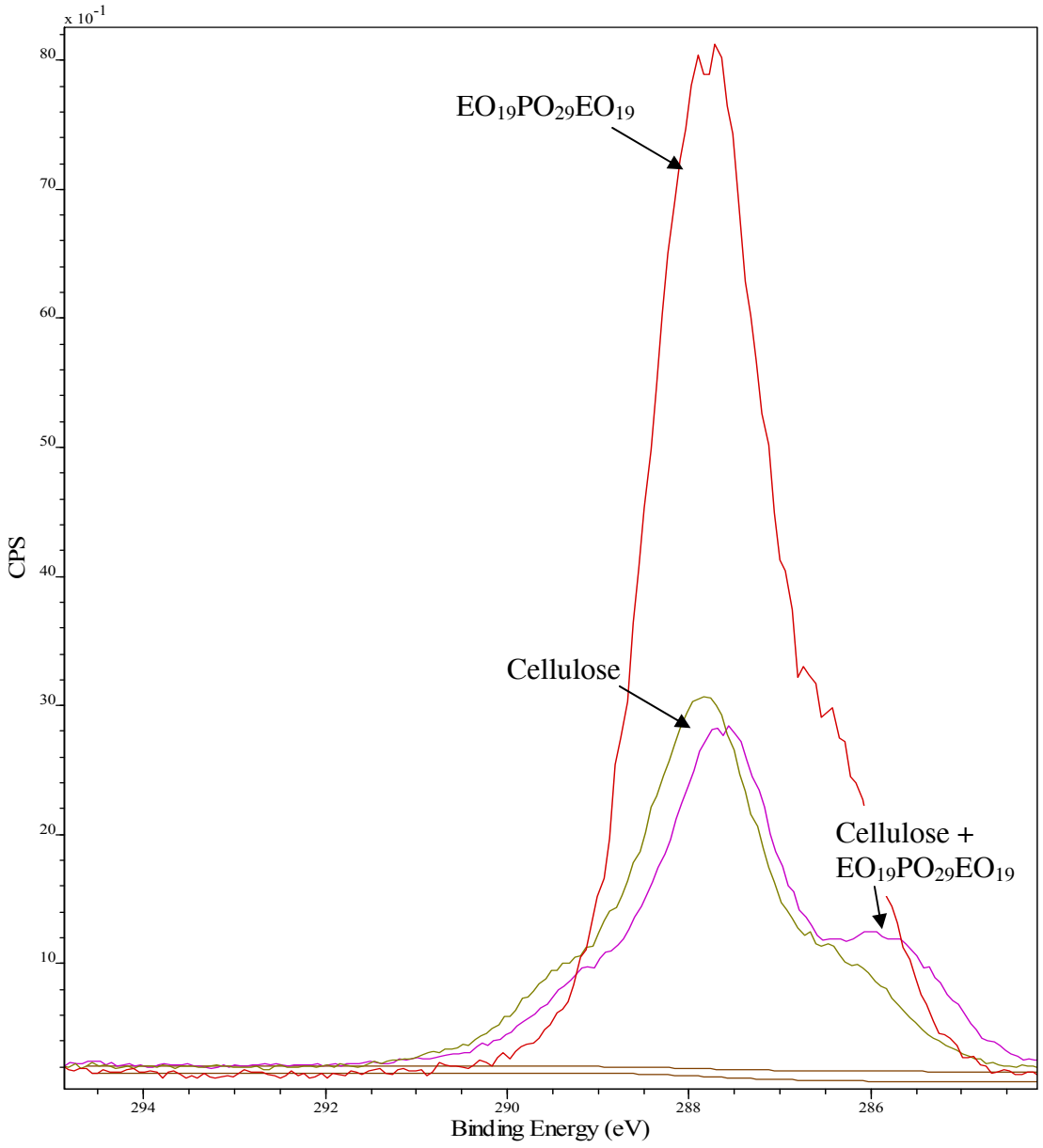

Figure 4. Normalized carbon 1s spectra: $EO_{19}PO_{29}EO_{19}$, cellulose, and cellulose+ $EO_{19}PO_{29}EO_{19}$.

To investigate the details of treatment effects of $EO_{19}PO_{29}EO_{19}$ to the chemical structures of the polymer surfaces, a multi-component model analysis was adapted for the C 1s peaks. The C 1s peaks of the $EO_{19}PO_{29}EO_{19}$ and the treated and untreated PE surfaces are shown in Figure 2. By means of curve fitting, a 4-component model was

created to fit the C 1s peak. These 4 components showed fine structures of carbon interacting with other atoms in the PE chains. [43] While comparing the two models for the treated and untreated PE substrate in Table 4, the 4th component shifted

Table 2. Binding energy and corresponding area percentage in the 4-component models for the untreated and treated PE surface

Sample	Binding energy (eV): Areas (%)of C 1s components			
	1	2	3	4
PE	285.71:61.88	286.02:30.94	286.49:6.19	286.88:0.99
PE+$EO_{19}PO_{29}EO_{19}$	285.34:48.60	286.02:24.31	286.95:22.66	289.83:4.43

Table 3. Binding energy and corresponding area percentage in the 4-component models for the untreated and treated PP surface

Sample	Binding energy (eV): Areas (%)of C 1s components	
	–C*H_2–/–C*H_3	**–C*(CH_3)H–**
PP	285.72 : 64.67	285.50 : 35.33
PP+ $EO_{19}PO_{29}EO_{19}$	285.75 : 71.08	285.85 : 28.92

Table 4. Binding energy and corresponding area percentage in the 4-component models for the untreated and treated cellulose surface

Sample	Binding energy (eV): Areas (%)of C 1s components		
	–C*OH	**–C*(C, H)**	**-O-C*-O-**
Cellulose	287.83:54.56	286.34:22.18	289.10:23.26
Cellulose+ $EO_{19}PO_{29}EO_{19}$	287.59:50.19	285.86:26.97	288.86:22.84

towards higher binding energy (289.83eV) after treatment. It was found that the carbon peak in $EO_{19}PO_{29}EO_{19}$ was at 289. 52eV. The higher binding energy

(289.83eV) of the 4th component of carbon on treated PE surface indicated that some $EO_{19}PO_{29}EO_{19}$ residue was perhaps left on the substrate after rinsing. According to Table 1, after treatment the amount of oxygen on the PE surface increased due to of the $EO_{19}PO_{29}EO_{19}$ residue.

The same curve fitting process was done to the C 1s peaks for PP and cellulose surfaces (Figure 3 and 4). A 2-component model showed two types of carbon: –C*H_2– /–C*H_3 and –C*(CH_3)H– in the PP chains. Table 3 shows the chemical shifts. After treatment a slight chemical shift was detected, confirming that PP remained a continuous layer on the silica support after the treatment. In addition, the oxygen peak was found to increase slightly, indicating little $EO_{19}PO_{29}EO_{19}$ remained on the treated PP after rinsing. A 3-component model was fit to the C 1s peak for the treated and untreated cellulose. Table 6 shows three kinds of carbon: -C*OH, -C*(C, H), and –OC*O- on the surfaces. Aliphatic carbon is typically shown in an XPS spectrum for cellulose. [44] The change was very little either in the binding energy and component percentage. It was suggested that no $EO_{19}PO_{29}EO_{19}$ was left on the cellulose surface after rinsing.

3.2 Friction coefficient

3.2.1 Polypropylene surface

PP surfaces were probed via LFM in air, water, and lubricant solutions. Topographical images and friction coefficient curves are shown in Figure 5. The PPO block of the tri-block copolymer had a higher affinity towards the PP surface than the PEO block. A buoy-anchor-buoy (B-A-B) arrangement of the tri-block copolymers in relation to the PP surface was proposed as shown in Figure 8. The anchoring PPO block tightly bounds on the PP surface resulting in a low mobility of the PPO block. The PPO block behaved as an inner well-packed layer, protecting the surface against abrasion. Meanwhile, two PEO blocks behaved as an outer canopy layer with high,

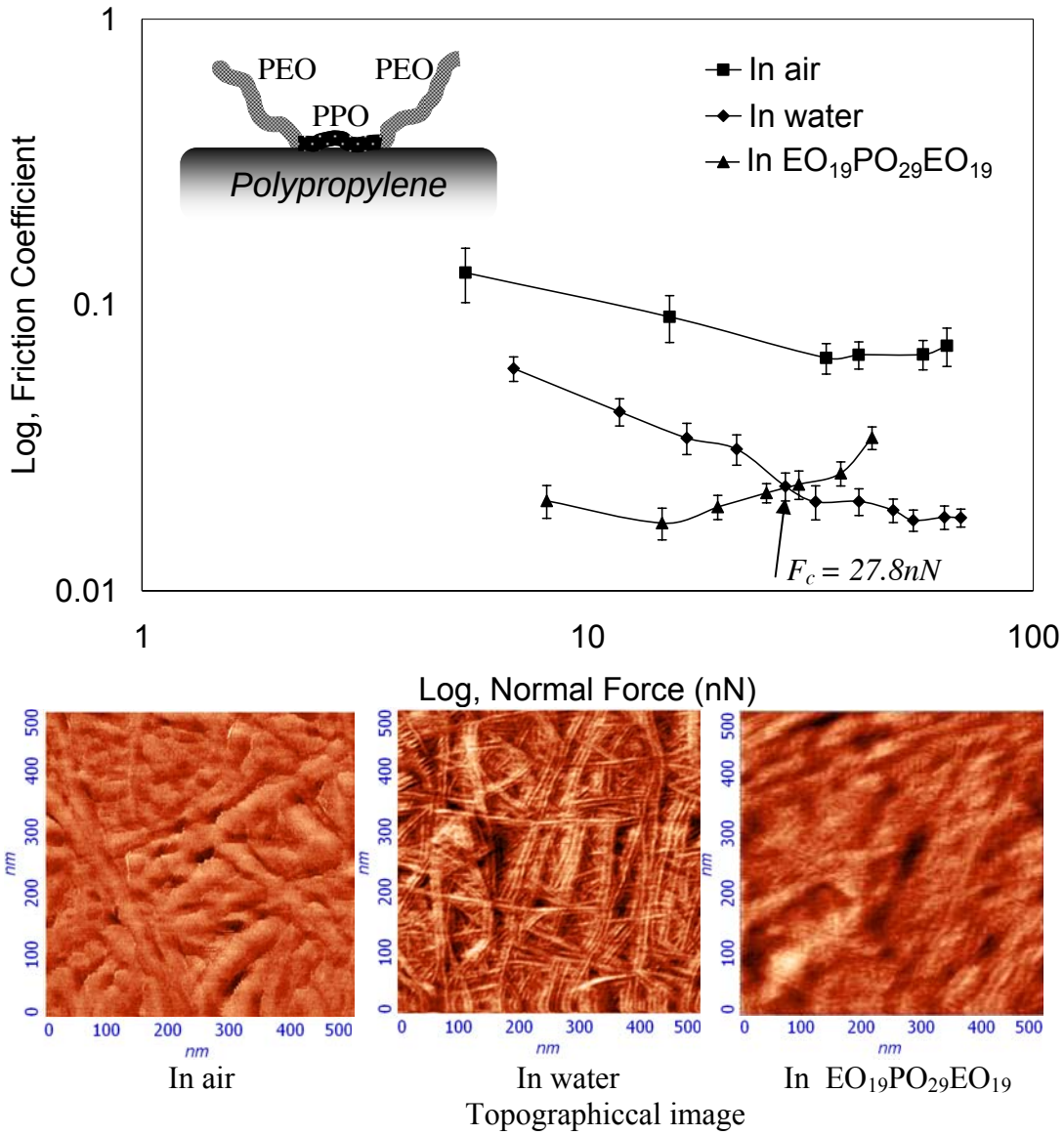

Figure 5. The proposed buoy-anchor-buoy structure and logarithmic relationship of friction coefficient and normal force on polypropylene surfaces in three conditions: in air, in water, in $EO_{19}PO_{29}EO_{19}$ solution. Friction coefficients decreased while the normal forces increased when the surfaces were in air and water. In $EO_{19}PO_{29}EO_{19}$ solution, the friction coefficients first kept constant and the average was lower than those in water. When the normal forces increased to a critical point, F_c = 27.8 nN, the friction coefficients increased. Topographical images in air, in water, in $EO_{19}PO_{29}EO_{19}$ solution.

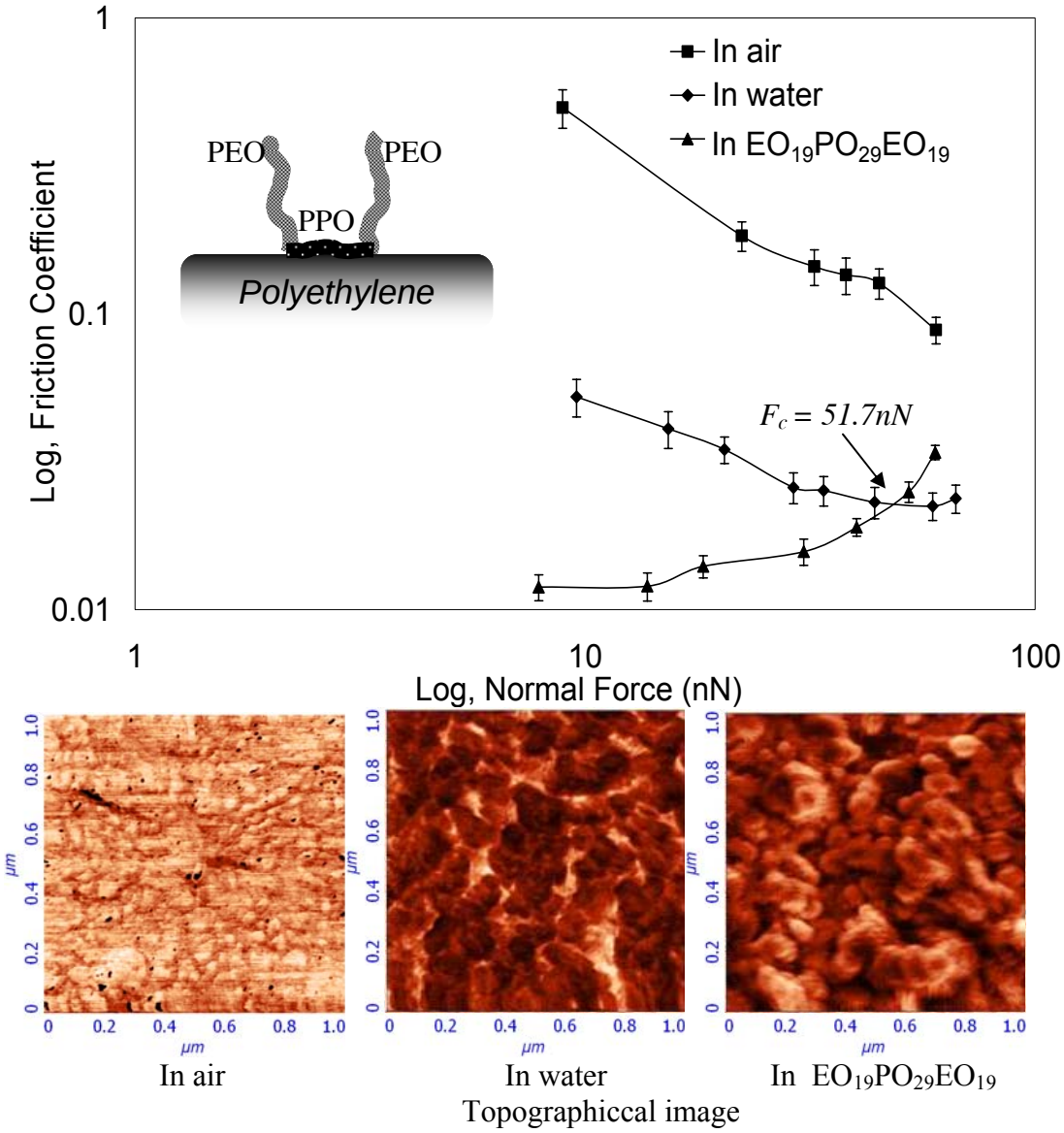

Figure 6. The proposed buoy-anchor-buoy structure and logarithmic relationship of friction coefficient and normal force on polyethylene surfaces in three conditions: in air, in water, in $EO_{19}PO_{29}EO_{19}$ solution. Friction coefficients decreased while the normal forces increased when the surfaces were in air and water. In $EO_{19}PO_{29}EO_{19}$ solution, the friction coefficients first kept constant and the average was lower than those in water. When the normal forces increased to a critical point, F_c = 51.7 nN, the friction coefficients increased rapidly. Topographical images in air, in water, in $EO_{19}PO_{29}EO_{19}$ solution.

liquid-like mobility and low shear resistance, serving as an effective lubricant. The PEO blocks were hydrophilic and floated away from the surface as tails. Similar self-assembled structures of the same tri-block copolymer were reported on hydrophobic non-polymeric surfaces. [22, 45, 46]

When the external force increased to a critical point of approximately 30nN, the friction coefficients rapidly increased to similar to those measured in air (Figure 5). This is most likely because the critical force caused a dramatic change in the molecular structure of the lubricant layers. The critical force most likely damages the self-assembled layers, destroying the organization in their structures and preventing them from functioning as an effective lubricant.

3.2.2 Polyethylene surface

Figure 6 illustrates the topographical images of polyethylene surfaces in air, water, and lubricant solutions as well as the friction coefficients curves against the normal force in the corresponding environments. Scratch and plowing was shown in the surface morphology when the PE surface was imaged in air. These marks disappeared after water was added, and a clearer morphology was obtained under the presence of lubricants in solution. Based on the finding that the PPO block in the tri-block copolymers had higher affinity towards the PE surfaces, it was proposed that a similar B-A-B structure is formed on the PE surface shown in Figure 6. A large stretching force occurred to the PEO blocks, extending them away from the PE surface. The outer PEO layer was more flexible on the PE surface than on the PP surface.The critical normal force was found to be 40nN. After the critical force, the self-assembled structure breaks down decreasing lubrication performance.

3.2.3 Cellulose surface

No dramatic difference in surface morphology was observed between the topographical images in water, air, and lubricant for the cellulose surface (see Figure

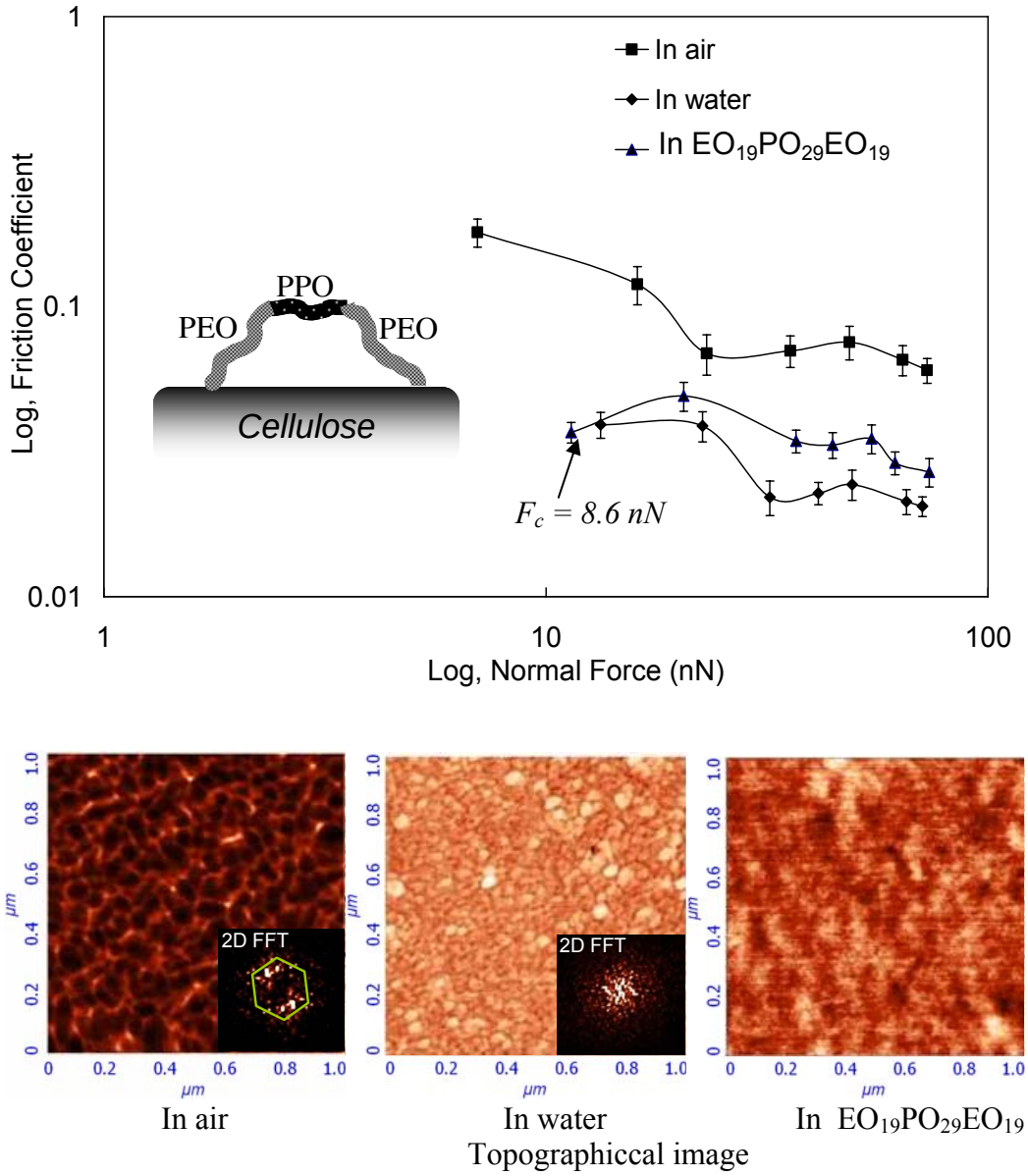

Figure 7. The proposed anchor-buoy-anchor structure and logarithmic relationship of friction coefficient and normal force on cellulose surfaces in three conditions: in air, in water, and in $EO_{19}PO_{29}EO_{19}$ solution. Friction coefficients decreased while the normal forces increased when the surfaces were in air and water. In $EO_{19}PO_{29}EO_{19}$ solution, the friction coefficients kept constant and the average was lower than those in air but higher than those in water. Topographical images in air, in water, in $EO_{19}PO_{29}EO_{19}$ solution.

7). The friction coefficient curves indicated that water reduced the friction coefficients similar to the phenomenon observed on PP and PE surfaces. The addition of lubricant, however, the friction coefficients with lubricants were higher than those measured in water alone. The critical normal force was 8.6 nN. It was lower than those for PP and PE surfaces. The

In contrast to the PP and PE surfaces, the PEO block had a higher affinity towards cellulose than the PPO block as discussed in the chapter 2. A reversed structure, anchor-buoy-anchor (A-B-A), was proposed for the cellulose surface shown in Figure 10. The PEO blocks anchored on the hydrophilic cellulose surface and the PPO block was repelled from the surface. [22] The PPO buoy block had poor mobility because it was constricted by the two anchored PEO blocks. The A-B-A structure of the copolymer layers could not produce an efficient lubrication. As for the cellulose surfaces, there was no critical force detected in the experimental range of normal forces, as in the cases of PP and PE. One possibly reason might be that the critical force was quite low and beyond the experimental range.

4. Lubrication mechanism on PP, PE and Cellulose surfaces

The lubricants reduced friction coefficients on PE and PP surfaces, but not on the cellulose surface. On the basis of the buoy/anchor structures in the PEO-PPO-PEO copolymers, we proposed a two-layer model to explain the mechanism of boundary lubrication on the model surfaces. Figure 8 shows a schematic diagram of the two-layer model consisting of two layers at a molecular scale. The molecular configuration of the two-layer model depends on interaction of the lubricant with the polymer coated surface. On the PP and PE surfaces (see Figure 8 (a) and (b), respectively), the PPO segments of the lubricant anchor on the solid surface to create a well-packed inner layer. Above the inner layer, an outer layer is constructed by soft segments that float away from the solid surface. The outer layer plays a critical role in boundary

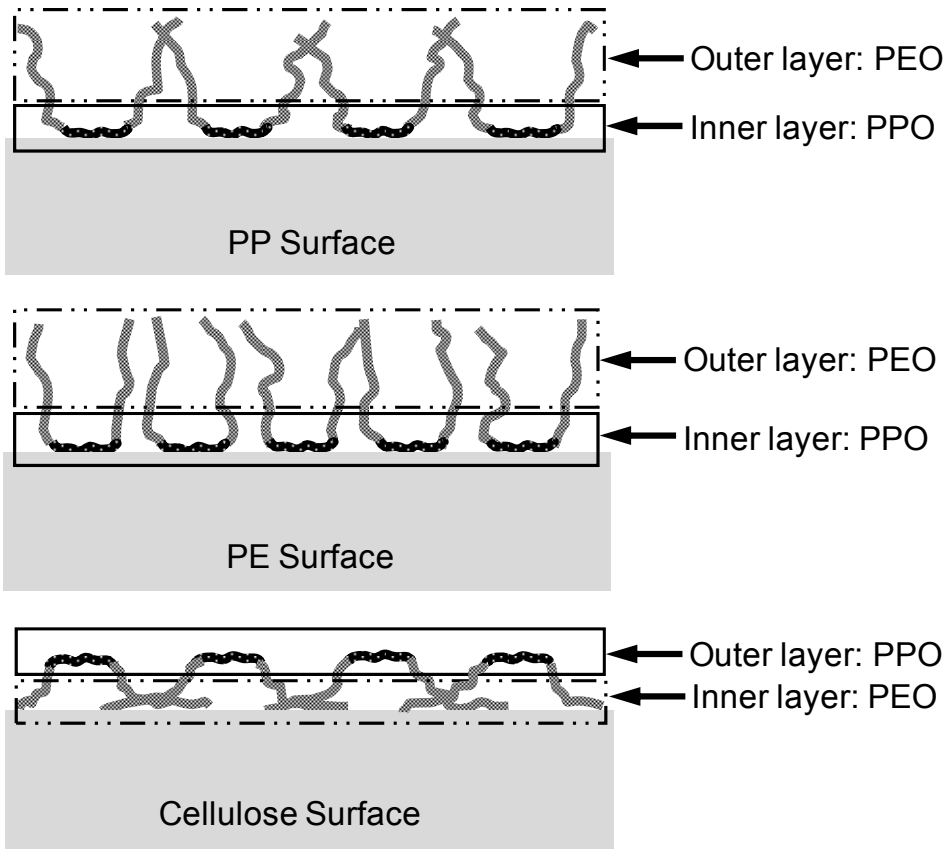

Figure 8. Schematic diagram of a double-layer model. (a) On the PP surface: an outer layer composed of the flexible PEO chains; an inner layer composed of the restricted PPO segments due to the B-A-B structure. The B-A-B structure corresponds with a low friction coefficient on surfaces. (b) On the PE surface: an outer layer composed of the flexible PEO chains, which are more perpendicular to the surface due to larger stretching force; an inner layer composed of the restricted PPO segments due to the B-A-B structure. The more perpendicular PEO chains in the B-A-B structure promote friction reduction on the surface. (c) On the cellulose surface: an outer layer composed of the restricted PPO segments due to the A-B-A structure; an inner layer composed of the hindered PEO segments with far less mobility. The A-B-A structure is associated with a high friction coefficient on surfaces.

lubrication. Molecules on the outer layer are highly flexibility. When a solid object slides on the surface, the outer flexible layer behaves like a liquid. The dislocation caused by the external forces is easily relieved, resulting in the friction reduction on the surface.

It is possible that high normal and lateral forces might penetrate the outer layer. The inner layer is well-packed and effectively prevents further penetration, resulting in the protection of the surface. In other words, the multilayer structure provides a gradient of sliding resistance on the surface. An energy dissipation mechanism states that friction costs energy which transforms into heat while two objects slide against each other. [47, 48]

There are several examples in literature where a similar friction reduction is observed in surfaces with extending flexible polymeric chains. One example is a polystyrene (PS)/polydimethylsiloxane (PDMS) diblock copolymer deposited on polystyrene surfaces. In this copolymer layer, the PS block penetrates the PS surfaces leaving flexible PDMS tails outstretched from the surface to produce low friction coefficients effectively functioning as a lubricating layer. [49] Hydrogels with brush-like dangling chains have been reported to produce a better lubrication than those without such flexible chains on their surfaces. [50-52] If the upper layers are crossed-linked, the networks with larger average length between adjacent crossed-linked points are more flexible and thus decrease the friction coefficient to a higher degree than those having tight cross-linking structures. This behavior is due to the mobility of the polymer chains [53].

On the cellulose surface (see Figure 8(c)), the A-B-A model suggests the outer layer is composed of restricted PPO segments and the inner layer composed of hindered PEO segments with far less mobility. Due to the lack of flexibility in the outer layer,

the A-B-A structure in the reverse two-layer model is associated with a high friction coefficient.

5. Conclusions

During boundary lubrication, important molecular processes such as molecular rearrangements, friction-induced chemical reactions, and self-assembled formations occur mainly due to molecular interaction forces. We have used lateral force microscopy to study the boundary lubrication of $EO_{19}PO_{29}EO_{19}$ tri-block copolymers on PP, PE, and cellulose model surfaces.

Surface friction coefficients indicated that the adsorption of the tri-block copolymers reduced friction on the PP and PE coated surfaces. A critical value for normal force was observed at 27.8 nN for the PP and 51.7 nN for the PE. When the normal forces were too large, the self-assembled structures of lubricant layers were destroyed and could no longer produce sufficient boundary lubrication.

Due to affinity differences between PEO and PPO for the polymer-coated surfaces, the B-A-B structure of the tri-block copolymers was proposed for the PP and PE surfaces while the A-B-A structure for the cellulose surface. A two-layer model was proposed which suggests the tri-block copolymers created a flexible outer layer of PEO blocks and a well-packed inner layer of PPO blocks on the PP and PE surfaces, resulting in low friction coefficients. In a contrast, the outer and inner layers were reversed on the cellulose surfaces. The outer layer consisted of the constrained PPO blocks (buoy), which could not contribute to friction reduction. These lubricating layers of PEO-PPO-PEO triblock copolymers did not permanently attach to the surfaces and could be removed after rinsing.

The PEO-PPO-PEO tri-block copolymers have been recognized to form unique molecular structures. The conformations and behavior of these molecular structures are essential to the function of lubricants as these molecular structures influence the

friction and wear behavior of materials. Correlating their lubrication properties with molecular self-assembled structures allows the intelligent design of efficient textile lubricants.

Acknowledgement

This work was supported by the National Textile Center under Grant No. C05-NS09. We thank Dr. Laura McJilton, Alejandra Andere Jones, and Christina Diaz for their English correction of the manuscript.

REFERENCES

1. Schick, M.J., Friction and Lubrication of Synthetic Fibers Part VII: Effect of Guide Temperature' Textile Research Journal, 1980. 50(11): p. 675-681.

2. Schlatter, C., R.A. Olney, and B.N. Baer, Concerning the Mechanisms of Fiber and Yarn Lubrication. Textile Research Journal, 1959. 29(3): p. 200-210.

3. Fort, T.J. and J.S. Olsen, Boundary Friction of Textile Yarns. Textile Research Journal, 1961. 31: p. 1007-1011.

4. Schick, M.J., Friction and Lubrication of Synthetic Fibers: Part II : Two-Component Systems Textile Research Journal, 1973. 43(4): p. 198-204.

5. Hansen, W.W. and D. Tabor, Role of Hydrodynamic Lubrication in the Friction of Fibers and Yarns. Journal of Applied Physics, 1956. 27: p. 1558--1559.

6. Schick, M.J., Friction and Lubrication of Synthetic Fibers Part I: Effect of Guide Surface Roughness and Speed on Fiber Friction Textile Research Journal, 1973. 43(2): p. 103-109.

7. Schick, M.J., Friction and Lubrication of Synthetic Fibers Part IV: Effect of Fiber Material and Lubricant Viscosity and Concentration Textile Research Journal, 1973. 43(6): p. 342-347.

8. Olsen, J.S., Textile Research Journal, 1969. 39(1): p. 31-37.

9. Schick, M.J., Friction and Lubrication of Synthetic Fibers Part V : Effect of Fiber Luster, Guide Material, Charge, and Critical Surface Tension of Fibers on Fiber Friction Textile Research Journal, 1974. 44(10).

10. Behary, N., et al., Using an electronic microbalance technique to study the stick-slip behavior of lubricated polypropylene fibers. Journal of Applied Polymer Science, 2003. 89(3): p. 645-654.

11. Postman, W., Spin Finishes Explained. Textile Research Journal, 1980. 50(7): p. 444-453.

12. Briscoe, B.J. and F. Motamedi, Role of Interfacial Friction and Lubrication in Yarn and Fabric Mechnics. Textile Research Journal, 1990. 60(12): p. 697-708.

13. Rosen, M.J., Surfactants and Interfacial Phenomena. 3 ed. 2004: John Wiley and Sons. 444.

14. Prasad, K.N., et al., Surface activity and association of ABA polyoxyethylene—polyoxypropylene block copolymers in aqueous solution Journal of Colloid and Interface Science, 1979. 69(2): p. 225-232.

15. Yu, G., et al., Micellisation and gelation of triblock copoly(oxyethylene/oxypropylene/oxyethylene), F127. Journal of the Chemical Society, Faraday Transactions 1992. 88: p. 2537-2544.

16. Alexandridis, P., et al., Surface Activity of Poly(ethylene oxide)-block-Poly(propylene oxide)-block-Poly(ethylene oxide) Copolymers. Langmuir, 1994. 10(8): p. 2604-2612.

17. Wanka, G., H. Hoffmann, and W. Ulbricht, The aggregation behavior of poly-(oxyethylene)-poly-(oxypropylene)-poly-(oxyethylene)-block-copolymers in aqueous solution Colloid & Polymer Science, 1990. 268(2): p. 101-117.

18. Schmolka, I.R., Block polymer nonionic surfactants in textiles. JAOCS, J. Am. Oil Chem. Soc. FIELD Full Journal Title:, 1982. 59(7): p. 322-7.

19. Malmsten, M. and F. Tiberg, Adsorption of ethyl(hydroxyethyl) cellulose at polystyrene. Langmuir FIELD Full Journal Title:Langmuir, 1993. 9(4): p. 1098-103.

20. Fu, Z. and M.M. Santore, Kinetics of Competitive Adsorption of PEO Chains with Different Molecular Weights. Macromolecules FIELD Full Journal Title:Macromolecules, 1998. 31(20): p. 7014-7022.

21. Brandani, P. and P. Stroeve, Kinetics of Adsorption and Desorption of PEO-PPO-PEO Triblock Copolymers on a Self-Assembled Hydrophobic Surface. Macromolecules FIELD Full Journal Title:Macromolecules, 2003. 36(25): p. 9502-9509.

22. Wu, C., et al., Atomic force microscopy study of E99P69E99 triblock copolymer chains on silicon surface. Langmuir FIELD Full Journal Title:Langmuir, 2000. 16(2): p. 656-661.

23. Alexandridis, P., Poly(ethylene oxide)/poly(propylene oxide) block copolymer surfactants. Curr. Opin. Colloid Interface Sci. FIELD Full Journal Title:Current Opinion in Colloid & Interface Science, 1997. 2(5): p. 478-489.

24. Eskilsson, K. and F. Tiberg, Equilibrium and kinetic properties of triblock copolymers at hydrophobic surfaces. Macromolecules FIELD Full Journal Title:Macromolecules, 1997. 30(20): p. 6323-6332.

25. Marques, C., J.F. Joanny, and L. Leibler, Adsorption of block copolymers in selective solvents. Macromolecules FIELD Full Journal Title:Macromolecules, 1988. 21(4): p. 1051-9.

26. Zhang, Q. and L.A. Archer, Boundary Lurication and Surface Mobility of Mixed Alkylsilane Self-assembled Monolayers. Journal of Physical Chemistry B, 2003. 107(47): p. 13123-13132.

27. Zhang, Q. and L.A. Archer, Interfacial Friction of Surfaces Grafted with One- and Two-Component Self-Assembled Monolayers. Langmuir FIELD Full Journal Title:Langmuir, 2005. 21(12): p. 5405-5413.

28. Carpick, R.W., et al., Friction force microscopy investigations of potassium halide surfaces in ultrahigh vacuum: structure, friction and surface modification. Tribol. Lett. FIELD Full Journal Title:Tribology Letters, 1998. 5(1): p. 91-102.

29. Ruan, J.-A. and B. Bhushan, Atomic-scale and microscale friction studies of graphite and diamond using friction force microscopy. Journal of Applied Physics, 1994. 76(9): p. 5022.

30. Sundararajan, S. and B. Bhushan, Static friction and surface roughness studies of surface micromachined electrostatic micromotors using an atomic force/friction force microscope. Journal of Vacuum Science and Technology A, 2001. 19(4): p. 1777-1785.

31. Devaprakasam, D., et al., Boundary lubrication additives for aluminum: A journey from nano to macro tribology. Tribol. Int. FIELD Full Journal Title:Tribology International, 2005. 38(11-12): p. 1022-1034.

32. Bluhm, H., et al., Anisotropy of sliding friction on the triglycine sulfate (010) surface. Appl. Phys. A: Mater. Sci. Process. FIELD Full Journal Title:Applied Physics A: Materials Science & Processing, 1995. 61(5): p. 525-33.

33. Carpick, R.W., D.Y. Sasaki, and A.R. Burns, Large friction anisotropy of a polydiacetylene monolayer. Tribol. Lett. FIELD Full Journal Title:Tribology Letters, 2000. 7(2,3): p. 79-85.

34. Marti, O., J. Colchero, and J. Mlynek, Combined scanning force and friction microscopy of mica. Nanotechnology, 1990. 1(2): p. 141-144.

35. Bhushan, B., H. Liu, and S.M. Hsu, Adhesion and Friction Studies of Silicon and Hydrophobic and Low Friction Films and Investigation of Scale Effects. Journal of Tribology, 2004. 126(3): p. 583-590.

36. Sasaki, N., K. Kobayashi, and M. Tsukada, Atomic-scale friction image of graphite in atomic-force microscopy. Physical Review B, 1996. 54(3): p. 2138-2149.

37. Behary, N., G.A. El Achari, and C. Caze, Tribological analysis of glass fibers using atomic force microscopy (AFM)/lateral force microscopy (LFM). Journal of Applied Polymer Science, 2000. 75(8): p. 1013-1025.

38. Song, J., et al., Development and Charaterization of thin polymer films relevant to fiber processing. Thin Solid Films, 2009. Article in Press.

39. Gunnars, S., L. Wagberg, and M.A.C. Stuart, Model films of cellulose: I. Method development and initial results. Cellulose, 2002. 9(3-4): p. 239-249.

40. Diakova, B., M. Kaisheva, and D. Platikanov, Thin liquid films from polyoxyethylene-polyoxypropylene-block copolymer on the surface of fused quartz. Colloids and Surfaces A: Physicochemical and Engineering Aspects, 2001. 190(1-2): p. 61-70.

41. Ha, H.-K., et al., Open air plasma chemical vapor deposition of highly dielectric amorphous TiO[sub 2] films. Applied Physics Letters, 1996. 68(21): p. 2965-2967.

42. Fu, Y., et al., Hydrogen-Bonding-Directed Layer-by-Layer Multilayer Assembly: Reconformation Yielding Microporous Films. Macromolecules, 2002. 35(25): p. 9451-9458.

43. Briggs, D. and N. Fairley, XPS of chemically modified low-density polyethylene surfaces: Observations on curve-fitting the C 1s spectrum. Surf. Interface Anal. FIELD Full Journal Title:Surface and Interface Analysis, 2002. 33(3): p. 283-290.

44. Shchukarev, A., et al., XPS study of living tree. Surf. Interface Anal. FIELD Full Journal Title:Surface and Interface Analysis, 2002. 34(1): p. 284-288.

45. Wang, A., et al., Direct force measurement of silicone- and hydrocarbon-based ABA triblock surfactants in alcoholic media by atomic force microscopy. J. Colloid Interface Sci. FIELD Full Journal Title:Journal of Colloid and Interface Science, 2002. 256(2): p. 331-340.

46. Florent, M., et al., Self-Assembly of Pluronic Block Copolymers in Aqueous Dispersions of Single-Wall Carbon Nanotubes as Observed by Spin Probe EPR. Langmuir, 2008. 24(8): p. 3773-3779.

47. Harrison, J.A., et al., Investigation of the atomic-scale friction and energy dissipation in diamond using molecular dynamics. Thin Solid Films, 1995. 260(2): p. 205-211.

48. Singer, I.L., Friction and energy dissipation at the atomic scale - a review, in Tribology Series, D. Dowson, Editor. 1994, Elsevier. p. 3-20.

49. Brown, H.R., Chain pullout and mobility effects in friction and lubrication. Science (Washington, D. C., 1883-) FIELD Full Journal Title:Science (Washington, DC, United States), 1994. 263(5152): p. 1411-13.

50. Gong, J.P. and Y. Osada, Surface friction of polymer gels. Progress in Polymer Science, 2002. 27(1): p. 3-38.

51. Lee, S. and N.D. Spencer, Aqueous lubrication of polymers: Influence of surface modification. Tribology International, 2006. 38(11-12): p. 922-930.

52. Tada, T., et al., Surface Friction of Poly(dimethyl Siloxane) Gel and Its Transition Phenomenon Tribology Letters, 2004. 17(3): p. 505-511.

53. Lee, S., et al., Boundary Lubrication of Oxide Surfaces by Poly(L-lysine)-g-poly(ethylene glycol) (PLL-g-PEG) in Aqueous Media Tribology Ietters, 2003. 15(3): p. 231-239.

CHAPTER 5

ADSORPTION AND LUBRICATION OF PEO/PPO TRI-BLOCK COPOLYMERS ON CELLULOSE AND POLYPROPYLENE THIN FILMS ---- A COMBINATION STUDY OF QCM, MD AND LRM

***ABSTRACT*:** The behavior of polyoxyethylene (PEO) – polypropylene (PPO) – polyoxyethylene (PEO) lubricants on cellulose and polypropylene films was studied. The adsorption of these lubricants onto the surface of polymer films was investigated using a quartz crystal microbalance with dissipation (QCM).The results showed a larger adsorption of lubricant molecules on PP surfaces as compared to cellulose. Molecular Dynamics (MD) simulations were employed to corroborate the difference in molecular absorption. Lateral Force Microscopy (LFM) was used to calculate the friction coefficients for the different samples. It was found that not only did the lubricant adsorption contributed to the reduction in friction, but also the hydrophobicity of the surface. In addition, force-distance curves demonstrate that large adhesion hysteresis was associated with relative high friction. The combination approach of a quartz crystal microbalance with dissipation (QCM), molecular dynamics simulation and lateral force microscopy was proven successful for the study of polymer thin films

.

KEYWORDS Adsorption, lubrication, thin films, quartz crystal microbalance, molecular dynamic simulation, lateral force microscopy

1. Introduction

Polymer thin films are usually found in a liquid-solid interface due to the adsorption of polymer molecules onto the solid surface. Their thickness is usually found in the nanometer to micron range. Such films play a critical role in several processes such as adsorption, lubrication, adhesion, electronic packaging, sensors, dielectric coatings, and lithographical resist layers. [1-3] As the film thickness decreases from the micron to the nanometer range, polymer properties become different from those of the bulk. [4, 5] Generally, the structure and properties of thin films are governed by key factors such as the mobility of polymer molecules near surfaces or within interfaces, the effects of confinement on polymers and their glass transition temperature [6].

Poly(ethylene oxide)-poly(propylene oxide)-poly(ethylene oxide) (PEO-PPO-PEO) are amphiphilic block copolymers used in a broad range of industrial applications such as dispersers, stabilizers, detergents, and emulsifiers [7]. Several studies have reported the formation of PEO-PPO-PEO thin films at liquid/solid interfaces. [8-12] Furthermore, it has been found that the adsorption and lubrication of PEO-PPO-PEO thin films are highly correlated with each other at the macro and nano scale. Cann and Smeeth *et al.* studied the film-forming properties of polyisoprene solutions on a solid surface via ultrathin film interferometry. [13, 14] The resulting films, with a thickness around 20nm, could prove useful for boundary lubrication on solid surfaces. Yamada *et al.* employed a surface force apparatus to examine a poly (dimethylsiloxane) (PDMS) thin film and discovered an effective friction reduction at a nanoscale in the confined and well-ordered PDMS films [15]. The study of the absorption effects on a lubrication system also been carried via quartz crystal microbalance (QCM), FTIR microspectroscopy [16, 17], ellipsometry [17, 18], and reflectance spectroscopy [19]. In this work, a quartz crystal microbalance with dissipation (QCM) was chosen to analyze the adsorption phenomena of PEO-PPO-PEO copolymers on polymer

surfaces. . This technique measures the changes in resonance frequency and energy dissipation of a quartz crystal resonator. The changes in resonance frequency are proportional to the mass added to or removed from a solid surface. On the other hand, the changes in energy dissipation are correlated with the viscoelastic properties of the absorbed layer on the surfaces. QCM has been employed in the study of absorption, swelling, lubrication, and wetting. For example, it was employed to study the adsorption of nanofibrils and poly (amideamine epichlorohydrin) on cellulose model surfaces when used as paper strength additives [20]. The dynamic analysis of frequency and dissipation showed evidence on the formation of layer-structures and nano-aggregates, which was determined to be a crucial effect on paper wetting and dry strength development. Recently, QCM was successfully used to study the adsorption of nonionic surfactants on polymeric model surfaces, such as polyethylene, polypropylene, Nylon, and polyester. The adsorption mechanism was found to be highly dependent on the surface nature [21]. Abedelmaksoud *et al.* were able to determine the sliding friction on the absorbed layer, with respect to the hard surface, by simultaneously measuring the shift in frequency and the broadening of the resonance. The absorption process can be in-situ tracked with a deeper understanding of friction behavior and molecular arrangement in the absorbed layer.

In order to probe the lubrication phenomena, lateral force microscopy (LFM) was employed in this work to examine friction properties of polymer thin films on solid surfaces [22]. LFM has been widely employed for direct measurement of friction and friction coefficients on thin lubricating film at the nanoscale [17]. Liu *et al.* used LFM to study the friction properties of surfactant monolayers. They found that external conditions such as humidity, temperature, and sliding velocity, had a significant impact on the friction behavior [22-24]. Esayanur *et al.* measured the frictional interactions between surfactant adsorbed surfaces using lateral force microscopy,

providing valuable insights into the role of dispersants acting as lubricants [25]. LFM has also provided an advanced tool to design and investigate the fabrication of high-performance polymer lubricants using C60-containing polyelectrolyte self-assembled films on micas [26]. It is also capable to directly identify and map surface frictional characteristics, providing an advanced and direct technique to study friction and lubrication phenomena at a nanoscale.

Besides the above mentioned experimental techniques, molecular dynamics (MD) simulations have been increasingly employed to investigate polymer interfacial phenomena at the atomic scale. MD has been used either individually or as a supplemental tool to experimental techniques. Prathab *et al.* theoretically predicted interfacial interactions between poly(methyl methacrylate) (PMMA) and many other engineering polymers of relevance by calculating solubility parameters in MD simulations [27] . By means of MD, Hower *et al.* investigated molecular configurations of proteins interacting with hydroxylated and methylated mannitol as well as sobitol terminated self-assembled monolayer (SAM) surfaces in the presence of explicit water molecules [28]. Wongkoblap *et al.* carried out both computation simulation and experimental studies to probe the adsorption of polar and non-polar fluids in carbon nanotube bundles [29]. Their model generated from simulation results were in agreement with the experimental data. However, little was found to study aqueous polymer solutions on solid surfaces. With the presence of water, the interface becomes more complex due to the formation of hydrogen bonds among polymers, water and solid surfaces.

In this study, we constructed hydrophobic and hydrophilic solid surfaces of polypropylene and cellulose respectively. The adsorption of PEO-PPO-PEO block copolymers in aqueous solutions on PP and cellulose surfaces was investigated using QCM. The friction coefficient and interfacial interaction of the thin PEO-PPO-PEO

films on solid surfaces were measured using LFM. A calculation method in MD simulation was proposed to predict theoretical interaction energy of the thin films in copolymer aqueous solutions on the solid surfaces. The MD results provided a theoretical explanation for the QCM and LFM experimental data. The correlation between the adsorption and lubrication was discussed.

2. Materials and Experiments

2. 1 Polymer coated surfaces

Prior to spin coating, silica wafers (Waferworld, FL) were washed with Piranha solution and cleaned using an ultraviolet-ozone (UVO) treatment. PP was spin coated onsilica wafers following the procedure used by Song *et al.* [21] 20 mg PP (M_n≈5000, M_w/M_n≈2.4, Sigma Aldrich) were dissolved in 10 ml xylene. The solution was stirred for more than 2 hours at a constant temperature of X degrees under a condensation system. Silica wafers (1cmx1cm) and pipettes were kept at a temperature of ca 85°C by means of an IR lamp. A drop of PP solution was spread on the wafer surface for subsequent spin-coating (WS-400A-6NPP, Laurell Technologies) at 2000 rpm for 20 seconds. The coated wafers were stored in an oven overnight at 80 °C to evaporate solvent residues.

To obtain silica wafes coated with cellulose, we followed a procedure reported by Song *et al.* [21] First, clean silica wafers were immersed in a polyvinylamide (PVAm, BASF) aqueous solution (100ppm) for 20 minutes. Milli-Q water was used to wash the PVAm-coated surfacein order to remove the PVAm excess and further dried with filtered nitrogen. . The presence of polyvinylamide on the surface of the wafer created effective binding sites for cellulose molecules. 50mg of micro-crystalline cellulose (MCC, Avicel) were dissolved in 2.5ml of 50vol% dimethyl sulfoxide (DMSO) in water. After complete dissolution, 7.5 ml DMSO were added to adjust the solution viscosity. A drop of cellulose solution was spread on silica wafers previously coated

with PVAm followed by spin-coating at 5000rpm for. The surface topography for bare silica, PP coated silica, and cellulose coated silica was imaged with Atomic Force Microscopy (Figure 1). The coating films had a thickness of 20 and 15 nm and a roughness of 1 and 2 nm for PP and cellulose respectively.

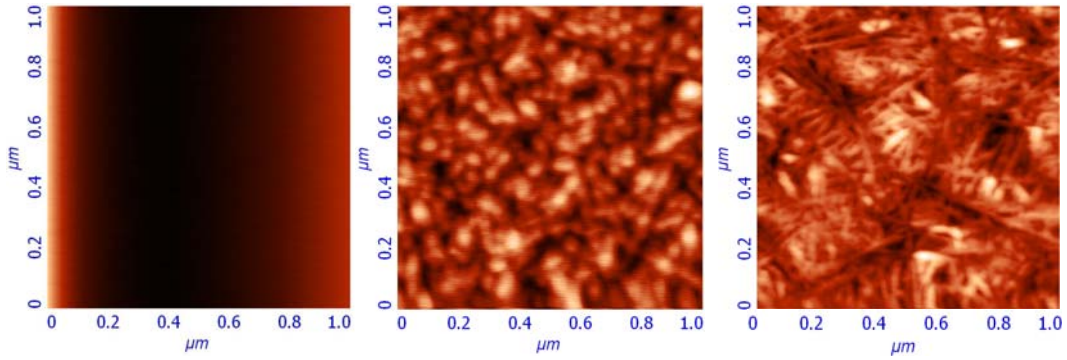

Bare silica Cellulose PP

a: Height images

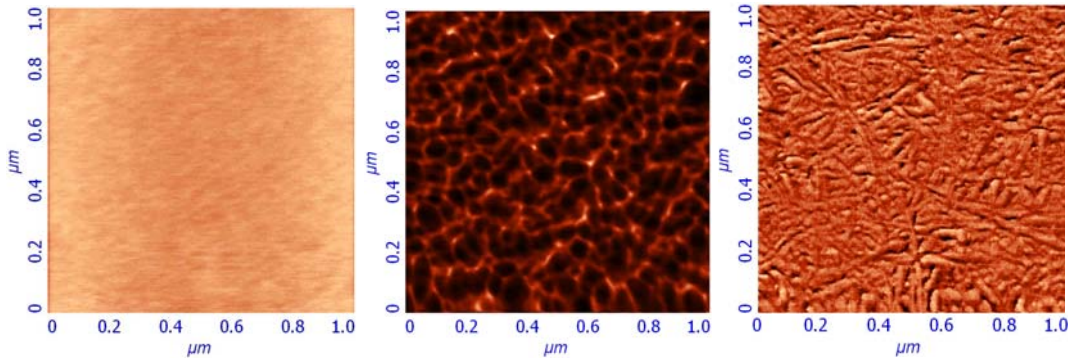

Bare silica Cellulose PP

b: Phase images

Figure 1. 1-µm AFM images of bare silica wafer, cellulose and PP thin films spin-coated on silica wafers (images obtained in air).

2. 2 Quartz Crystal Microbalance (QCM)

A QCM E4 model (Q-sense, Inc. Sweden) was used to study the adsorption and dynamics of triblock copolymers on polymer surfaces. The resonant frequency (f) change of the crystal depends on the total oscillating mass. For the case of thin and

rigid adsorbed layers, the Sauerbrey equation (Eqn. 1) [30] can be used to calculate the change in the adsorbed mass:

$$\Delta m = -\frac{c\Delta f}{n},$$

where C = 17.7 ng Hz^{-1} cm^{-2} for a 5 MHz quartz crystal. n = 1,3,5,7 is the overtone number.

The surface of QCM sensors was modified with an ultrathin layer of PP or cellulose films by the spin coating procedure described in the previous section. The temperature was kept constant at 25 ± 0.02 ºC for all experiments. The triblock copolymer, $EO_{37}PO_{56}EO_{37}$ (BASF Co.), was used in this study. Copolymer solutions with concentrations of 0.0001%, 0.001, 0.01% 0.1% and 1% w/w were prepared for QCM experiments to obtain adsorption curves.

2. 3 Molecular Dynamics Symulations (MD)

MD work was performed using the Material Studio 4.1 software (Accelrys Inc., San Diego, CA). The force-field of COMPASS (Condensed-phase Optimized Molecular Potentials for Atomistic Simulation Studies) was applied to build models. The detailed discussion on COMPASS can be found in the literature [31, 32]. An oligomer method has been successfully developed of adopting oligomeric forms of these polymers in the MD simulations [33-35]. The target density of PP and cellulose were defined as 0.873g/cm^3 and 1.446g/cm^3 respectively, which were comparable to those reported previously [36, 37]. The PP and cellulose oligomer chains were first built by corresponding monomers and then were used to construct a polymer slub with a dimension of 200×33×26Å for PP and 200×33×32Å for cellulose, respectively. Another water layer (1.00g/cm^3, 200×33×40Å) was built and piled up on the confined polymer surfaces. A single tri-block copolymer, $EO_{37}PO_{56}EO_{37}$ was generated in the water layer and placed on the polymer surface. The water layer with a single copolymer molecule simulated a 1% copolymer aqueous solution. A vacuum space

was placed on the top to avoid the interruption of the periodical border. Representative models before simulations are illustrated in Figure 2a and 2c. Then MD simulations were performed under the constant volume and temperature (NVT) ensemble. Models built with 3D periodicity were equilibrated for 5ps in the NVT ensemble at 298K. Systems were then subjected to 1000 ps of dynamics with the trajectories being saved every 10 ps. The final frames are shown in Figure 2b and 2d.

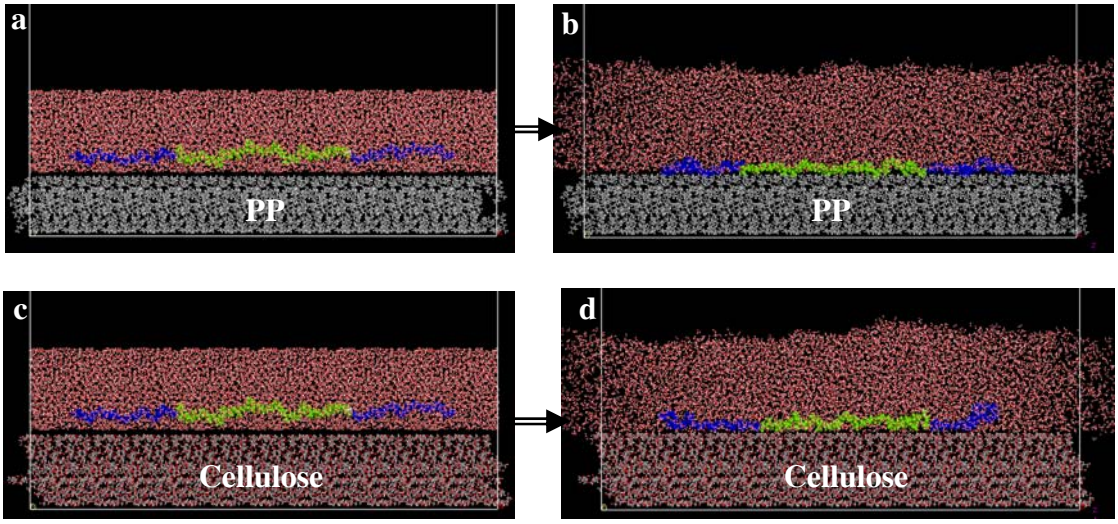

Figure 2. MD scheme on the MD simulation when the interaction energy was calculated on PP and cellulose surfaces. (Left) Original models of a single triblock copolymer molecule in water on PP(a) and cellulose(b) surfaces. Colors represents particular: carbon atoms—grey, hydrogen—white, and oxygen—red. The PAG polymers are colored with different sections: butyl group—purple, PPO— green, and PEO—blue. (Right) the final frames after the NVT dynamic simulation are shown for PP (b) and cellulose (d) surfaces.

The interaction energy represents the work of adhesion necessary to separate a single copolymer molecule from the PP or cellulose surface interacting with each other. The interaction energy is proportional to the difference between the energy of the total system E_{total} and those of the individual layers $E_{surface}$ and $E_{polymer}$. The energy difference should be normalized in order to obtain the interaction energy at a

molecular level. We adopted a surface area method reported by Chauve et al[38]. This method calculates the interaction energy of the polymer in the middle of a sandwich model by dividing the energy difference by two times the surface areas. Because there was only one interacting interface in our model, the energy difference was only divided by the surface area $S_{surface}$ to obtain the interaction energy $E_{interaction}$ (cal/cm^2) in equation (1).

$$E_{interaction} = -(E_{total} - E_{surface} - E_{polymer}) / S_{surface} \qquad (1)$$

Results are shown in Figure 5.

2. 4 LFM and force spectroscopy

Atomic force microscopy (TEGRA Prima, NT-MDT) in lateral force mode was employed to measure the friction forces on bare silica, PP, and cellulose surfaces. Scans were performed in air, DI water and in the lubricant solution (1% by weight) for each surface. Before each scan, surfaces were cleaned with DI water and 95% ethanol, and then air-blow dried. Contact mode probes (MikroMasch) were made from silicon nitride, with a force constant of 0.35N/m. For the tests under water and lubricant solution, the liquids were injected in a liquid metal cell where the wafer samples were placed. The scanning was done at 1Hz for a scanning size of 1 μm. Both height and lateral force images consisting of 256×256 pixels were collected simultaneously in LFM.

Distance-force curves are the probe responses during the approach-retract cycle in force spectroscopy (FS). Force measurements were conducted after each scan and distance-force curves were obtained accordingly. The force curves illustrated the mechanical properties of the polymer thin films. The shape and slope of the curves depended on the surface characteristics.

3. Results and discussion

3.1 Adsorption

In order to understand the adsorption mechanism and properties of the adsorbed layers on a molecular scale, adsorption experiments were conducted on polymer coated silica wafers using QCM. Frequency and dissipation of three overtones were recorded simultaneously and plotted in a single chart. Because the third overtone vibration reached the largest area in the sensor compared to the other two, the third overtone was chosen to illustrate the changes in resonance frequency and energy dissipation. The changes in frequency and dissipation are shown in Figure 3 as a function of time for $EO_{37}PO_{56}EO_{37}$ adsorbed on PP surfaces. Before each experiment, water was continuously injected in the sample loop until stable baselines were obtained for both frequency and dissipation simultaneously. Following this, a 0.0001% w/w copolymer solution was injected in the loop, resulting in a rapid drop of frequency and a small increase in dissipation. These changes were indicative of the adsorption of the copolymer on the sensor surface. The increase in dissipation was no more than 3×10^{-6} dissipation units, which indicated that the adsorbed $EO_{37}PO_{56}EO_{37}$ film was loosely bound on the surface. In addition, the adsorption process of the nonionic lubricants was found to be quite rapid, as required in many practical applications. It took approximately 10 minutes to allow both adsorption and dissipation curves to reach a plateau. The experiment was continued for another 10 minutes to ensure that an equilibrium state was achieved. Afterward, water was injected to rinse the system. The equilibrium was disturbed followed by an increase in frequency, but no observable change in the dissipation curve. These changes were indicative of the removal of loosely bound lubricant molecules on the surface by rinsing. After the first cycle of absorption and rinsing, the experimental procedure was

continuously repeated for the remaining solutions in order of increasing concentration. The results are displayed in Figure 3. The inset shows the small changes in dissipation when concentrations of 0.001% and 0.01% were used.

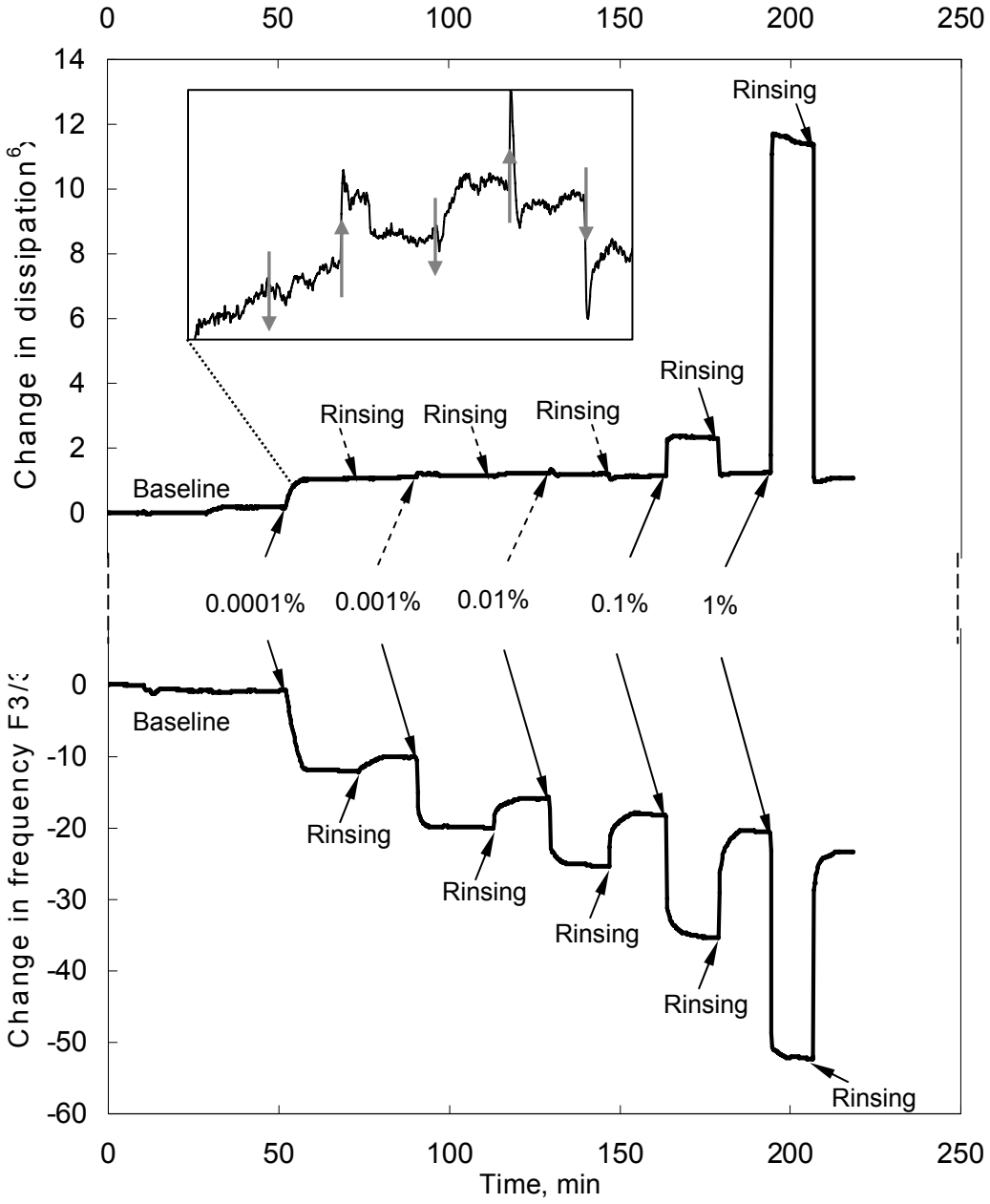

Figure 3. QCM results showing changes in frequency and dissipation for $EO_{37}PO_{56}EO_{37}$ on PP surfaces.

The adsorption mass in a QCM measurement can be divided into two categories: total or reversible adsorbed mass, indicated by the first plateau in one cycle, and irreversible adsorbed mass, related to the second plateau in one cycle. The irreversible adsorbed mass, which eliminates the influence of bulk polymers, is more important than the total adsorbed mass for boundary lubrication. As seen in Figure 3, the equilibrium state for a given cycle was associated with higher frequency and lower dissipation than the previous cycle, indicating an increase in the irreversible adsorbed mass. Therefore, the adsorbed mass kept accumulating in the thin layer, however the molecular conformation on the surface did not change significantly below a concentration of 0.1%. At concentrations above 0.1%, the amount of lubricant molecules absorbed on the surface was high enough to cause changes in the structure of the absorbed layers. Meanwhile, rinsing caused a large drop in the frequency curve, indicating that a large portion of absorbed mass was removed due to loose binding of lubricants on the surface.

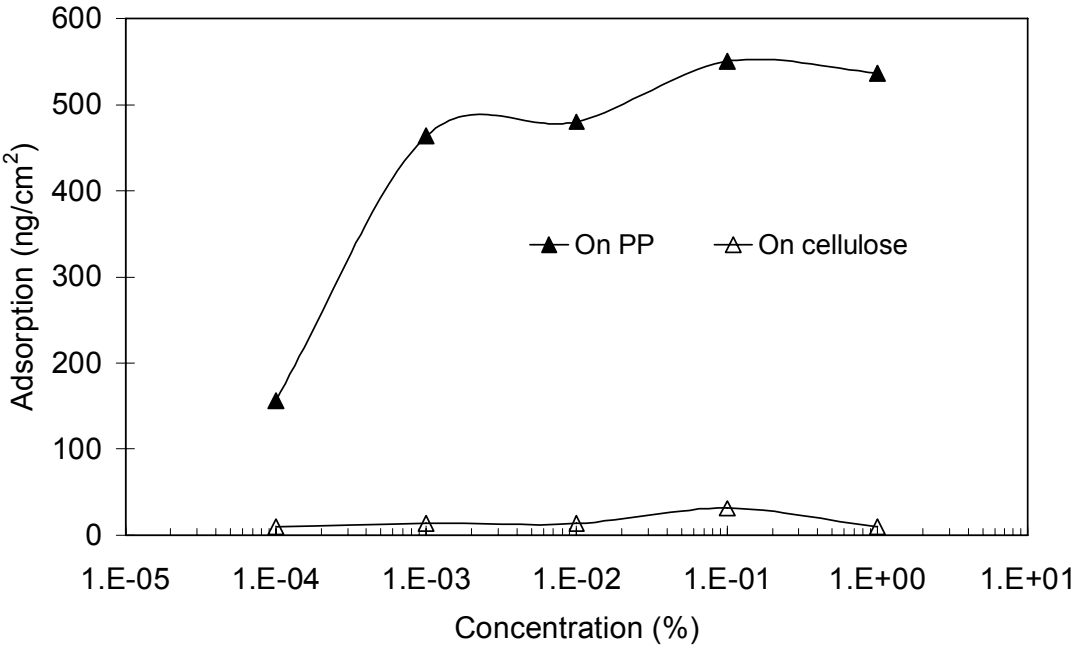

Figure 4. Adsorption Isotherms of $EO_{37}PO_{56}EO_{37}$ on PP and cellulose surfaces.

The same procedure was also repeated on cellulose surfaces. The equilibrium adsorption mass after rinsing, related to irreversible adsorption, was recorded as a function of concentration. The amount of lubricant adsorbed was calculated from the frequency change by using the Sauerbrey equation (Eqn.1). The absorption mass of $EO_{37}PO_{56}EO_{37}$ was plotted as a function of lubricant concentration (Figure 4). The adsorption of tri-block copolymers on cellulose surfaces was less than that on PP surfaces. The difference in adsorption on substrates indicated the lower affinity of the tri-block copolymers towards hydrophilic cellulose surfaces. As a result of a greater affinity to the water, most of the lubricant molecules were removed from the cellulose surfaces during the rinsing cycle. In contrast, a large adsorption of tri-block copolymers on PP surfaces was observed, indicating a higher affinity of the tri-block copolymers towards the hydrophobic PP surfaces. The irreversible adsorption of $EO_{37}PO_{56}EO_{37}$ on the PP surface approached saturation as the lubricant concentration increased, as indicated by the decrease in time for frequency to stabilize after rinsing (Figure 3).

3.2 Interaction energy

Interaction energies of a single tri-block copolymer molecule on PP and cellulose coated surfaces were calculated in vacuum and water using MD simulation, shown in Table 1. For the simulation in water, the equivalent copolymer concentration was

Table 1. Interaction energy between tri-block copolymer molecules and polymer surface calculated by MD simulations.

Surfaces	**Interaction energy of the tri-block copolymer (Kcal/mol)**	
	In vacuum	**In water**
PP	-610.5 ± 43.1	-646.8 ± 122.3
Cellulose	-647.6 ± 43.3	-472.7 ± 87.4

calculated to be 1% w/w. This concentration was used for friction coefficients measurements. The interaction energy calculated by MD simulations was capable to quantify the affinity of the tri-block copolymers with the polymer-coated surfaces. In vacuum, the values of the interaction energies between the tri-block copolymer and the PP and cellulose surfaces coated surfaces were similar. When taking into account the addition of water molecules to the system, the absolute interaction energy significantly decreased for the cellulose surface while slightly increasing for the PP surface. The variation in interaction energy was attributed to the nature of polymer-coated surfaces. The addition of water to the system resulted in a lower affinity between the tri-block copolymer and the cellulose coated surface. Due to this low affinity, the copolymer preferentially remained in solution. In contrast, the addition of water increased the interaction energy with the hydrophobic PP. The MD results were in agreement with the data from QCM in that the tri-block copolymers had larger adsorption on PP surfaces than on cellulose surfaces.

3.3 Lubrication

The coefficients of friction for a bare silica surface showed a significant decrease when measured with LFM in water and lubricant solution as compared to air (Figure 5). Water reduced the friction coefficients more than the copolymer solutions. A similar trend was observed for cellulose surfaces, shown in Figure 6. Contact angle measurements, determined in a previous study,[39] for bare silica and cellulose coated wafers were 25.7±1.5° and 28.6±3.4°, respectively. The acute angle indicated both surfaces were hydrophilic.[40] The reduction of friction due to water for the cellulose coated surface was smaller as compared to silica. The molecular weight of the tri-block copolymer impacted the reduction in friction only for the cellulose surface, with the higher molecular weight resulting in a lower coefficient of friction. The friction coefficients for silica remained constant while varying for the cellulose surface over

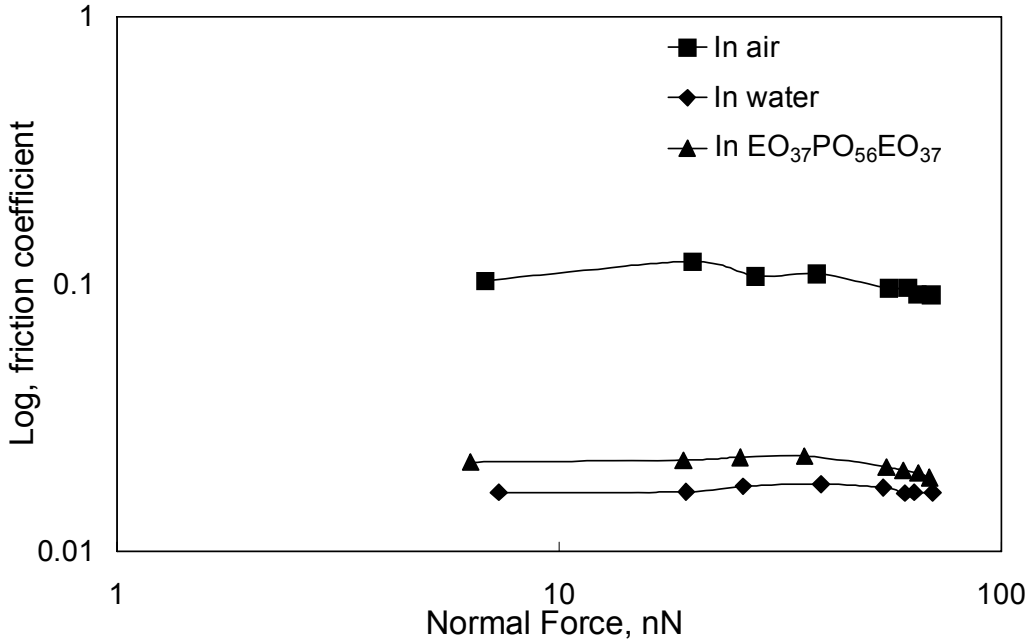

Figure 5. Friction coefficient curves on a bare silica surface.

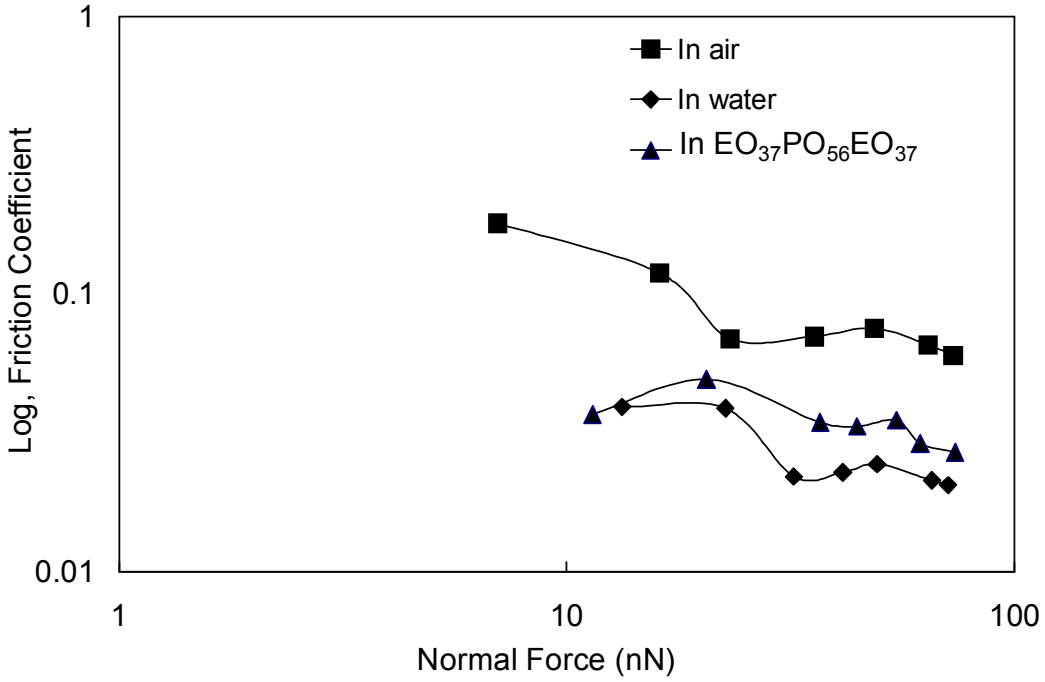

Figure 6. Friction coefficient curves on a cellulose surface.

the normal force range. Although both cellulose and silica surfaces are hydrophilic, they are different in terms of mechanical properties. Silica surfaces are hard and tough, as shown by the independence of the coefficient of friction with the normal force.

Cellulose coated surfaces are relatively soft and deformable compared with silica, resulting in a dependence of the coefficient of friction with the normal force.

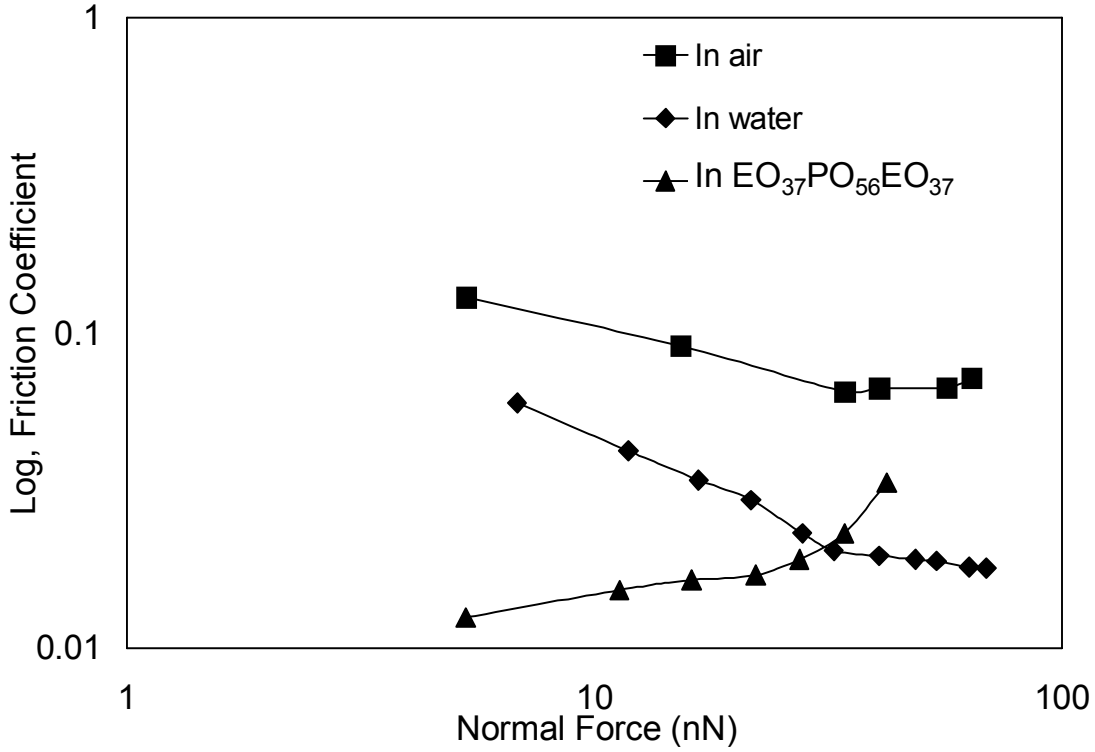

Figure 7. Friction coefficient curves on a polypropylene surface.

At small normal forces, the presence of aqueous tri-block copolymer solution lowered the friction coefficient, as shown in Figure 7. At a critical force of 27.4 nN, the friction coefficients increased and became greater than the friction coefficient in water. This suggests that at forces greater than the critical force, a change in the molecular arrangement of the adsorbed tri-block copolymer layers occurred. One possibility is that the layers are destroyed by forces greater than the critical force and prevent them from functioning as an effective lubricant.

3.4 Distance-force curve

Distance force curves are shown in Figure 8 for the three different surfaces in the different environments. The energy dissipation within an approach-retract cycle, known as adhesion hysteresis (AH), is the difference between the energy required to

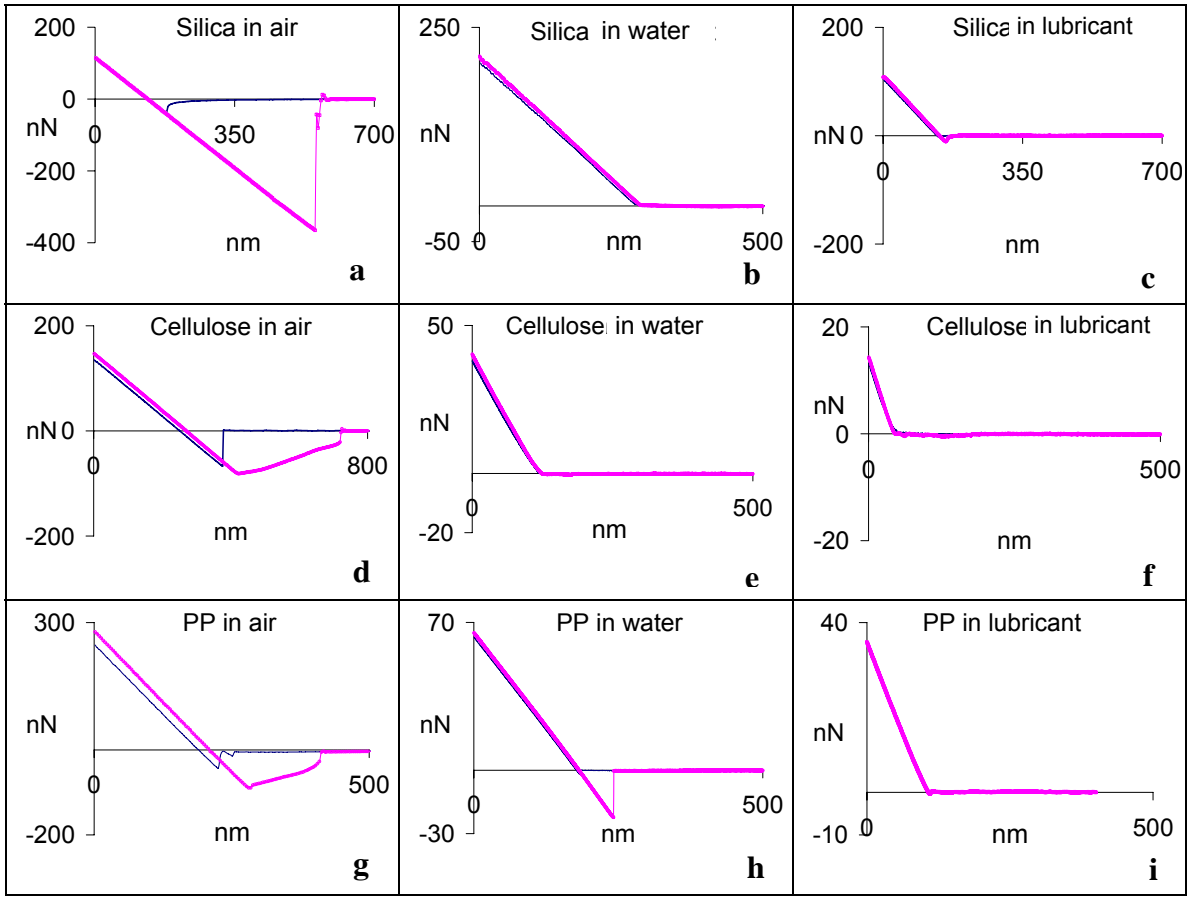

Figure 8. Distance-force curves are obtained on silica (a, b, c), cellulose (d, e, f), and PP (g, h, i) surfaces in different environment: in air (a, d, g), in water (b, e, h), in lubricant solution (c, f, i). Large dissipation hysteresis was found on all surfaces in air, which corresponded to large friction coefficients in air.

bring the AFM tip in contact with the surface and the energy needed to separate the tip from the surface. The AH is determined by measuring the area of the closed loop during an approach-retract cycle. The tri-block copolymer effectively reduces the hysteresis effect on all substrates, as shown in Figure 8. In the case of hydrophobic surfaces, water had a comparable effect as that of the copolymer solution while hysteresis effect was still observed on the PP surface. Just as with the coefficient of friction behavior, the larger AH was observed in air. Polymeric surface layers can be classified into three categories: solid-like, liquid-like, and amorphous.[41] Dry surfaces showed a larger AH as compared with surfaces immersed in liquids, the silica surface being the largest of the three.

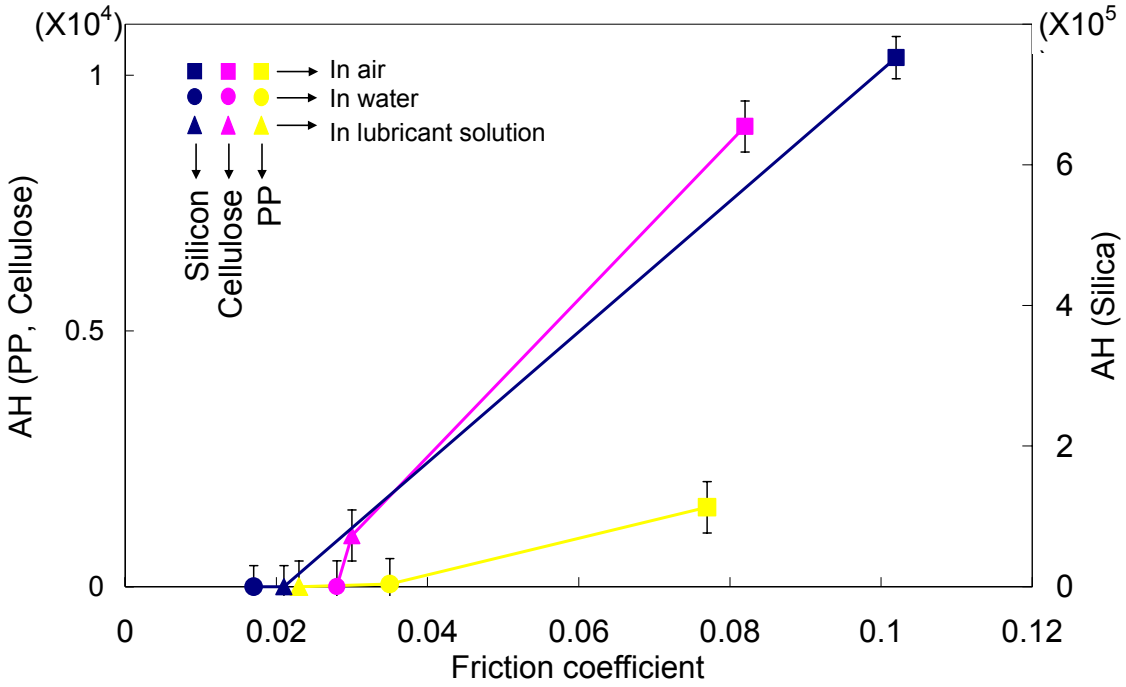

Figure 9. Correlation between adhesion hysteresis (AH) and friction coefficient on polymer surfaces in air, in water, and in lubricant solution. In air, high friction coefficients correspond to high adhesion hysteresis. In water and lubricant solution, low friction coefficients correspond to low adhesion hysteresis.

When the surfaces were immersed in water or lubricant solutions, the AH was dramatically reduced. In this case, the polymer coated surfaces behaved similarly to the liquid state, resulting in low AH and friction coefficients. In the liquid-like state, chain entanglements readily occurred as soon as the AFM tip came into contact with the surface. The interacting molecules disentangled rapidly and easily so that the system was always at equilibrium, resulting in no AH. The PP surfaces showed a small AH, possibly attributed to the hydrophobicity of PP which prohibited wetting on the surface. Silica and cellulose surfaces were hydrophilic and so water easily wetted the surfaces. Wetting could transform the surface layer to a truly liquid-like state, which results in no AH on wet silica and cellulose surfaces.

The adhesion hysteresis was quantitatively illustrated by the area of the approach-retraction cycle. It was plotted as a function of friction coefficient, which was measured on the corresponding surfaces as well as the corresponding conditions (in air, in water, or in lubricant solution). It was found in Figure 9 that adhesion hysteresis was large when friction coefficient was high in air. There was a linear relationship between adhesion hysteresis and friction coefficient, suggesting that adhesion hysteresis on distance-force curve could be an effective indicator of friction behavior on a surface. Therefore, except for LFM measurement, force curve measurement could be an alternating method to qualitatively study friction phenomena.

4. Conclusion

The combined study of QCM, MD simulation and LFM techniques is a capable approach for understanding the absorption and lubrication of triblock copolymers, $EO_{19}PO_{29}EO_{19}$ and $EO_{37}PO_{56}EO_{37}$, on polymer coated surfaces. The time-dependent QCM study showed that a larger mass of tri-block copolymers was adsorbed on PP than on cellulose surfaces. The MD simulations calculated the interaction energy of a single $EO_{19}PO_{29}EO_{19}$ tri-block copolymer molecule in an aqueous solution with

cellulose and PP coated surfaces. A larger adsorption was observed for PP surfaces as compared to cellulose. The friction coefficients from LFM measurements indicated that friction and lubrication were dependent on the surface nature. Using tri-block copolymers as lubricants, the hydrophobicity of PP surfaces resulted in low friction and good lubrication while the hydrophilicity of cellulose surfaces did not. In addition, force spectroscopy provided an alternative method to evaluate friction coefficients in terms of AH by a linear relationship between friction force and AH.

Acknowledgement

The authors thank the financial support of this work by National Textile Center (No. C05-NS09). We thank Dr. Laura McJilton, Alejandra Andere Jones, and Christina Diaz for their English correction of the manuscript.

REFERENCES

1. Bartczak, Z., et al., The morphology and orientation of polyethylene in films of sub-micron thickness crystallized in contact with calcite and rubber substrates. Polymer, 1999. 40(9): p. 2367-2380.

2. Cohen, Y. and S. Reich, Ordering phenomena in thin polystyrene films. Journal of Polymer Science: Polymer Physics Edition, 1981. 19(4): p. 599-608.

3. Prest, J.W.M. and D.J. Luca, The alignment of polymers during the solvent-coating process. Journal of Applied Physics, 1980. 51(10): p. 5170-5174.

4. Fell, H.J., et al., Unexpected orientational effects in spin-cast, sub-micron layers of poly(alkylthiophene)s: A diffraction study with synchrotron radiation. Solid State Communications, 1995. 94(10): p. 843-846.

5. Frank, C.W., et al., Structure in thin and ultrathin spin-cast polymer films. Science, 1996. 273(5277): p. 912-915.

6. Karim, A. and S. Kumar, Polymer surfaces, interfaces and thin films. 2000, Singapore: World Scientific.

7. BASF Technical Brochure and BASF Co. 1989: Parsippany, NJ.

8. Baker, J.A. and J.C. Berg, Investigation of the adsorption configuration of polyethylene oxide and its copolymers with polypropylene oxide on model polystyrene latex dispersions. Langmuir, 1988. 4(4): p. 1055-1061.

9. Brandani, P. and P. Stroeve, Adsorption and Desorption of PEO−PPO−PEO Triblock Copolymers on a Self-Assembled Hydrophobic Surface. Macromolecules, 2003. 36(25): p. 9492-9501.

10. Green, R.J., et al., A surface plasmon resonance study of albumin adsorption to PEO-PPO-PEO triblock copolymers. Journal of Biomedical Materials Research, 1998. 42(2): p. 165-171.

11. Green, R.J., et al., Adsorption of PEO-PPO-PEO triblock copolymers at the solid/liquid interface: a surface plasmon resonance study Langmuir, 1997. 13(24): p. 6510-6515.

12. Shar, J.A., T.M. Obey, and T. Cosgrove, Adsorption studies of polyethers Part 1. Adsorption onto hydrophobic surfaces. Colloids and Surfaces A: Physicochemical and Engineering Aspects, 1998. 136(1-2): p. 21-33.

13. Cann, P.M. and H.A. Spikes, The behavior of polymer solutions in concentrated contacts: immobile surface layer formation. Tribol. Trans. FIELD Full Journal Title:Tribology Transactions, 1994. 37(3): p. 580-6.

14. Smeeth, M., H.A. Spikes, and S. Gunsel, The formation of viscous surface films by polymer solutions: boundary or elastohydrodynamic lubrication? Tribol. Trans. FIELD Full Journal Title:Tribology Transactions, 1996. 39(3): p. 720-725.

15. Yamada, S., Nanotribological properties of molecularly thin polymer melt films studied using the surface forces apparatus. Hyomen Kagaku FIELD Full Journal Title:Hyomen Kagaku, 2008. 29(9): p. 550-557.

16. Molenda, J., M. Gradkowski, and C. Kajdas, Identification of surface phenomena by FTIR microspectroscopy. Tribologia FIELD Full Journal Title:Tribologia, 1997. 28(5-6): p. 773-781.

17. Zhao, J.C., Miao; An, Yanqing; Liu, Jianxi; Yan, Fengyuan, Preparation of polystyrene brush film by radical chain-transfer polymerization and micromechanical properties. Applied Surface Science 2008. 255(5, Pt. 1): p. 2295-2302.

18. Fukuzawa, K.S., T.; Yoshida, T.; Zhang, H.; Mitsuya, Y., Visualization of dewetting of molecularly thin lubricant on magnetic disks by ellipsometric microscopy. IEEE Transactions on Magnetics 2006. 42(10): p. 2495-2497.

19. Yanagisawa, M., An adsorption of perfluoropolyethers on silica surfaces for thin film magnetic disk overcoats. Tribology Transactions, 1999. 36(3): p. 484-90.

20. Ahola, S., M. Osterberg, and J. Laine, Cellulose nanofibrils-adsorption with poly(amideamine) epichlorohydrin studied by QCM-D and application as a paper strength additive. Cellulose (Dordrecht, Neth.) FIELD Full Journal Title:Cellulose (Dordrecht, Netherlands), 2008. 15(2): p. 303-314.

21. Song, J., et al., Development and Charaterization of thin polymer films relevant to fiber processing. Thin Solid Films, 2009..

22. Liu, Y., T. Wu, and D.F. Evans, Lateral Force Microscopy Study on the Shear Properties of Self-Assembled Monolayers of Dialkylammonium Surfactant on Mica. Langmuir, 1994. 10(7): p. 2241-2245.

23. Liu, Y., et al., Structure and Frictional Properties of Self-Assembled Surfactant Monolayers. Langmuir, 1996. 12(5): p. 1235-1244.

24. Jia, J.B., Jonathan W, Friction Dependence on .alpha.-Relaxations in a Tethered Polymer Monolayer. Nano Letters, 2007. 7(5): p. 1304-1307.

25. Esayanur, M.S.Y., Suresh B.; Rabinovich, Yakov I.; Moudgil, Brij M., Interaction force measurements using atomic force microscopy for characterization and control of adhesion, dispersion, and lubrication in particulate systems. Journal of Adhesion Science and Technology, 2005. 19(8): p. 611-626.

26. Huang, L., et al., Fabrication and AFM/FFM studies of C60-containing polyelectrolyte self-assembled films. Chin. J. Polym. Sci. FIELD Full Journal Title:Chinese Journal of Polymer Science, 2002. 20(3): p. 197-203.

27. Prathab, B.S., V.; Aminabhavi, T. M., Molecular dynamics simulations to investigate polymer-polymer and polymer-metal oxide interactions. Polymer, 2007. 48(1): p. 409-416.

28. Hower, J.C., Y. He, and S. Jiang, A molecular simulation study of methylated and hydroxyl sugar-based self-assembled monolayers: Surface hydration and resistance to protein adsorption. Journal of Chemical Physics, 2008. 129(21): p. 215101/1-215101/7.

29. Wongkoblap, A.D., D. D.; Wang, K., Adsorption of polar and non-polar fluids in carbon nanotube bundles: Computer simulation and experimental studies. Journal of Colloid and Interface Science, 2009. 331(1): p. 65-76.

30. Sauerbrey, G., Verwendung von Schwingquarzen zur Wägung dünner Schichten und zur Mikrowägung Zeitschrift für Physik A Hadrons and Nuclei, 1959. 155(2): p. 206-222.

31. Sun, H., P. Ren, and J.R. Fried, COMPASS force field: Parameterization and validation for phosphazenes. Computational and Theoretical Polymer Science, 1998. 8(1-2): p. 229.

32. Sun, H., COMPASS: an ab initio force-field optimized for condensed-phase applications-overview with details on alkane and benzene compounds. Journal of Physical Chemistry B, 1998. 102(38): p. 7338.

33. Kavassalis, T.A., P. Choi, and A. Rundin, Calculation of 3D solubility parameters using molecular models. Molecular Simulation, 1993. 11(2-4): p. 229-241.

34. Choi, P., T.A. Kavassalis, and A. Rudin, Estimation of Hansen solubility parameters for (hydroxyethyl)- and (hydroxypropyl)cellulose through molecular simulation. Industrial & Engineering Chemistry Research, 1994. 33(12): p. 3154-3159.

35. Kela, L., et al., Interactions between cationic amylose derivatives and a pulp fiber model surface studied by molecular modelling. Journal of Molecular Structure: THEOCHEM, 2007. 819(1-3): p. 1-12.

36. Mazeau, K.H., L., Molecular Dynamics Simulations of Bulk Native Crystalline and Amorphous Structures of Cellulose. The Journal of Physical Chemistry B, 2003. 107(10): p. 2394-2403.

37. Sun, C.C., Quantifying errors in tableting data analysis using the Ryshkewitch equation due to inaccurate true density. Journal of Pharmaceutical Sciences, 2005. 94(9): p. 2061-2068.

38. Chauve, G., et al., Cellulose poly(ethylene-co-vinyl acetate) nanocomposites studied by molecular modelling and mechanical spectroscopy. Biomacromolecules, 2005. 6(4): p. 2025-2031.

39. Li, Y., O.J. Rojas, and J.P. Hinestroza, Adsorption and Association of PEO-PPO-PEO Tri-block Copolymer Solutions on Polypropylene, Polyethylene, and Cellulose Surfaces. 2009.

40. Schwartzberg, H.G., In Food Packaging and Preservtion. Modeling of gas vapour transport through hydrohphilic films, Ch. 7, ed. M. Mathlouthi. 1986, New York: Elsevier Applied Sci.

41. Zeng, H., et al., Adhesion and Friction of Polystyrene Surfaces around Tg. Macromolecules, 2003. 39(6): p. 2350-2363.

CHAPTER 6

CONCLUSIONS AND FUTURE WORK

1. Summary and conclusions

The preceding work makes several important contributions to the field of fiber science and lubrication science as follows:

- It was demonstrated that Lateral Force Microscopy is a feasible technique capable of probing lubrication phenomena at the nanoscale in polymeric surfaces. The technique requires small amounts of lubricant and of polymer and it can provide qualitative and quantitative information valuable in assessing lubrication performance for textile relevant surfaces. Furthermore, it was found that several parameters obtained from LFM measurements, such as adhesion hysteresis and critical normal force, can be used as quantitative predictors of lubrication formulations.
- Lateral Force Microscopy and Atomic Force Microscopy measurements validated existing hypotheses, some stated as early as 1900s, regarding the influence of the chemical structure of a lubricant molecule on the friction behavior of coated textiles. Visual confirmation of conformational changes in the polymeric substrate caused by the deposition of the lubricant solutions were obtained and used to propose the molecular behavior of the lubricant molecule. These measurements were complimentary to independent analytical techniques such as Quartz Crystal Microbalance adsorption studies and molecular dynamic simulations.
- Thin films of some polymeric materials such as polypropylene can effectively be used as model surfaces to study fiber lubrication behavior at the nanoscale. However, in some cases, such as cellulose and polyethylene, dewetting of the

surface by the lubricant solution can present significant experimental challenges.

- Critical normal force measurements, adhesion hysteresis and adsorption behavior of lubricant on polymeric surfaces were found to correlate to lubrication performance. These three independent variables have the potential to be used in an equation capable of predicting the behavior of lubricant formulations.

2. Future Work

While the experimental results of this work may have validated old hypotheses and provided quantitative verification of the influence of molecular interactions between lubricant and surface on friction behavior, several questions remain unanswered. It is recommended that future work may be initiated in the following areas:

- Establish a mathematical relationship capable of predicting lubrication performance for a determined set of lubricant and surfaces: In this study hints of a mathematical linear relationship between friction coefficient μ with interaction energy, absorption behavior and critical normal force were found to exist. We adapted Buckingham π theorem to nondimensionalize these terms. A new dimensionless term we created was $V_i = E \cdot M \cdot F_c^{\,2} \cdot v^2$, where E: Interaction Energy (Kg•m^2/s^2), M: Adsorption (Kg/m^2), F_c: Critical Normal Force (Kg•m/s^2), v: Scanning Velocity (m/s). We plotted μ with this new number V_i (see Figure 1). The curve approximately shows an exponential relationship, this gives us a hint that friction coefficient is predictable by these parameters we studied in the work. In the future, other type of textile relevant polymers, polyester, Nylon, and other type of lubricants can be used in the same study so that there will be more data that can be used to establish a

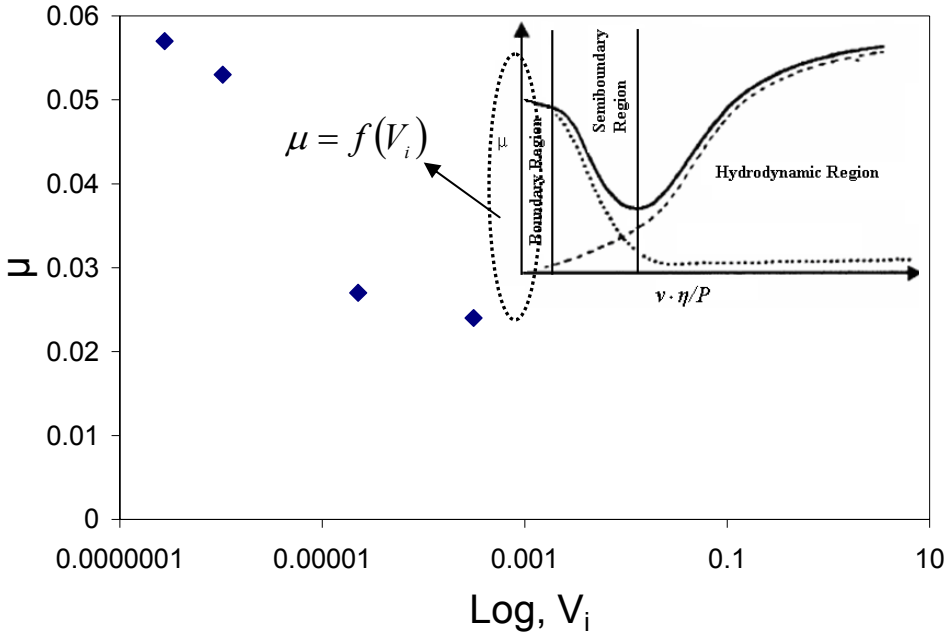

Figure 1. A nonlinear relationships ($\mu = f(V_i)$) between the new dimensionless number V_i and friction coefficient μ in boundary lubrication region.

mathematical model that is able to predict the boundary lubrication behavior. It is recommended that further studies with Pluronic® surfactants of different molecular weights and molecular configuration may be initiated in order to establish quantitative relationships between the molecular characteristic of the lubricant, i.e. the ratio of PEO/PPO and the MW of the molecule, and its lubrication performance. This type of relationships may open a new avenue for establishing a more intelligent criterion in the formulation of textile lubricants.

- Probe the lubrication behavior of multicomponent formulations: In this study only a type of molecules was studied. However commercial lubricant formulations are composed of several ingredients and it is possible that the presence of several components may induce synergetic effects that can alter the molecular conformation of the lubricant molecules. It is recommended to use

the existing AFM liquid cell to perform LFM experiments in which the concentration and number of components of the lubricant solution may be varied with precision.

- Incorporate the unique geometrical configuration of fibers as a factor in friction phenomena: In this study thin films were used as textile model surfaces to establish the feasibility of LFM as a probing technique. However textile fibers have a unique cylindrical shape, an in many cases non-cylindrical shapes i.e. lobular, star-like, ribbon-like, etc., which can play a role in friction and lubricant adsorption behavior. It is recommended that a cylindrical fiber be used as a model surface in future studies and probed in the longitudinal and axial directions. Preparing these types of samples could be quite challenging but novel advances in nanofabrication (i.e. FIB and micromachining) may be used to isolate a single fiber or to produce a cylindrical specimen with defined geometric characteristics in order to study the effect of geometry in friction phenomena.
- Incorporating adsorption dynamics as a factor in understanding transient friction behavior: The preceding study was performed at adsorption equilibrium. However textile lubrication is a very dynamic process and it is likely that adsorption kinetics may influence the lubrication behavior of a specific molecule. It is recommended that the existing AFM liquid cell may be coupled with the outlet of a QCM apparatus to perform in-situ LFM measurements using a high-speed scanner. While there are technological challenges to perform these measurements they may provide a new insight on the formation of lubricating layers on polymeric surfaces as a function of time.